# A 3D geological model for the East Rand Basin, South Africa

**DC Labuschagne**

**21618100**

Dissertation submitted in fulfilment of the requirements for the degree *Magister Scientiae* in Geography and Environmental Management at the Potchefstroom Campus of the North-West University

Supervisor: Mr T de Klerk

May 2015

## Acknowledgements

I wish to express my sincere appreciation and gratitude to the following persons and institutions for their contribution to this study:

My Heavenly Father, for His love, support, guidance and for giving me the privileges and abilities to study;

Mr Theuns de Klerk, who supervised and gave me guidance on my study;

Mr Dirk Cilliers, who helped me on the GIS tools;

Dr Reinier Dennis, for supplying me with all the data to complete this study;

The NRF, who funded me for my study;

The North-West University, Potchefstroom Campus, who gave me the opportunity to do this study;

My family and loved ones, who encouraged and supported me with all their love throughout my studies; and

My friends and colleagues for their assistance and support.

## Abstract

The primary aim of this dissertation is to map the geology of the East Rand Basin accurately by creating a 3D model. This was done by using borehole data from the National Groundwater Archive Geodatabase, which the Department of Water and Sanitation collected, and the average depths derived from the literature. Triangulated irregular networks (TINs) and digital elevation models (DEMs) surfaces were created from these data points to determine the depths for areas with no borehole data. Using these surfaces, three methods were used to create three main models. These models were then compared to one another, other geological maps and cross-sections to determine the most accurate and practical model of the three. It was found that the quality and quantity of the data from the National Groundwater Archive Geodatabase were not sufficient for these models; therefore, the results and accuracy of each layer was questionable. This dissertation found that these methods can be used for basic geological studies if the data are of the same quality and quantity. However, if the data are more evenly distributed and higher in quantity, these methods can be used to create more accurate models. Furthermore, the use of commercial software was recommended in this study. The reason for recommending these tools is that they have been specifically designed to create geological layers from boreholes within the ArcGIS software. These tools also allow the user to create cross-sections within ArcGIS.



**KEY WORDS: EAST RAND BASIN, GIS, 3D MODELLING, TIN, DEM**

## Abbreviations

2D – Two-dimensional

3D – Three-dimensional

AMD – Acid Mine Drainage

DEM – Digital Elevation Model

DWA – Department of Water Affairs

DWS – Department of Water and Sanitation

EMM – Ekurhuleni Metropolitan Municipality

Frm. – Formation

GIS – Geographical Information Systems

Grp. – Group

NGA – National Groundwater Archive

SACS – South African Committee for Stratigraphy

Spgrp. – Supergroup

TIN – Triangulated Irregular Network

WISA – Water Institute of Southern Africa

# Table of Contents

## List of tables

## List of figures

# Chapter 1: Introduction

## 1.1 Introduction

Geology involves studying the history and the function of the earth. By looking at layers of rock and ice, geologists can uncover clues about the climate, plant life and animal life of the past. Geology helps geologists predict potential environmental problems so that it can be understood, and so that ways to reverse, avoid or address these problems can be found. These problems include sinkholes, earthquakes, landslides and land erosion. Geology also assists geologists to study mining and to help find ways to extract resources such as gold, iron, coal and gas from the earth so that these resources can be manufactured into jewellery (gold) or used as energy sources (coal and gas) (Langholt, 2013).

South Africa is known as a very diverse and unique place, without equal on the globe when it comes to geology. South Africa occupies only 1% of the earth's land surface and was once the world's largest producer of gold, chromium, diamonds, vanadium, manganese and platinum. Therefore, South Africa is also known as the treasure house when it comes to valuable minerals. South Africa serves as a home to very large reserves such as iron, titanium, coal, fluorspar, zinc and refractory minerals (McCarthy & Rubidge, 2005).

The Witwatersrand was known as one of the biggest carriers of gold reserves in South Africa. The Witwatersrand Supergroup, which contains the West Rand Group and the Central Rand Group, is up to 7 km thick and makes up a part of the Western, Central and East Rand Basin's (also known as voids) geology (DWA, 2013a). These three basins have a total length of about 86 km in the west-east direction (Van Wyk *et al*., 2013). Soon after the discovery of gold in 1886, gold-mining commenced in the East Rand Basin and peaked between the 1940s and the 1950s (Scott, 1995 and DWA, 2013a). The East Rand Basin (Figure 1.1), which covers the East Rand, including the towns of Brakpan and Springs, is an oval-shaped basin of ± 30 km long and 20 km wide in which dips of strata are relatively shallow, and has a mine lease area of about 768 km2.

The East Rand Basin falls within the Ekurhuleni Metropolitan Municipality (EMM) (Figure1.1). This region has a Highveld summer rainfall, mild summers and freezing temperatures during the winter season. Various dams and streams, such as the Blesbokspruit, form part of this region, which is also home to a number of South Africa's biodiversity and is covered by the grassland biomes. Various agricultural and mining activities, which contribute to the economy, are also found within the region.

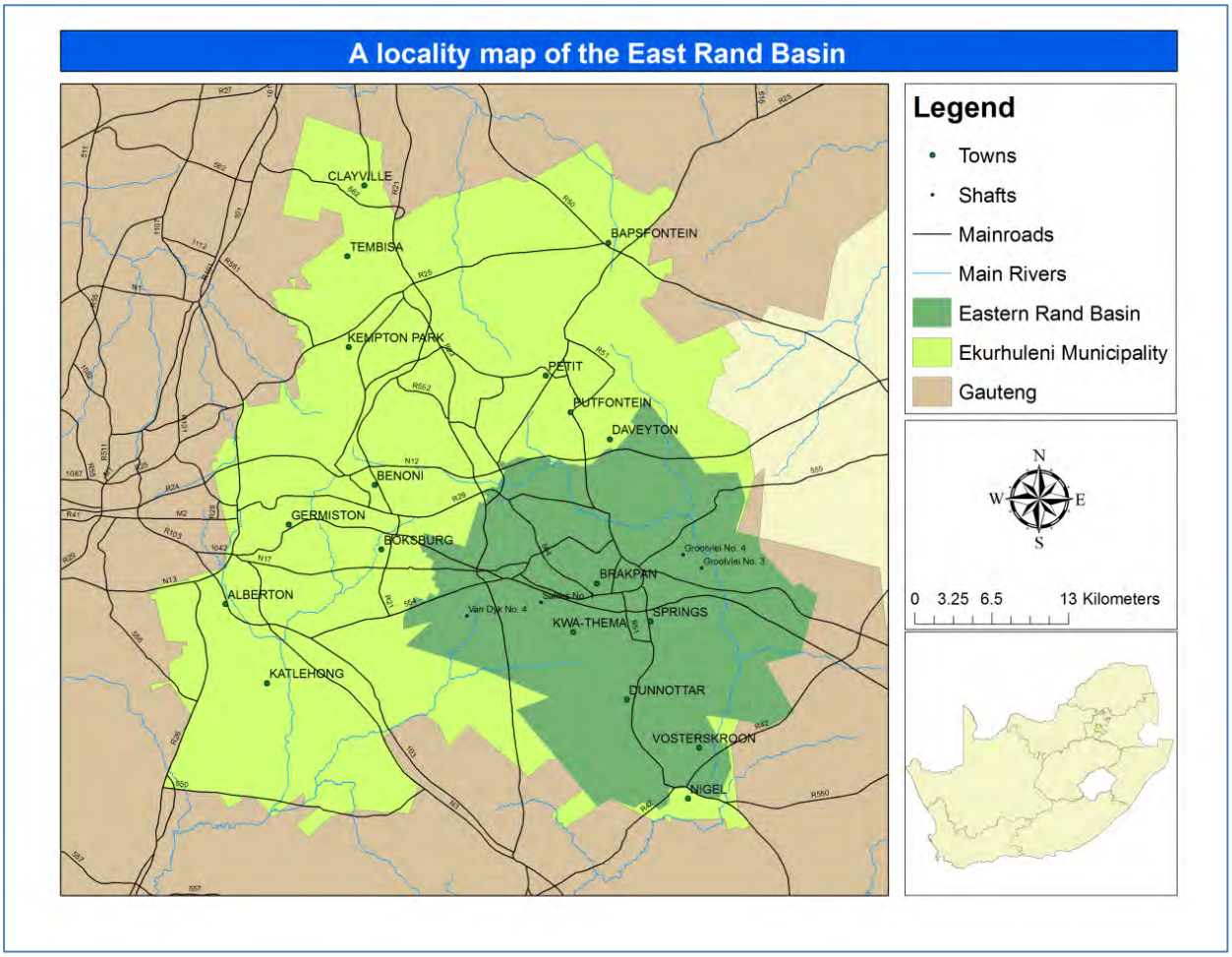


**Figure 1.1: Map indicating the location of the East Rand Basin in South Africa (Annexure A)**

Highly weathered lower Karoo sediments cover most of the East Rand Basin and overlie the Witwatersrand rocks and the extensively developed rocks of the Transvaal Supergroup. The basin is also home to various intrusive bodies. The most prominent of the bodies are the diabase and seyenite dykes and sills. Although this basin is largely mined out, it has supported about 28 mines and produced about 10 000 tons of gold (DWA, 2013a and EMM, 2007).

According to DWA (2013a) there are shallow perched aquifers that are mainly found in the sandstone and mined-out coal horizons. The Malmani Subgroup dolomite of the Chuniespoort Group is exposed due to the Karoo strata that have been eroded by the Blesbokspruit River. The effect of this exposure is that the surface water comes directly in contact with the dolomite aquifer, improving groundwater recharge rates. According to Scott (1995) the underground water has historically been pumped from the East Rand Basin since the early mining activities in the 1950s and 1960s, but since 1991 pumping has stopped and the water continued to flood the mines. Dewatering at the No. 3 shaft of Grootvlei at 740 m below surface started again in 1996

and stopped in early 2011 (Van Der Merwe & Lea, 2003 and Creamer Media, 2011). Scott (1995) estimated that groundwater flowing from the dolomites to underground workings represent the bulk of all water ingress to the mines. Two distinct dolomite aquifers occur within the Eastern Basin (Scott, 1995 & DWA, 2013a), as indicated on the map below:

- In the northern part of the area, the dolomite overlies the Witwatersrand sediments; and
- In the south-western portion of the area, the dolomite aquifer overlies the Ventersdorp Supergroup rocks.

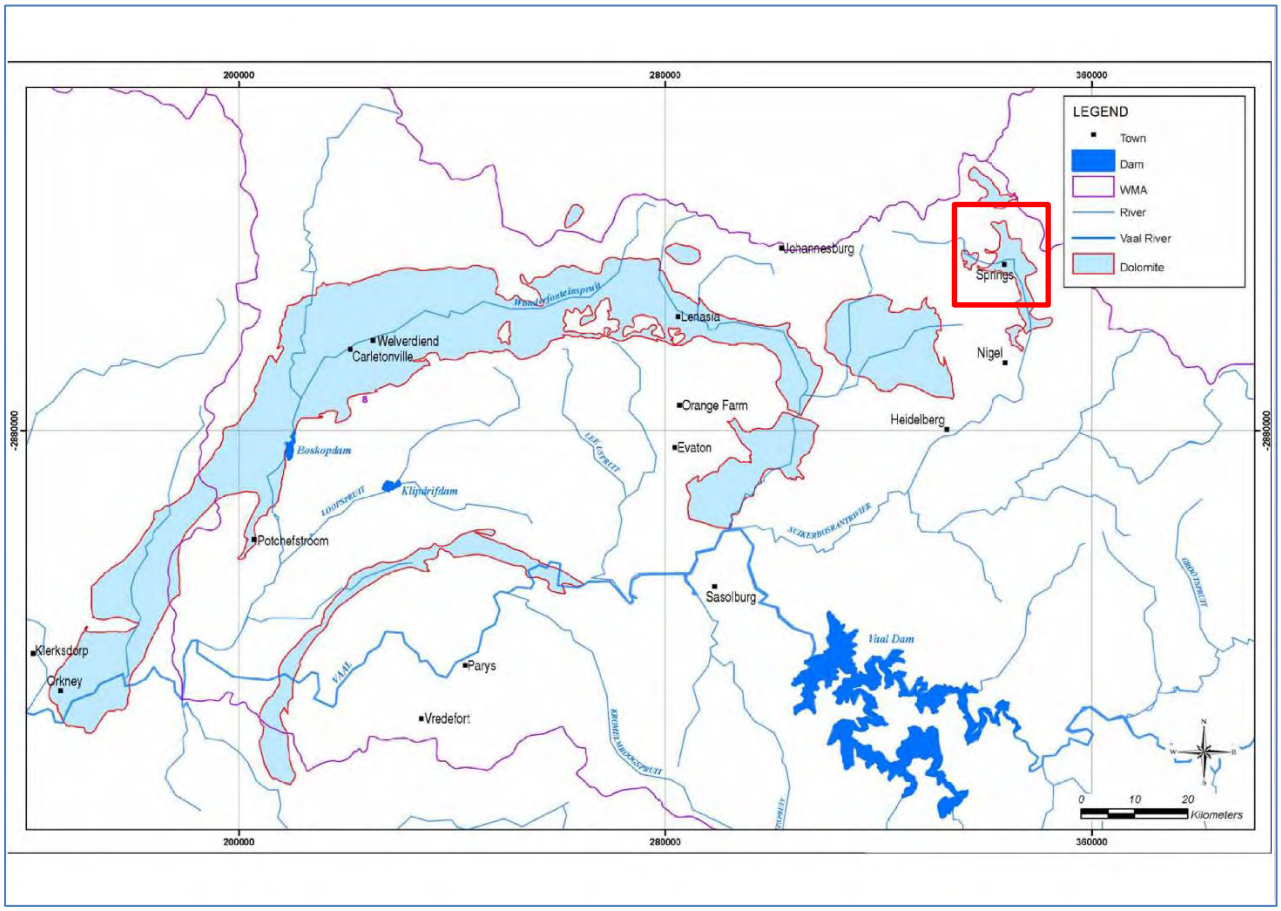


**Figure 1.2 : Map indicating the Far East to Far West dolomites (DWAF, 2006)**

A 3D geological model will be helpful in this case to identify and understand the geology of the Eastern Basin, and will indicate these aquifers and the various structures associated with them.

For the research done on this area, no complete 3D geological model of the current East Rand Basin as a whole could be found, which shows the current state of the geology after the historical and recent mining activity structures. Therefore, exact decisions can be made only with the help of surface and subsurface techniques or older geological maps. These techniques

are carried out on or above the land surface or involve lowering instruments into boreholes. The most common of these techniques is borehole logging. Boreholes are normally drilled to depths of tens to hundreds of meters. The data obtained by making use of these techniques can be illustrated by geologic cross-sections and isopach and structure contour mapping. These illustrations are normally 2D and obtaining the data can be expensive (Water Encyclopedia Science and Issues, 2013).

Figure 1.3 below indicates the difference between a basic 2D geological map and a 3D map, where the exact change in topography can be seen. Earth scientists operate in a world where the third dimension assumes a far greater importance than is required in everyday life. Therefore the ability to visualise the East Rand Basin as a three-dimensional object rather than a two-dimensional sketch will be very useful (McCarthy & Rubidge, 2005). When using all the current well/borehole data from the National Groundwater Archive Geodatabase (DWS, 2014) a 3D geological model can be created with the help of ArcGIS. This will help with the visualisation of the geology and the geological features of the Eastern Basin. ArcGIS 10.2 as GIS software will be used to manipulate the huge amount of data that was collected in the field over the years. A geodatabase will help to store, categorise and access the data in the GIS environment. The data will then be converted to a Digital Elevation Model (DEM) or Triangulated Irregular Network (TIN), which gives a 3D surface representation of the terrain. After creating the 3D model it could be viewed and analysed from any angle, unlike a 2D map.

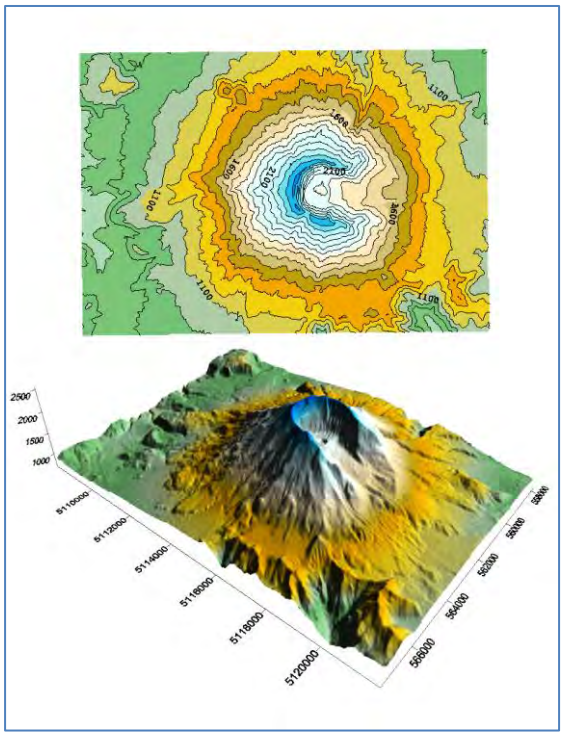


**Figure 1.3: Indicating the difference between 2D and 3D geological maps of the same area (Wikipedia, 2014a)**

The recent development of software for 3D reconstruction has opened a new frontier in the Earth Sciences, leading to n-dimension analyses of the spatial extension of any kind of geological structure and to 3D virtual models. Nowadays, ArcGIS as a GIS software also consists of a 3D GIS mapping function (Zanchi *et al*., 2007). Therefore, ArcGIS will be used in this area to help produce an exact 3D geological model of the Eastern Basin. Using a 3D geological model will lead to new perspectives and insights that would not be readily apparent from a planimetric map of the same data (ESRI, 2013). This model can be used for making cross-sections, fence diagrams and block diagrams that will help with research in this area. If the ArcGIS is not able to create this model, the restrictions will then be explained and recommendations will be made.

A 3D geological model, such as the models that will be created in this study, will help governments and water utilities create water supply plans and to assess the impacts of groundwater abstractions from the surrounding mines. The model will also be valuable to geologists as they will be able to identify the groundwater potential, and they will also have a more dynamic perspective of the extent of aquifers or the location of potential sinkholes. The model will also improve research, investigations and make scientific interpretations more precise (DeMeritt, 2012).

### 1.2 Problem statement

The above information leads to the following problem statement: With the latest GIS software of today, will it be possible to accurately map the Eastern Basin's geology without the using surface or subsurface techniques?

### 1.3 Research aims and objectives

- To map the spatial distribution of the geology in the East Rand Basin;
- To identify the geological structures of the area;
- To design a geodatabase for the management and storage of the geological data;
- To create a model of the East Rand Basin's geology; and
- To compare the cross-sections derived from the models with existing cross-sections of the area.

## 1.4 Study layout

Chapter 2 of this dissertation will focus on the review of the existing literature on the history, the mining activities and the underlying geology of the East Rand Basin. Chapter 3 will focus on the concept of GIS, the type of data that will be used and the three ArcGIS methods that will be used to create the 3D geological models. Chapter 4 of this dissertation will capture the results of the three models. These results will include reviews about the quality of the data and the effectiveness of the three ArcGIS methods. Finally, Chapter 5 will capture the conclusions drawn from the data quality, the ArcGIS methods and the interpretation of the results. Chapter 5 will also provide recommendations on further studies that will focus on 3D modelling with the help of ArcGIS.

# Chapter 2: Literature review

## 2.1 Introduction

In this chapter, a background of the East Rand will be given and the underlying geology of the East Rand Basin will be discussed. A description of the history of the various mining activities; the influences and implications of the mining activities; the geology; the geological structures; and the stratigraphic column of the Eastern Rand Basin will also be included.

## 2.2 Background of the East Rand and the East Rand Basin

The Afrikaans word “Witwatersrand” can be translated as “ridge of white waters”, where ridge refers to the Afrikaans word “rand”. This word has also been adopted as the South African currency, which indicates the economic significance of gold mining in the country. It was the discovery of gold by George Harrison in the Witwatersrand which led to the existence of the East Rand (Scott, 1995, DWA, 2013a and EMM, 2007).

The rainfall of the East Rand region is known to be typical to the Highveld summer rainfall, which occurs from October to April. The average annual rainfall varies from 715 mm to 735 mm. Frost does occur frequently from mid-April to September, which makes temperatures below freezing common during winter times. This area is home to mild summers with temperatures seldom above 30°C. During spring and winter, northerly and north-westerly winds occur and during summer north-easterly to north-north-easterly winds occur (EMM, 2007).

There is a large number of pans across the Ekurhuleni area. These pans cover a total area of 3 559 ha within the Ekurhuleni Metropolitan Municipality area and are mostly seasonal. There are also a few lakes created by mines, which are used for recreational parks. Germiston Lake, Benoni Lake and Boksburg Lake are the three main lakes used for recreational purposes within the Ekurhuleni Metropolitan Municipality area, but which fall outside the East Rand Basin area. A few dams, such as the Jan Smuts Dam, Alexander Dam, Nigel Dam and Cowles Dam, are found within the East Rand Basin area, along with various rivers and streams (see Figure 2.1 together with Annexure B – A land use map of the Ekurhuleni Metropolitan Municipality) (EMM, 2007 & Scott, 1995 ):

**Table 2.1: Spruit / River that occur in the East Rand Basin (EMM, 2007 & Scott, 1995)**

| Spruit/River | Description |
|---|---|
| **Blesbokspruit** | • One of the two main streams that flow through the area of the East Rand Basin.<br>• This catchment covers a total area of 1427 $km^2$<br>• Originates in the North of Benoni and Daveyton.<br>• Flows southwards through Springs and Nigel towards the Vaal River.<br>• Accepted by the RAMSAR Convention (see*below table).<br>• The eastern part contains extensive natural wetlands, whereas the western part is impacted on by agriculture, human settlements and mining activities.<br>• Forms part of the Vaal River Barrage catchment and flows into the Suikerbosrand River, where it joins the Klip River.<br>• Flows over alluvium covered dolomite.<br>• Contains the Cowles Dam, which is situated on dolomite.<br>• Most of the Blesbokspruit catchment (98.8%) occurs in the East Rand Basin. |
| **Rietspruit** | • One of the two main streams that flow through the East Rand Basin area.<br>• Covers an area of 820 $km^2$.<br>• Drains the western part of the East Rand Basin.<br>• Originates South-west of Benoni and ends up joining the Klip River.<br>• 29.4% of the Rietspruit catchment is present in the East Rand Basin.<br>• Due to the seepage of the surrounding active tailings dams, the streams forming the Rietspruit won't dry up. |
| **Kaalspruit** | • Originates in Kempton Park and flows in a northern direction to join the Hennops River in Centurion.<br>• Polluted by human settlements and agricultural activities. |

**Table 2.1: Continues**

| Spruit/River | Description |
|---|---|
| **Jukskei Spruit** | • A number of the Jukskei Spruit's tributaries drain a portion of the south-western areas of the service delivery areas (built-up areas) in the north. |
| **Rietvlei River** | • Originates in the smallholding areas of Kempton Park and flows in a northern direction towards the Rietvlei Dam.<br>• Primarily supplied by agricultural run-off.<br>• Kempton Park's sewage works are responsible for the pollution in this river however some of the pollution is filtered out by a number of wetlands that fall between the dam and the sewage works. |
| **Klip River** | • Originates in Katlehong.<br>• Joins the Vaal River below the Vaal Dam.<br>• Polluted by industries, agricultural activities and human settlements. |

* "The Convention on Wetlands, signed in Ramsar, Iran, in 1971, is an intergovernmental treaty which provides the framework for national action and international cooperation for the conservation and wise use of wetlands and their resources. There are presently 155 Contracting Parties to the Convention, with 1 674 wetland sites, totalling 150 million hectares, designated for inclusion in the Ramsar List of Wetlands of International Importance." The Blesbokspruit was accepted in 1995 and the number given to this spruit is 343 (WISA, 2015).

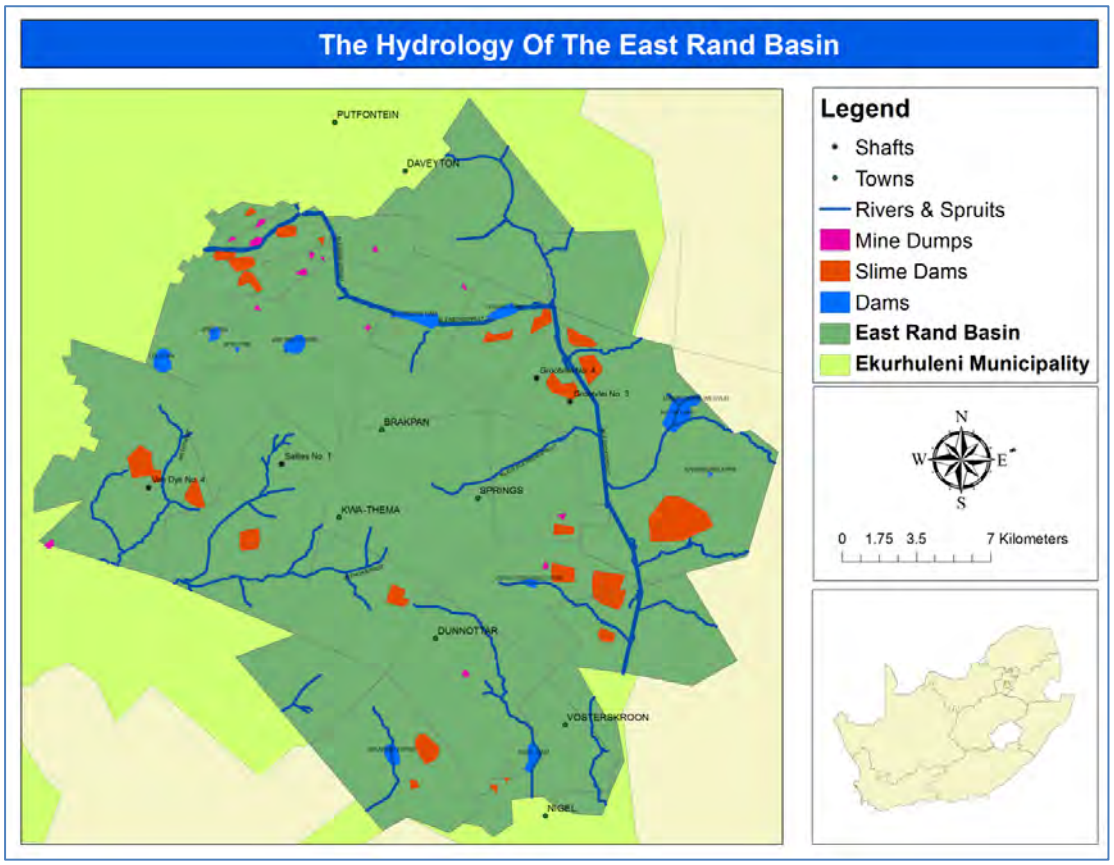


**Figure 2.1:** **Map indicating the hydrology and shafts of the East Rand Basin (Annexure C)**

A large percentage of South Africa's biodiversity is represented in the Ekurhuleni Metropolitan Municipality area. The EMM is mostly covered by grassland biomes, in which grass dominates and geophytes are abundant. Trees are found along the river courses and on koppies, but are usually absent. Agriculture activities such as dry land agriculture, intensive agriculture, irrigated agriculture and urban agriculture consume 31 435 ha of the EMM's total land area, compared to the 16 842 ha of the activities associated with mining. These activities include slime dams, quarries/borrow pits, mine dumps and disturbed land (EMM, 2007).

Before George Harrison discovered gold in the quartz pebble conglomerates on the farm Langlaagte on the Witwatersrand in March 1886, the land was occupied by a farming community. The proclamation of the Witwatersrand Goldfield was first gazetted in September 1886. The conglomerates had been traced along the entire outcrop length for a distance of 45 km and where the conglomerates were covered beneath younger rocks in the east and west, the initial activity was confined to the outcrop. These outcrops became known as the Central and West Rand Goldfield, which forms part of the Witwatersrand Goldfields. In 1887 West Rand Consolidated was the first mining company to operate in the West Rand Goldfield. The East

Rand Goldfield developed between 1888 and 1940 when diamond drilling led to the discovery of the eastern extension of the Central Rand. The Goldfields mentioned here can also be referred to as the Western, Central and East Rand Basin (DWA, 2013a and Durand, 2012). These various goldfields / basins are indicated in Figure 2.2 below.

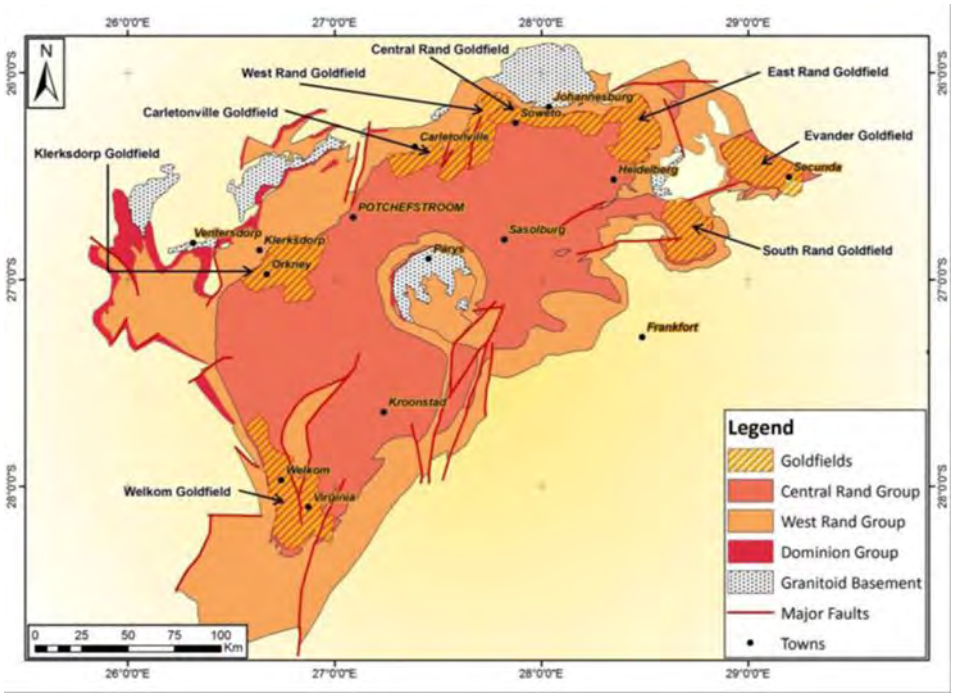


**Figure 2.2: Simplified geological map of the Witwatersrand Basin showing the location of the main goldfields (DWA, 2013a)**

The Witwatersrand also became the most densely populated region in the country. Various cities and towns originated in the Witwatersrand area over the years, of which Johannesburg was one of the largest metropolitan areas in Africa (Winde & Stoch, 2010). Just like the city of Johannesburg, several towns exist within the EMM, such as Germiston, Springs and Brakpan, and developed as the mining activities took place. Three main black townships are found within the study area that originated on the borders of these towns to provide basic housing for the mine workers. These towns include Kwa-Thema, Duduza and Tsakane (DWA, 2013a and Durand, 2012). The main towns / townships and cities of the EMM that fall within the study area are highlighted in Table 2.2 below (EMM, 2007; Encyclopaedia Britannica Online, 2014a and b; SAWEB, 2014; Nigel Business Directory, 2014):

**Table 2.2: The main towns / townships / city within the East Rand Basin.**

| Town / Township / City | Existance |
|---|---|
| Brakpan | Existed in 1886, but expanded when coal (in 1888) and gold (in 1905) was discovered. |
| Springs | Originated from a coal-mining camp in 1885 and was then sustained in 1908 when the mining of gold started and then Springs was incorporated in 1912. |
| Kwa-Thema (Springs) | Established in 1951 to house the African families who were removed from Payenville. |
| Tsakane | Founded in the 1960's when the native people from around Brakpan were relocated to a new designated area. |

The residents / mine workers that live within these settlements, mostly informal settlements, consisted not only of the ethnic groups of South Africa, but also people from the neighbouring countries of South Africa, such as Zimbabwe and Mozambique, and various other African countries such as Malawi (DWA, 2013a and Durand, 2012).

The extreme expansions of the settlements led to various sustainability problems, such as the supply of drinking water and basic sanitation, which the government had to deal with. Where there had still been limited access to resources, inhabitants of the townships were using polluted media such as water, soil and tailings, even though these were illegal or dangerous (DWA, 2013a and Durand, 2012).

## 2.3 Mining activity within the East Rand Basin

As mentioned above, mining in the East Rand Basin started a few years after the discovery of gold. The mining activities in the East Rand Basin reached an all-time high between the 1940s and 1950s. There were 24 mines and 90 shafts in 1955, but the fixed gold price and the high working costs led to the closure of many mines between the late 1950s and the 1960s. The open and closure rates of these mines are illustrated by Scott (1995) in Figure 2.3.

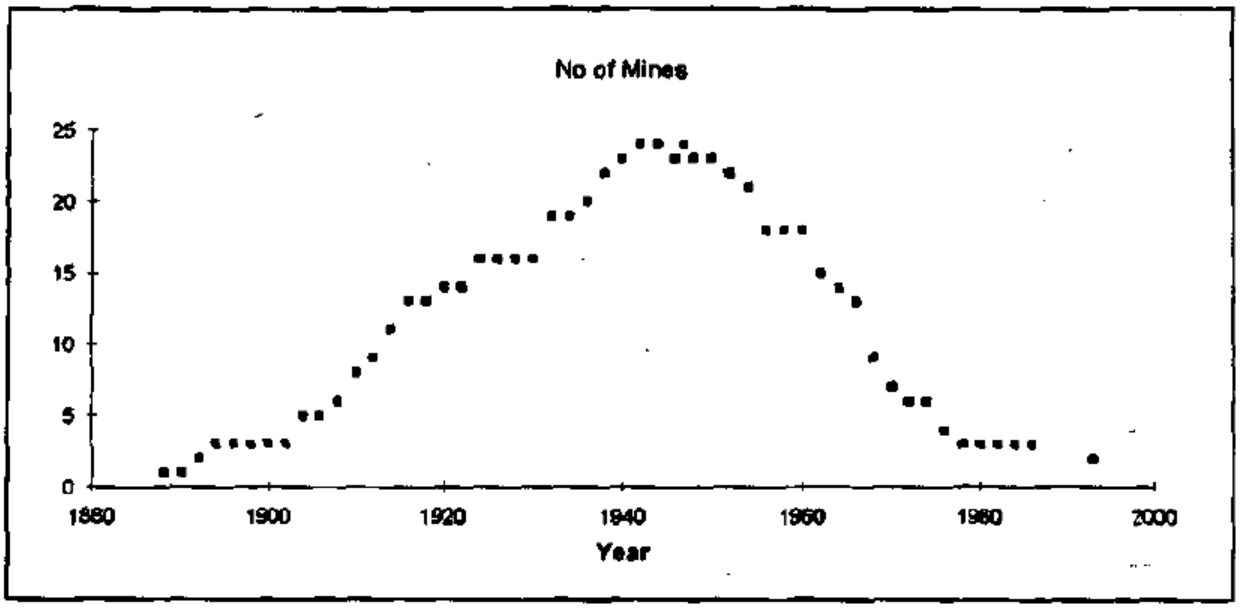


**Figure 2.3: Illustration of the number of mining companies operating on the east rand over the years (Scott, 1995)**

In 2013 active mining was still taking place in this basin, although most of the mines are inactive, closed or abandoned (DWA, 2013a). According to Scott (1995), three main reefs were mined over the years for their economical deposits. They are:

1. The Main Reef – extensively mined (Figure 2.4).
2. Kimberly Reef – incipiently mined (Figure 2.5).
3. Black Reef – sporadically mined.

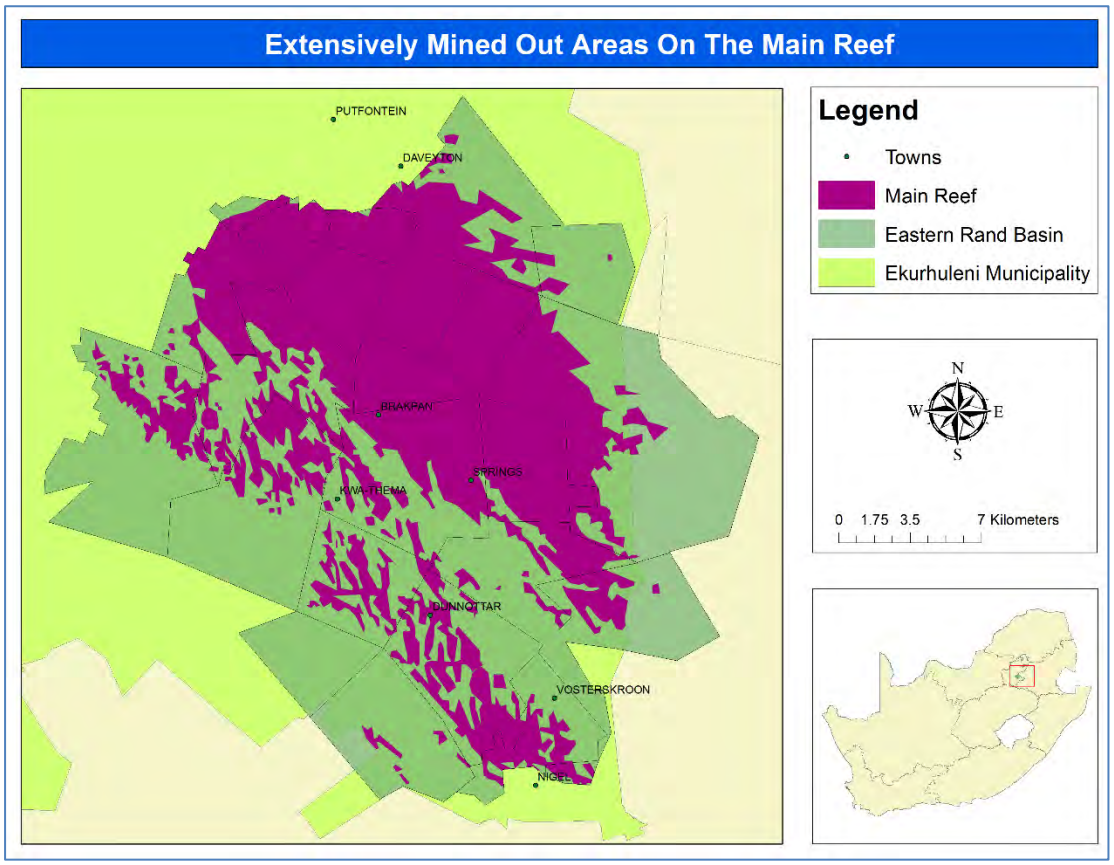


**Figure 2.4:** **The extensively mined-out areas on the Main Reef according to Scott (1995) (Annexure D)**

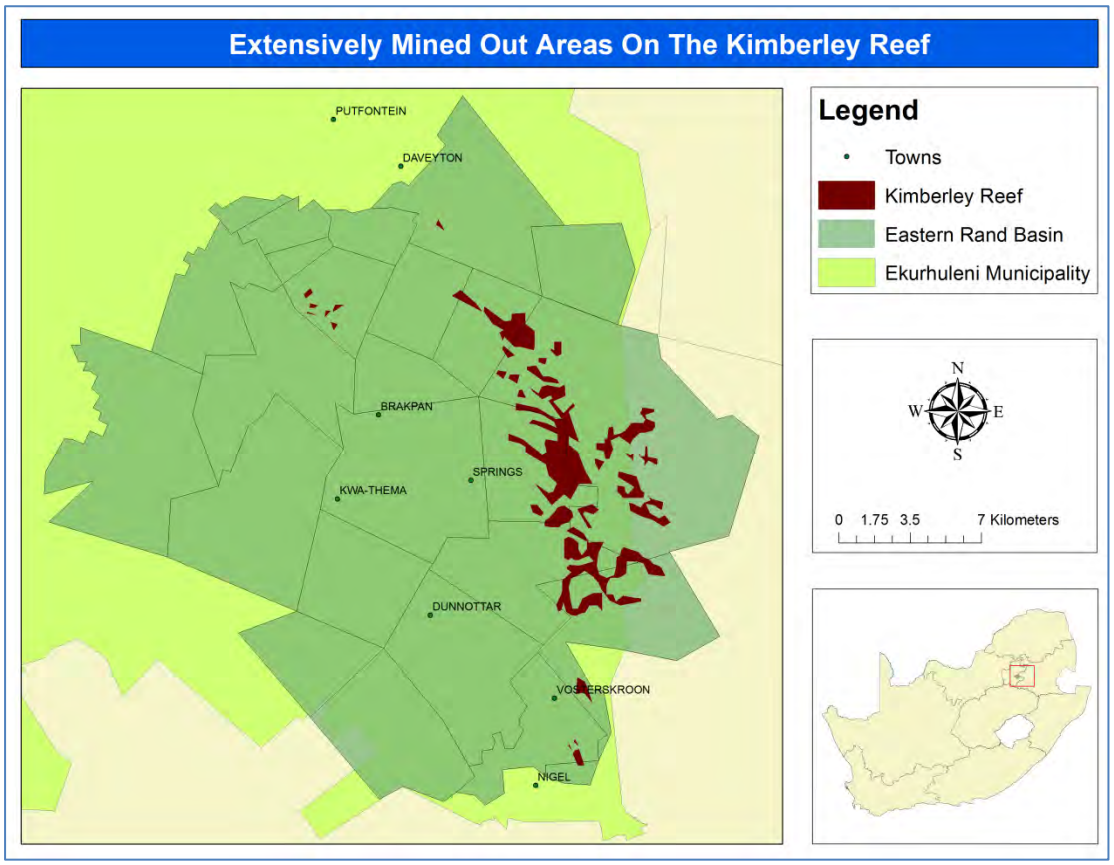


**Figure 2.5: The extensively mined-out areas on the Kimberley Reef according to Scott (1995) (Annexure E)**

Gold mining was not the only mining activity happening in the basin; coal mines started operating soon after, from the early 1890s, and ended in the late 1940s. The Main Reef was the main focus in the East Rand Basin when it came to gold mining. A depth of 2 300 m below surface at the Vlakfontein Gold Mine, which lies in the Vlakfontein lease area (Figure 2.6), was founded as the deepest mine workings on the Main Reef (DWA, 2013a). Various other mines, indicated in Figure 2.6, are located within the East Rand Basin. According to Scott (1995) the mines within the East Rand Basin are interconnected underground. This interconnection leads to the altering of the subsurface water flow conditions.

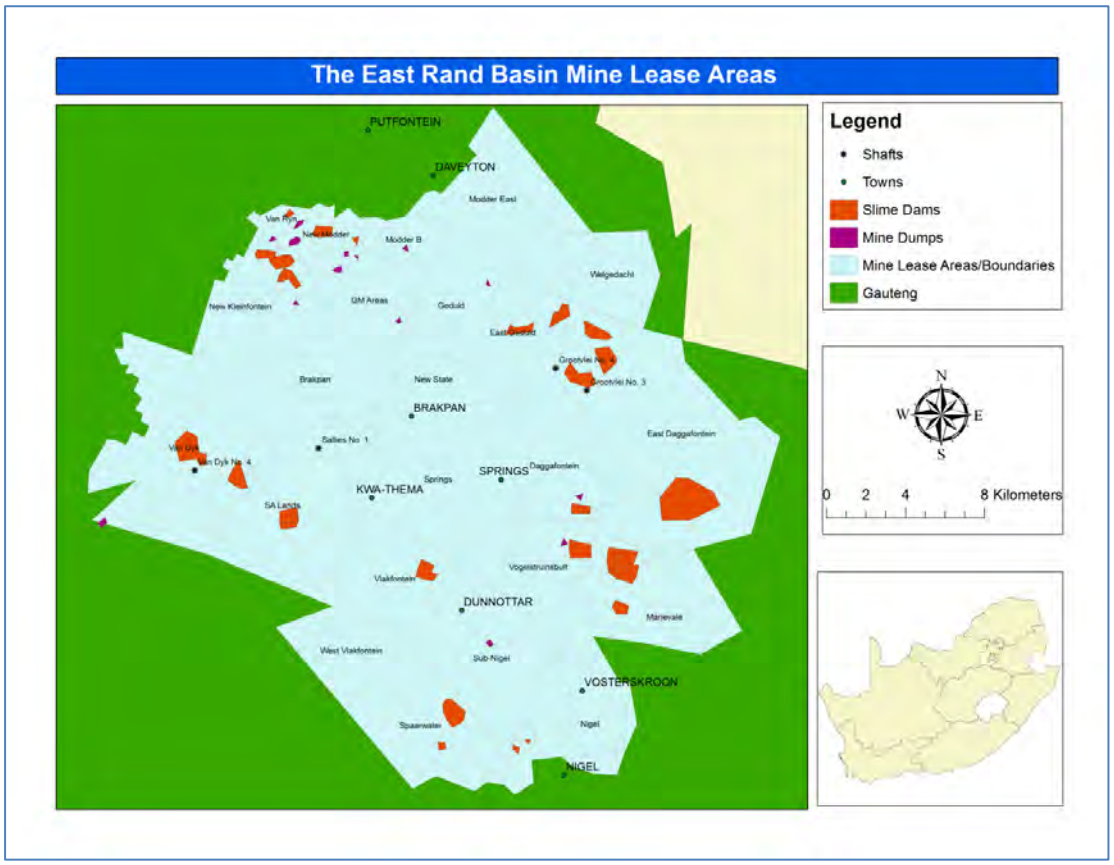


**Figure 2.6: Map of the East Rand Basin showing the mine lease areas (Annexure F)**

These mines are associated with various mining methods which are used to extract the coal and gold ore from the earth's crust. The two most common methods and their effect on the environment of the study area will be explained:

### 2.3.1 Shaft mining / Shaft sinking

Shaft mining / shaft sinking (see Figure 2.7) is used to vertically access the underground mining facilities. According to the ILO (2011), an underground mine is like a factory deep below the earth's surface. Here the miners work to recover the minerals of economic value by drilling, charging and blasting. A shaft is made up of various components such as the entrance, service cage, shaft station, skips and a head frame. The entrance of the shaft can be given two different names, depending on whether the entrance is above ground (shaft or portal) or underground (winzes). Winzes are known as the vertical underground entrances driven downwards from the surface / level to another level (Hamrin, 2009 and Wisegeek, 2014).

The service cage is normally the vertical central shaft of a shaft mine used for transporting the mine workers from the surface to the lower parts of the mine. This cage normally consists of multiple horizontal or close to horizontal underground openings that are also referred to as

branches. These branches are extended off the cage, like a tree. These branches are known as levels or drifts. The shaft station will then be the positioned where the levels or drifts are connected to the service cage (Hamrin, 2009 and Wisegeek, 2014).

Skips are the names given for the small shaft conveyors that fall outside the service cage. Unlike a service cage, skips are smaller and are used for hoisting the mined ore or waste from the subsurface to the surface. Skips can also be used as a ventilation system, or to transport water and fuel via pipelines (Matsui, 2014; Wisegeek, 2014; De La Vergne, 2008).

On the surface a head frame, which consists of a hoist motor, is found. This frame is used to winch the lifts within the shaft up or down. This frame is usually constructed of steel and concrete (Wisegeek, 2014 De La Vergne, 2008).

The impact of gold mining on the environment and the geology, using shafts, will be discussed in 2.3.3.

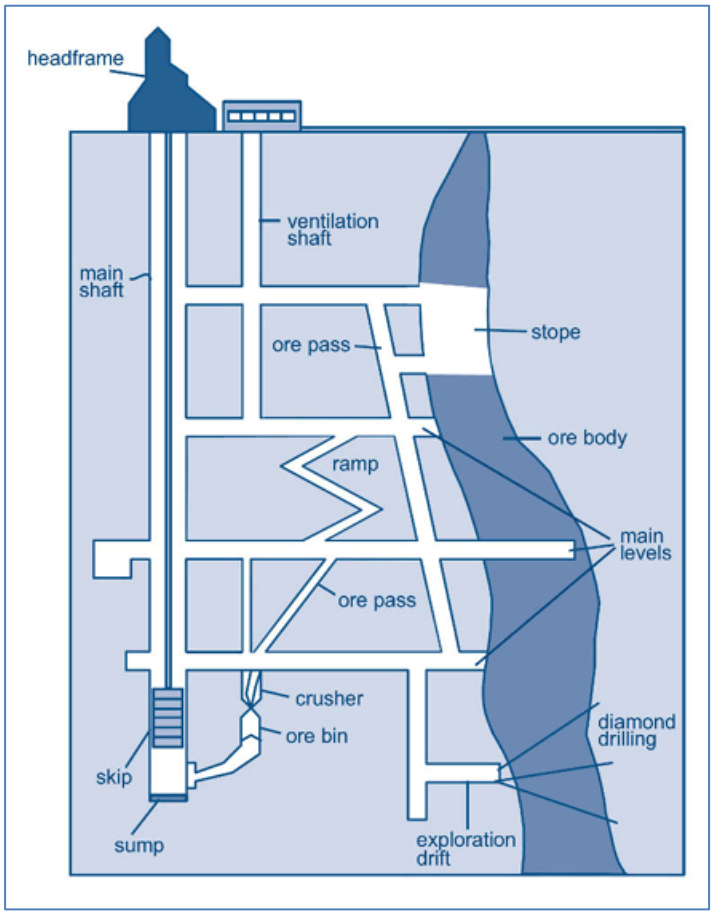


**Figure 2.7: Cross-section of an underground mine (Environment Canada, 2009)**

### 2.3.2 Opencast mining / Open-pit mining

Opencast mining / open-pit mining (see to Figure 2.8), which is normally associated with coal mines, is a process where rock and minerals are excavated in long strips of up to a few meters thick, out from beneath the earth's surface or overburden, and then eliminated from the pit or borrow. This method is used only when the rocks or minerals, better known as ore, are found relatively close to the earth's surface; that is, where the overburden layer is thin or the material of interest is structurally inappropriate for the tunnelling method (GreatMining, 2014; Satyanarayana, 2012; Schissler, 2006). The Mine-Engineer (2012) seconds this by defining opencast mining / open-pit mining as the mining type where a cut or excavation is made on the surface of the ground to extract the ore left open for the total operational phase.

When it comes to the walls of the pit, the angles used to dig these walls are less than vertical to minimize the damage and hazards caused by rock falls. These walls are normally stepped features, like stairs, of which the incline part is called the batter and the flat part of the step the bench. A bench can also be defined as the ledge that forms a single level of operation, above which the minerals or waste are mined back to. These benches are mined simultaneously at different elevations and parts throughout the pit. A haul road is situated at the side of each pit, forming a ramp that trucks could use to export the ore or waste rock. Waste rock is rock that is too low in grade to be mined economically (GreatMining, 2014; Mine-Engineer, 2012; Hamrin, 2009).

There are two types of piles outside the pit, namely the overburden / waste rock dump, and secondly the discard dump or settling pond. The overburden / waste rock dump is the identified site where all the overburden / waste is transported to and left to pile up, while the tailings dam or settling pond is where all the discharged slurry – made up of all the unrecoverable and uneconomic metals, minerals, chemicals, organics and process water – is pumped to (GreatMining, 2014, SPC, 2014 and Engels, 2014).

Due to the availability of coal in the East Rand Basin, the mining activity associated with this type of mining has led to extensive mining within the East Rand Basin. This mining took place on top of the Witwatersrand rocks (Brakpan) and on top of the dolomites (Springs) within the East Rand Basin (GreatMining, 2014).

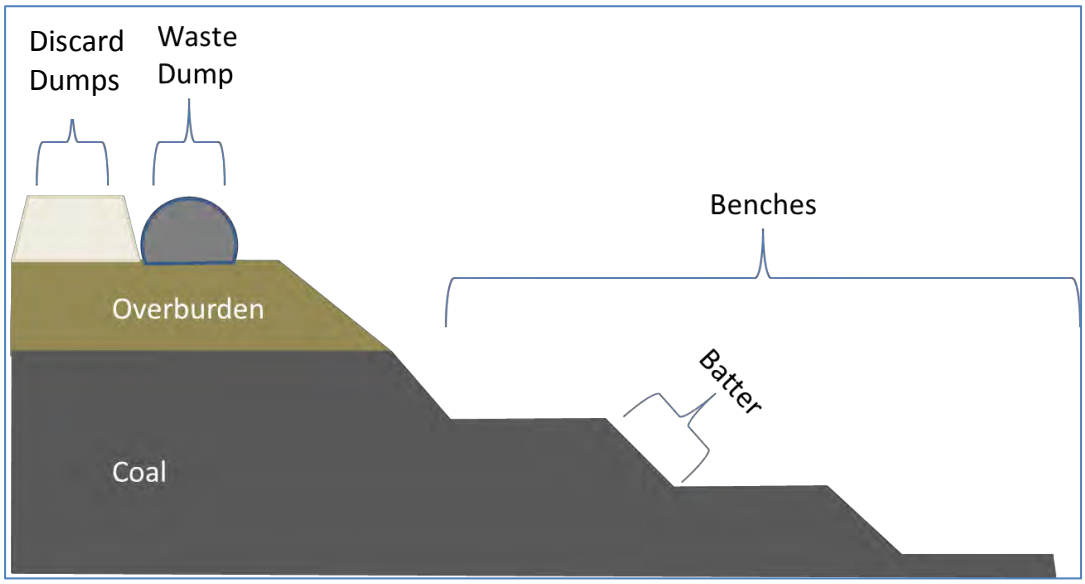


**Figure 2.8:** **Opencast mining adopted from GreatMining (2014), SPC (2014), Engels (2014) Mine-Engineer (2012), Hamrin (2009), Satyanarayana (2012) and Schissler (2006)**

### 2.3.3 The impact of the mining methods on the East Rand Basin

The workings of these coal mines were relatively shallow, some of which were up to 50 m below surface. In the early 1900s these shallow mines resulted in subsidence due to insufficient support and to pillar robbing of the Great Eastern Collieries and the Largo Collieries (GreatMining, 2014).

Broad depressions were the result of these collapsing collieries, which can fill with water and appear as small pans when looked at from the surface. In other areas vertical sided / inverted cone-shaped collapses occurred. Several of these features contain permanent water, which is at the same depth as the rest water level in the nearby boreholes. The rest water level, also known as the static water level, can be defined as the groundwater level of a borehole which is not influenced by abstraction or recharge (Scott, 1995 & Groundwater Dictionary by DWAF, 2014).

When mining the above reefs for gold, the hard rock that has lain unexposed for years is exposed. After the mining of this hard rock, cavities remain, which could then be filled by means of water ingress or could subside. The sinkholes related to gold mining are formed in the dolomites due to cavities (see 2.3.3.3). When crushed, the hard rocks expose radioactive elements, asbestos-like minerals, and metallic dust to the air and water. During separation, residual rock slurries, which are mixtures of pulverized rock and liquid, are produced as tailings,

toxic (pyrite). Radioactive elements from this liquid can leak into the bedrock or water resources if not properly contained (GreatMining 2014).

As the water takes on these harmful concentrations of minerals (pyrite) and heavy metals, it becomes a contaminant. This contaminated water can pollute the environment surrounding the mine and beyond. One of the main processes associated with this type of contaminated water is known as Acid Mine Drainage (see 2.3.3.1). This contaminated water also fills these cavities, which create aquifers. These aquifers then need to be dewatered (see 2.3.3.2) to avoid the contaminated water from reacting with the surrounding rock. Most underground mining operations increase sedimentation in nearby rivers through their use of hydraulic pumps and suction dredges. The sediment then poses a threat to the biomes in the river system and to the animals which feed on the river banks, as the sedimentation that accumulates along the river banks may contain harmful metals and minerals. Deforestation due to mining leads to the disintegration of biomes and contributes to the effects of erosion (MIT, 2014). When it comes to the East Rand Basin, three main problems occur:

#### 2.3.3.1 Acid Mine Drainage (AMD)

As mentioned above, mining produces various rock piles, sand and slime dumps or tailings dams. These features are then left behind by the abandoned mines. These features collectively contain one mineral or product, pyrite ($FeS_2$), which is known to be the main mineral of AMD. AMD is one of the most understood processes in the world of today. It arises primarily when the pyrite mineral reacts with oxygenated water and air. This reaction is then followed by two processes: the first process is the production of sulphuric acid ($H_2SO_4$) and ferrous sulphate ($FeSO_4$), and the second process is the production of orange-red ferric hydroxide ($Fe(OH)_3$) and more sulphuric acid. The source of pyrite is found mostly in South Africa's gold deposits within the Witwatersrand Basin; but also within the coal deposits, many of which are not located close to the Witwatersrand Basin (Van Wyk *et al.*, 2013 and Scott, 1995).

After the extraction of gold the conglomerates, which contain about 3% pyrite, are deposited on tailings dumps. These gold tailings dumps have become a distinct feature of the landscape around the gold mines and have been discharging polluted water, such as AMD, into the surrounding areas for decades. This type of pollution is known as diffuse pollution and is visible in the case of the Blesbokspruit in Springs, due to the tailings dumps abounded in the upper catchments (McCarthy, 2011). These dumps can be seen in Figure 2.1.

Another form of pollution is caused when the pyrite is oxidised by rain water. This forms the sulphuric acid (acidic mine void water) mentioned above (Van Wyk *et al*., 2013 and McCarthy, 2011). This acid then percolates through the tailings dump, dissolving the heavy metals

(uranium) in transit, and emerges at the base of the tailings dump to join the local groundwater as a pollution plume (McCarthy, 2011).

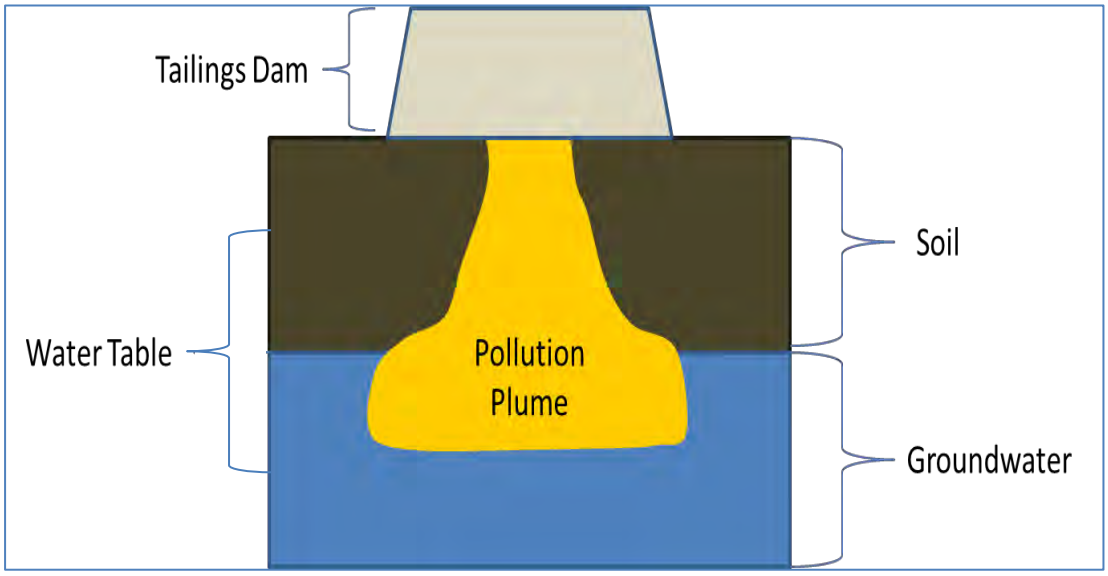


**Figure 2.9: Illustration of a pollution plume adopted from McCarthy (2011).**

The polluted water then emerges on the surface in the rivers and streams draining the areas around the tailings dumps; therefore, the streams, such as the Blesbokspruit, around the dumps are known to be acidic and have high sulphate and heavy metal concentration (McCarthy, 2011).

#### 2.3.3.2 Dewatering and rewatering

As mentioned under Section 1.1, during the peak of mining activity in the 1950s to 1960s, pumping historically took place at numerous locations within the East Rand Basin, due to the rising water levels within the mine voids. In the late 1970s, dewatering took place from Sallies No. 1 shaft and Grootvlei shafts No. 3 and No. 4 (Figure 2.1) only, but Sallies soon stopped in 1991 and Grootvlei in January 2011 (DWA, 2013a and DWA, 2013b). Since the closing of these mines, the underground voids have been left to fill with water (DWA, 2013a). This filling action is known as rewatering. Rewatering of the mine voids is caused by a combination of excessive surface water ingress generated by surface run-off and to a smaller amount recharge from an overlying fractured and weathered aquifer system (Van Wyk *et al.*, 2013). As the ingress took place over the years, each individual mine was responsible for their own dewatering as they were physically separated from one another by the boundary pillars that were left between them. As time passed these boundary pillars where mined for various safety reasons and to extract the remaining gold. This resulted in an unhindered flow of water between the mines (Van Wyk and Munnik, 1998).

Recharge of the dolomitic aquifers on the East Rand by mine water will be a problem if there is a significant water movement through the dolomite, since the dolomite will be dissolved (Scott, 1995). According to Scott (1995) the recharge from the rainfall directly on the exposed dolomite is enough to sustain a natural groundwater aquifer. Recharge of the dolomitic aquifers also occurs through the continuous seepage from the surrounding tailings dumps.

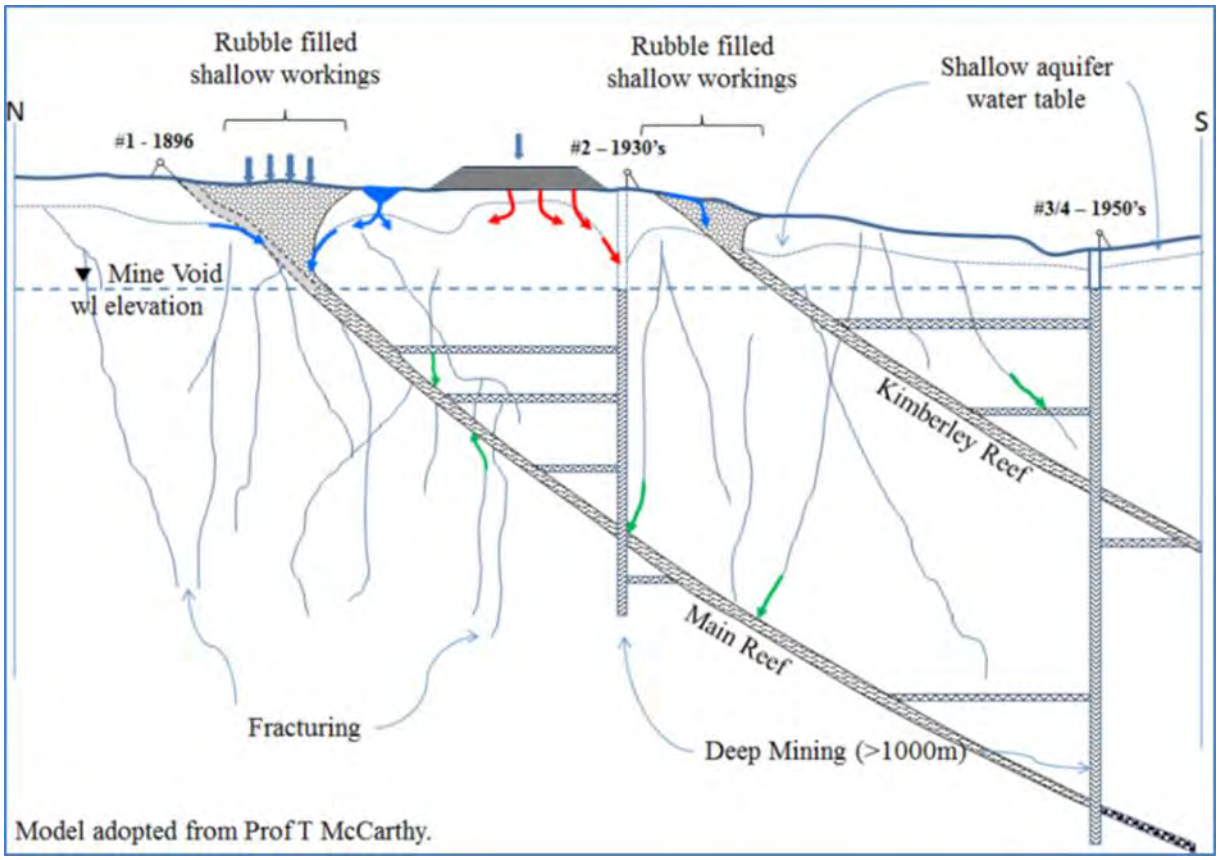


**Figure 2.10: Example of different stages of mining and shaft development and hypothetical subsurface flow regimes. Arrows indicate groundwater flow directions from surface (ingress and deep fissure flow (Van Wyk *et al.*, 2013)**

As mentioned, the water in the voids will then interact with the sulphide within the rock formations to form acid mine drainage (see 2.4.1), also known as acid rock drainage. According to DWA (2013a) the water level within the mine voids of the East Rand Basin is rising steadily and will continue to rise until the water is pumped from the voids. If the voids are not pumped, the water will start to decant into the surrounding dolomitic aquifers and will then start to decant at the earth's surface. A prediction has been made that the critical levels of the voids within the East Rand Basin will be reached and will start decanting late in 2016. This decanting is likely to occur at several points, especially within the Nigel area, as well as at unidentified locations

across the basin, due to variation in water levels (DWA, 2013a and Council for Geoscience, 2010).

Dewatering may seem as a positive action, but with dewatering comes discharging of the mine void water into surrounded wetlands and rivers. Discharging leads to other problems, including changing the water quality and quantity of that wetland and stream, especially when discharging into the Blesbokspruit, since it is already severely deteriorated with a present ecological state of the river as unacceptable (DWA, 2013a). Originally the Blesbokspruit responded to seasonal fluctuations in the water table only, since it was an ephemeral stream. Today it is known as a perennial drainage due to the discharging of effluent water from municipal sewage works (DWA, 2013b). Discharging also leads to the accumulation of heavy metal in the soils that make up the river banks, which could lead to fatalities of livestock.

#### 2.3.3.3 Sinkholes

According to the Council for Geoscience (2012) some parts of South Africa's ground surface are prone to sudden, catastrophic collapse which may cause death, injury or structural damage. The associated features are known as sinkholes (Figure 2.11) and usually occur in the areas where the underlying geology is dolomite. Approximately 25% of Gauteng is underlain by dolomite, which poses a risk to the safety of many people and the structures where they work and live. The carbonated rock formation within Gauteng, in which the East Rand Basin is situated, consists of the Malmani Subgroup of the Chuniespoort Group (see 2.4).

Sinkholes are known to form where acidic water moves through underground cracks, such as surface water ingress. The water then reacts and then slowly dissolves the surrounding carbonated rocks, such as dolomite ($CaMg(CO_3)_2$). As the dolomite dissolves, a void is left behind; this void then collapses when the weight from the above geological or soil layers could not be supported (Council for Geoscience, 2012 and Berlin, 2013).

Dewatering (see 2.3.3.2) also contributes to the forming of sinkholes. When a dolomitic aquifer is being dewatered, the groundwater level / rest level drops. This causes the soil that was "resting" above it to collapse inwards.

According to SAPA (2012), families that were living in Tsakane Extension 10 in The East Rand had to be relocated to the stands in Langville, because sinkholes were developing within the Tsakane land area.

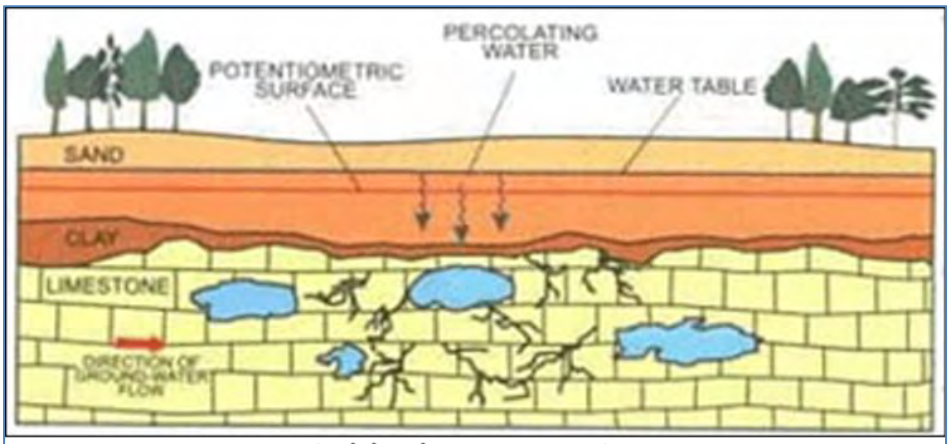


Sinkhole Formation

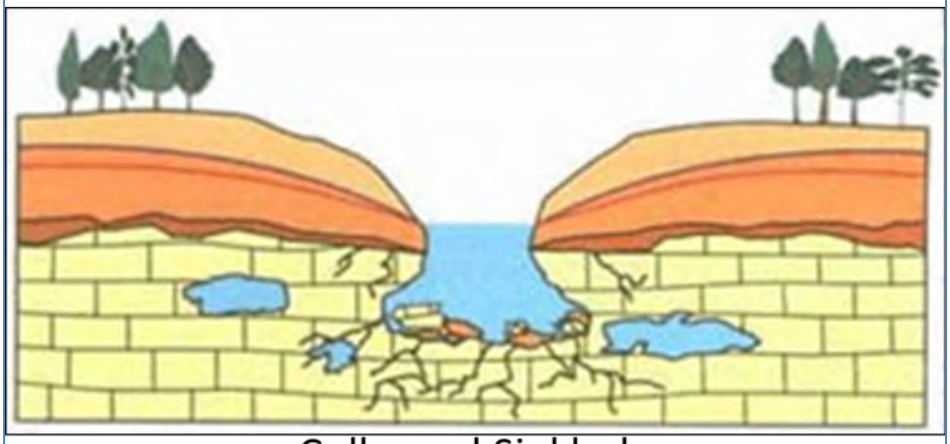

Collapsed Sinkhole

**Figure 2.11: How sinkholes form (BLG, 2014)**

## 2.4 Geology of the East Rand Basin

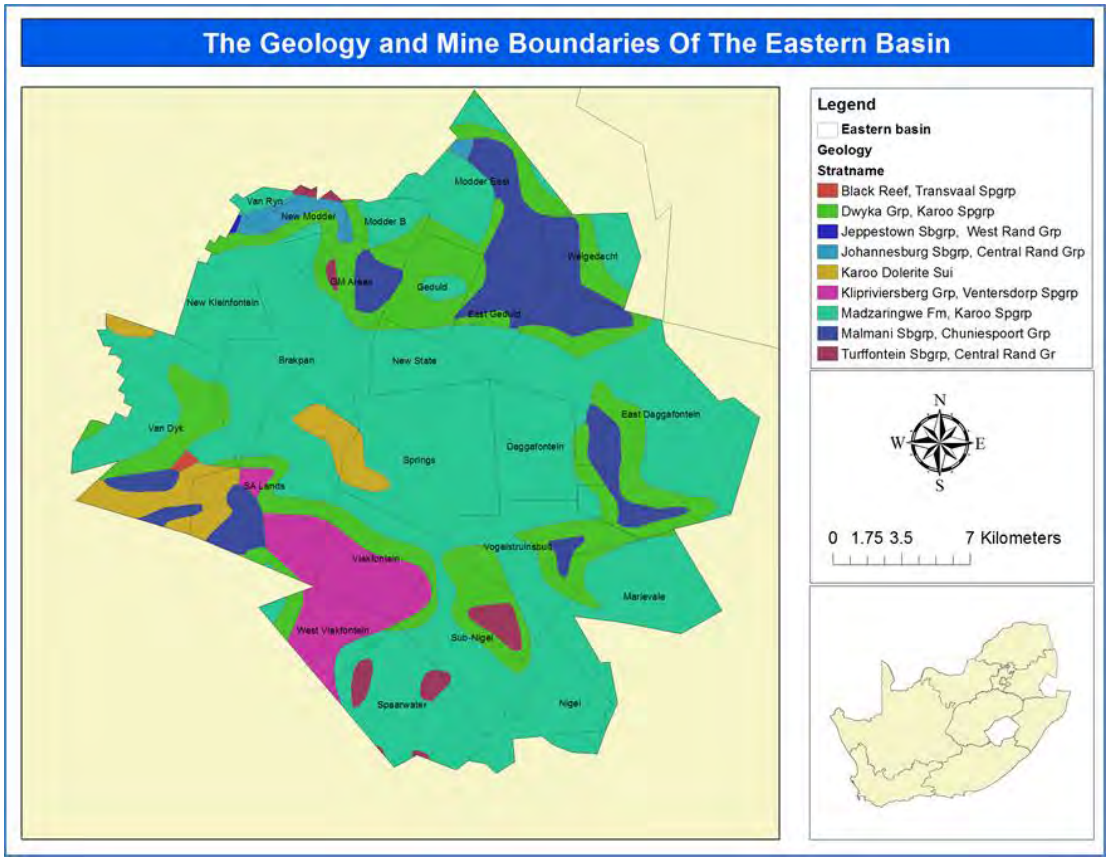


**Figure 2.12: Geological map on the mine boundaries of the East Rand Basin (Annexure G)(Spgrp: Supergroup, Grp: Group, Sbgrp: Subgroup and Fm: Formation)**

The East Rand Goldfields are known to be the best developed goldfields and the most extensively mined fluvial fan within the Witwatersrand Basin (Beater, 1982). The East Rand Goldfields are also known as the East Rand Basin in hydrological terms and is one of the sub-basins of the Witwatersrand Basin (DWA, 2013a). The Witwatersrand Basin is oval in shape and has a major axis of about 350 km extending in a north-easterly direction, and a minor axis of about 200 km extending in a north-westerly direction (DWA, 2013a). The East Rand Basin, which is known to be a relatively shallow sub-basin, is an oval-shaped basin of about 30 km long and 20 km wide, in which dips of strata are relatively shallow, and it has a mine lease area of about 768 $km^2$ (BKS, 2011 & Scott,1995).

The Springs Monocline, a zone of steepened dip, connects the East Rand Basin with the Witwatersrand Basin in the west. The East Rand Basin's geology differs substantially from the Western and Central Rand Basins. Sediments which make up the basin have been gently folded and lies unconformably on the pre-Witwatersrand basement rocks; therefore, an

asymmetrical south-west, plunging syncline is formed by the rocks of the Witwatersrand Supergroup. The northern limb dips about 45° and the southern limb about 25° (Scott, 1995).

The geology of this region is primarily known to be sedimentary strata that are associated with the Witwatersrand Supergroup and the younger sediments of the Transvaal Supergroup strata (Hobbs & Cobbing, 2007 and Beater, 1982). The Witwatersrand Supergroup is thicker in the western parts in the Van Dyk and Brakpan mining areas, and thinner in the eastern parts of the East Rand Basin (Beater, 1982).

According to McCarthy (2006) the base of the Central Rand Group, which is the younger group of the Witwatersrand Supergroup, is defined by the 1-1.5 m thick South Reef (Main Reef). Mosoane (2003) states that the conglomerates of the Johannesburg Subgroup, which is a subgroup of the Central Rand Group, are thoroughly developed to the west and are characterised by the partings, which are about 1 m between the Main Reef and Main Reef Leader, and 30 m between the Main Reef Leader and the South Reef. The conglomerates of the lower most Main Reef are poorly sorted due to the pebbles being up to 5 cm in diameter. The pebbles of the Main Reef are found to be coarser than those of the Main Reef Leader, with pebbles up to 8 mm in diameter. The Main Reef is dark in colour due to the chlorite found in the footwall. The South Reef is less well-sorted than the Main Reef and the Main Reef Leader, occurring as individual pebble bands with arenaceous partings. Although the South Reef is of lower grade, it is still the most persistent of the conglomerate layers (Mosoane, 2003). These Reefs are illustrated in Figure 2.13 through a cross-section of the East Rand Proprietary Mines (ERPM), by Mosoane (2003):

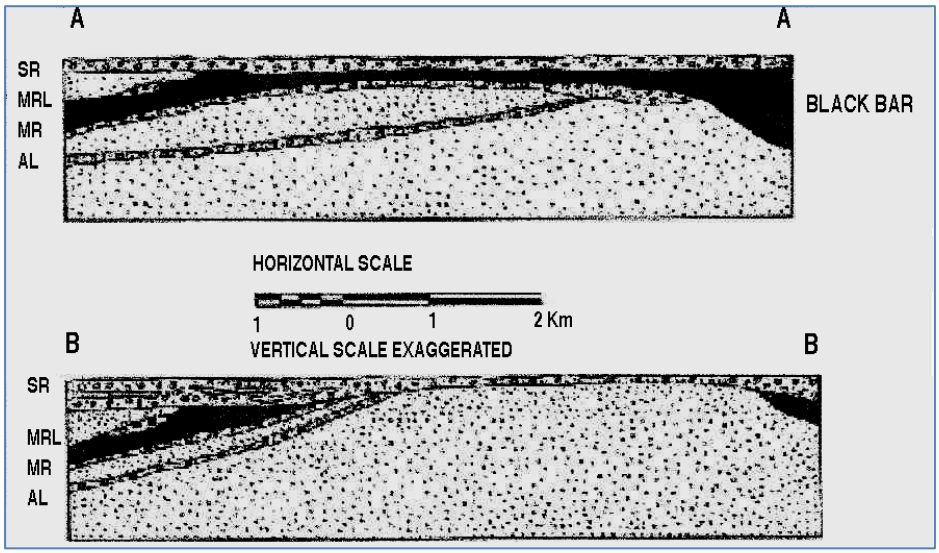


**Figure 2.13: A cross-section of the South Reef (SR), Main Reef Leader (MRL) and Main Reef (MR) within the East Rand Proprietary Mines (ERPM), Adjacent Layers(AL) (Mosoane, 2003)**

Beneath the above-mentioned reef a disconformity truncates (cuts) the Main and Blyvooruitzicht Formations across the Springs monocline, and has eroded until the Jeppestown Subgroup. This subgroup is the youngest subgroup of the West Rand Group, is part of the Witwatersrand Supergroup, and has a thickness of between 350-500 m within the East Rand Basin (Scott, 1995; SACS, 2006; Beater, 1982). According to Truswell (1977) the Jeppestown Formation is made up of shales that are reddish in colour and alternate with sandstones that are red, yellow or dark in colour. On the western part of the basin the Witwatersrand sediments are covered by the Ventersdorp Supergroup (Scott, 1995). The Ventersdorp Supergroup consists of amygdaloidal and porphyritic lavas, which are up to 450-500 m thick but have been eroded over the north-eastern part of the basin by pre-Transvaal erosion (De Bever, 1997 and Beater, 1982). The Black Reef Formation and dolomite of the Transvaal Supergroup then overlie the Ventersdorp Supergroup (Scott, 1995).

According to Scott (1995) the closure of the syncline occurs in the central and eastern parts. It is here where the Ventersdorp Supergroup and Witwatersrand Supergroup are covered by the Karoo Supergroup. These highly weathered lower Karoo sediments of up to 80 m thick also cover more than 90% of the rest of the East Rand Basin. These Karoo sediments consist of shale, sandstones and coal beds of the Ecca Group with the Dwyka formation at its base. Peneplanation took place before the area was covered by the Karoo Supergroup (De Bever, 1997).

Over the south-westerly parts of the basin the Black Reef quartzite has been deposited on the Ventersdorp lavas. The quartzite of this reef is known to be mature quartic sandstone, which is known to represent a phase of beach-type deposits (Truswell, 1977). The Black Reef quartzite has a total thickness of 10-30 m across the basin. This deposition was progressively followed by upper and lower Witwatersrand Rocks, northwards and eastwards. A slight and often indistinct angular unconformity appears at the base of the Black Reef quartzite formation between the Witwatersrand and Ventersdorp Supergroups (De Bever, 1997).

The Black Reef quartzite and the Malmani dolomite of the Transvaal Supergroup together cover about two-thirds of the East Rand Basin and reach a maximum depth of 400 m on the Daggafontein / Grootvlei boundary (De Bever, 1997). The Malmani dolomite is known to be rich in chert and light of colour in the lower and upper dolomite zones. These zones, according to Erikson *et al.,* (2006), are also known as the five formations (Figure 2.14) which subdivide the Malmani Subgroup. These formations together have an overall thickness of +/-370 m (Scott, 1995). At the basal transitional zone, the Oak Tree Formation, the dolomite is known to be dark in colour due to the absence or little chert and the high quantities of clastic sediment. This clastic sediment is known to consist of quartzite and carbonaceous mudstone. Algal

stromatolites are also found in abundance within the dolomite, which specify that the Malmani dolomite accumulated in shallow water environments (Truswell, 1977 & Ngcobo, 2006). Due to weathering, the Malmani dolomite is also visible in the flood plain of the Blesbokspruit (Scott, 1995). Four subsidiary basins are formed by the Government areas, New State areas, Daggafontein and Marievale mines on its uneven floor, from north to south along the syncline. These basins are separated by anticlinal warps (De Bever, 1997).

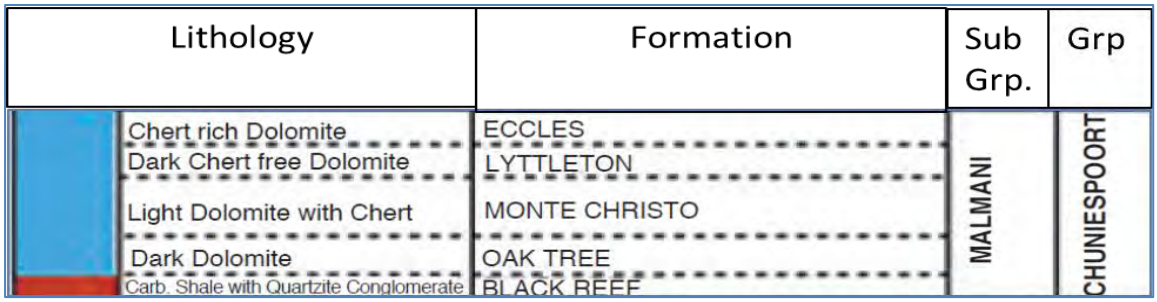


**Figure 2.14: The different Malmani formations (Ngcobo, 2006)**

When it comes to structure, the East Rand Basin is marked by prominent folds and major faults (Figure 2.15). These include the Vogel's Jeffrey's fault, which is the most important since it is sinistral and displaces 1 200 m. The other is the Grootvlei tear fault. The Vogel's Jeffrey's fault is known to be a conjugate fault set. A conjugate fault set can be defined as the cross-cutting set of fault planes with an ideal intersection angle of 60º and 120º, with both having right- and left-handed shear senses (Allaby and Allaby., 1999). The Vogel's Jeffrey's tear fault can be observed on the Springs and Vogelstruisbult mines, whereas the Grootvlei tear faults can be observed on the Geduld, East Daggafontein and the New State mines. These faults strike east to west, while another fault set strikes north-west to south-east (Scott, 1995 and Pitts, 1990). According to De Bever (1997) only small scale faulting is present in the Black Reef. A series of west-east trending pre-Transvaal wrench-faulting caused by a late compressional event is present in the area. The East Rand Basin is separated from the Mapleton Basin by a northwest trending anticline called the Marievale-van Dyk.

According to Scott (1995) there are also two distinct dolomite aquifers present in the basin:

- The one occurs in the northern part of the area. It has a thickness of up to 200 m and overlies the Witwatersrand Supergroup. A set of sills called the Green Sill is found within this dolomite below 60 m. Perched water tables, characterised by relatively shallow water levels, were developed by these sills. Major fissures can be found within this dolomite leading into the mine workings. These fissures are more significant in the Black Reef since a high amount of the off-reef development is within the dolomite.

- The other aquifer is found in the south-western portion of the basin. The aquifer overlies the Ventersdorp Supergroup and forms a hydraulic barrier between it and the Witwatersrand Supergroup. These Witwatersrand sediments are known as the Boksburg Gap, since it is a barren part of the basin. This dolomite is home to caves in some places, with possible sinkhole development adjacent to the Alberton / Heidelberg road. Mine dewatering did not lead to the existence of these sinkholes, but they developed due to poor run-off control and water accumulation in burrow pits adjacent to the paved road; therefore, most of the attention over the years has been focused on the northern aquifer.

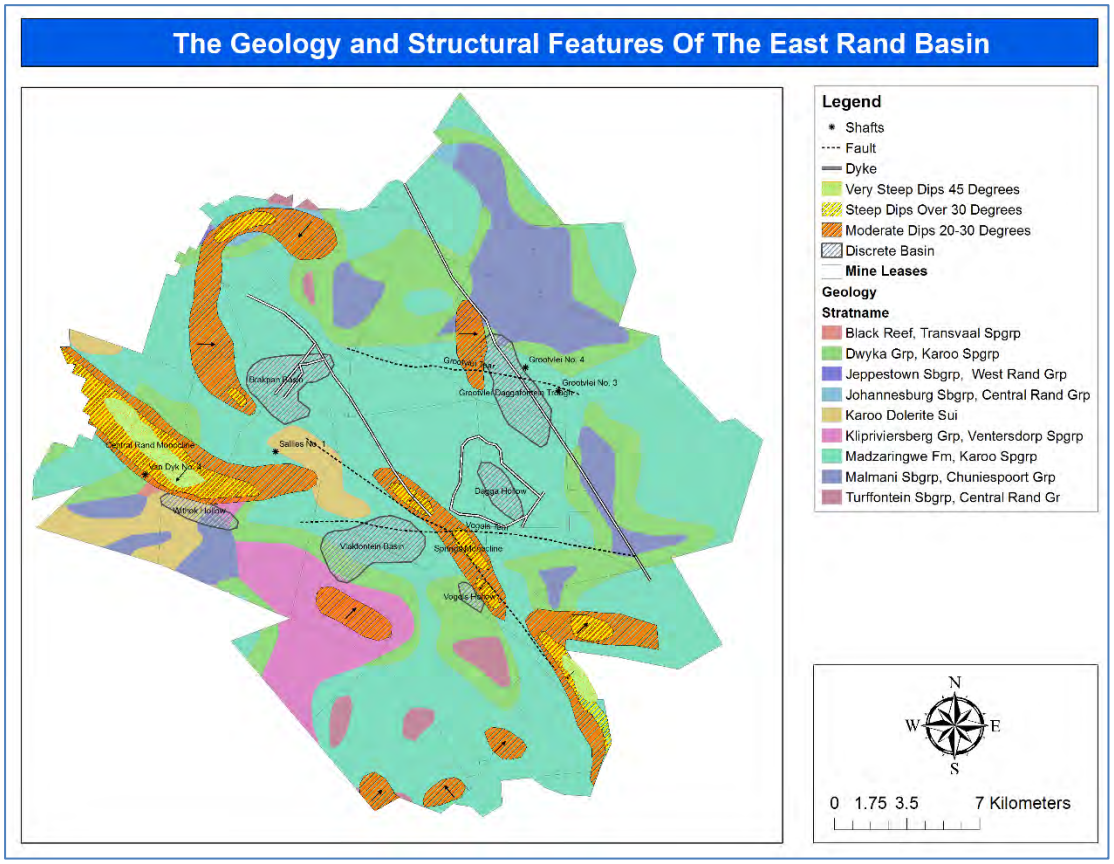


**Figure 2.15: Map indicating the main structural features and basins of the East Rand Basin adopted from De Bever (1997) (Annexure H)**

Now that the geology has been described, various available stratigraphic columns, together with the above-mentioned geological information, will be used to create a new lithostratigraphic column to indicate the average thickness of the various layers (see 2.5).

## 2.5 The East Rand Basin's lithostratigraphic column

The purpose of this new lithostratigraphic column is to serve as an updated / modern version, capturing various people's opinions on which depth each geological layer in the East Rand Basin is found and how thick each of these layers is.

The stratigraphic columns that will be used to compile a new stratigraphic column are as follows (Figure 2.16):

- Stratigraphic column used by Scott (1995).
- Stratigraphic column of Antrobus and Whiteside used in Beater (1982).
- Stratigraphic column used by SACS Task Group (2006).

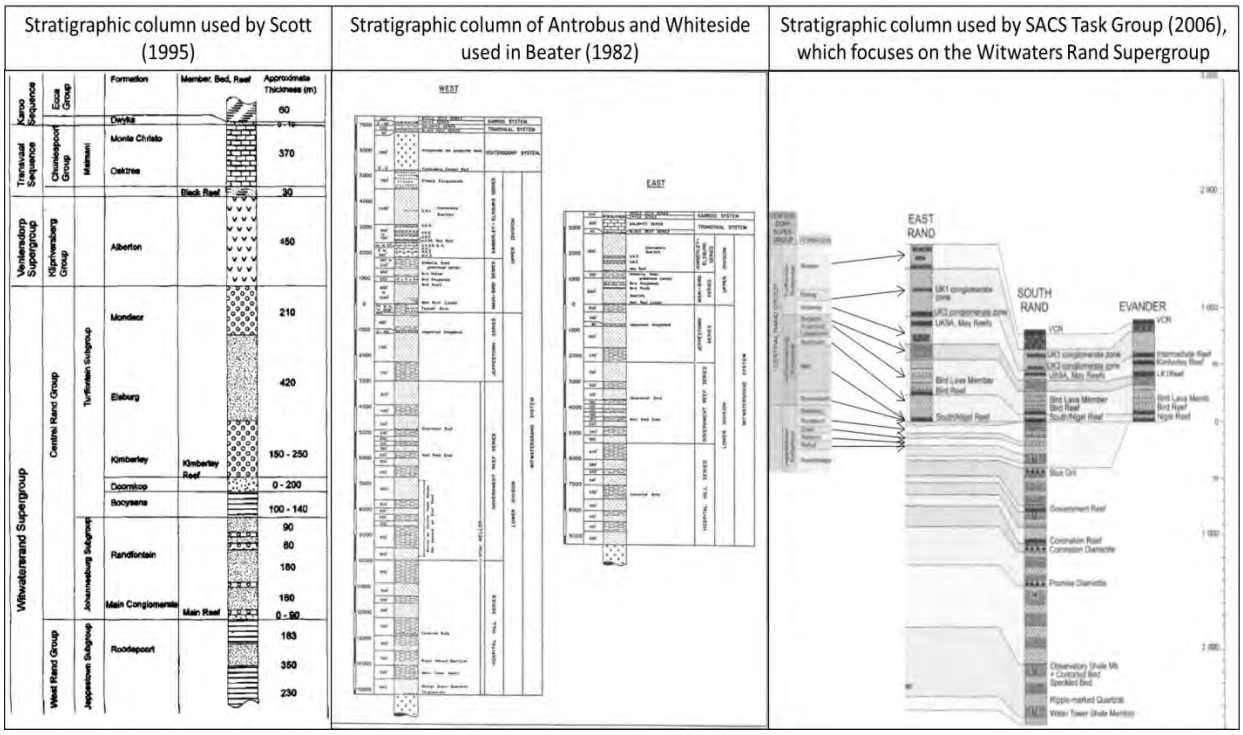


**Figure 2.16: The stratigraphic columns that are used to compile a new stratigraphic column (Annexure I)**

The Antrobus and Whiteside stratigraphic column clearly indicates that the western part of the East Rand Basin's geology differs from the eastern part of the East Rand Basin's geology. This was also mentioned in section 2.4 and therefore the newly compiled lithostratigraphic column will not indicate the various depths at which each layer is found, but only the average thickness of each geological layer. The stratigraphic column of Antrobus and Whiteside is older than those

of SACS and Scott and still illustrates the depths and thicknesses in feet. Therefore, the depth and thickness measurements need to be converted from feet to metres before it is used to calculate the average thickness. Where the thickness of SACS and Scott correspond with those of the West and East columns of Antrobus and Whiteside, the average of the four depths is calculated. But when the readings differ substantially, a minimum and maximum depth (such as the Black Reef) is given. The reason for this is that the geological layer is affected by the thinning mentioned under section 2.4. The new table will also illustrate to which subgroup, group and supergroup each geological layer belongs. The Ventersdorp Supergroup is also present in this new table, although it only appears in the western region of the East Rand Basin. The reason for adding this Supergroup is that the new table is merely an illustration of the average thickness and the order of the various geological layers within the East Rand Basin. The new table is given below in Figure 2.17.

| Supergroup | Group | Subgroup | Formation | Reef | Layer | Thickness (m) |
|---|---|---|---|---|---|---|
| Karoo Supergroup | Ecca | | | | | 60 |
| | Dwyka | | Dwyka | | | 0-15 |
| Transvaal Supergroup | Chuniespoort | Malmani | Eccles Lyttleton Monte-Christo Oak Tree | | | 75-370 |
| | | | | Black | | 10-30 |
| Ventersdorp Supergroup | Klipriversberg | | Alberton | | | 0-455 |
| Witwatersrand Supergroup | Central Rand | Turffontein | Mondeor | | | 210-260 |
| | | | Elsburg | | | 400-420 |
| | | | Kimberley | Kimberley | | 150-250 |
| | | | Doornkop | | | 0-200 |
| | | Johannesburg | Booysens | | | 100-130 |
| | | | Krugers-dorp | | | 100-250 |
| | | | Rand-fontein | | | 250-300 |
| | | | Main | Main/ South | | 0-90 |
| | West Rand | Jeppestown | Roode-poort | | | 90-100 |
| | | | Crown | | | 30 |
| | | | Babrosco | | | 100-350 |
| | | | Rietkuil | | | 110-230 |

**Figure 2.17: The newly created lithostratigraphic column for the East Rand Basin**

The methods and materials that will be used to capture the geology of the East Rand Basin within a 3D geological model will be explained and described in the next chapter.

# Chapter 3: Method and Materials

## 3.1 Introduction

In the following chapter the term GIS and 3D GIS will be explained. This will include an explanation of the main data types, such as vector and raster data. The difference between the two terrain surface models TINs and DEMs, which will be used to illustrate the geology in each geological 3D model, will also be included in this explanation. Furthermore, the methods and tools used to create the three different 3D models – model A (a)(b)(c), model B and model C – to represent the subsurface geology of the area will be explained.

## 3.2 GIS

A geographical information system, better known as GIS, is a computer-based system that is capable of capturing, managing, analysing and modelling a variety of geographical information. According to Chrisman (2002) three components are captured within geographical information. These components include (Chrisman, 2002 and Siabato & Manso-Callejo, 2011):

- **The space / location component (Where?) -** Also known as the geometric component. This component can be understood in a number of ways, of which the simplest is that space is made up of diverse places that are different from each other. The objects that are connected with space have variable length, width and height. These objects are known to be a certain distance and direction from one another and are mostly illustrated by a two-dimensional map.

- **The time component (When?) -** Also called the basic temporal component. Time regularly plays a silent role when it comes to maps, though there is always some implicit or explicit temporal reference. This concept is needed to locate a geographic feature at a specific time. A good example would be to look at a map as a snapshot, which is only valid for a specific moment in time.

- **The attribute component (What?) -** Can be defined as the descriptive component. This is the component that contains the descriptive information / properties of the other two (space / location and time) components. The descriptive information / properties are known to be qualitative or quantitative. These attributes are normally found within the attribute tables in the GIS specific software. An example of these tables can be seen in Figure 3.14.

These three components need to be present to create a map. According to Sinton (cited by Langran & Chrisman, 2014) the measure of one component requires that a second component

be controlled and that the third component be fixed. These three components can then be represented by two types of data, such as vector data and raster data.

Vector data (Figure 3.1) consist of points, lines and polygons stored and encoded as a collection of x and y coordinates. These points, lines and polygons are then represented by feature classes within the GIS software. The point features, just as the boreholes used in this study, are given a single x and y coordinate whereas a linear feature, such as the mine boundaries used in this study, is given a string of point coordinates and thus a polygon feature, such as national parks, is stored as a closed loop of coordinates. When it comes to describing discrete features such as buildings, a vector model could be very useful, but when it comes to varying features such as soil, the vector model would be less useful (Korte, 2001). The advantages and disadvantages of vector data according to Gobi (2007) are as follows::

Advantages:

- Vector data can be illustrated in its original resolution and form without the need for generalisation.
- The output of the graphics is usually more appealing (traditional cartographic representation).
- Most data are in the form of vector data, which means no conversion of data is needed.
- Accurate geographic location of the data is maintained.

Disadvantages:

- Each vertex's location needs to be stored explicitly.
- For an analysis to be successful, the data must be converted into a topological structure. This involves intensive processing and extensive data cleaning.
- If the vector data is edited after the topological structure was built, the topological structure would require rebuilding.
- The spatial analysis and filtering within a polygon is impossible.

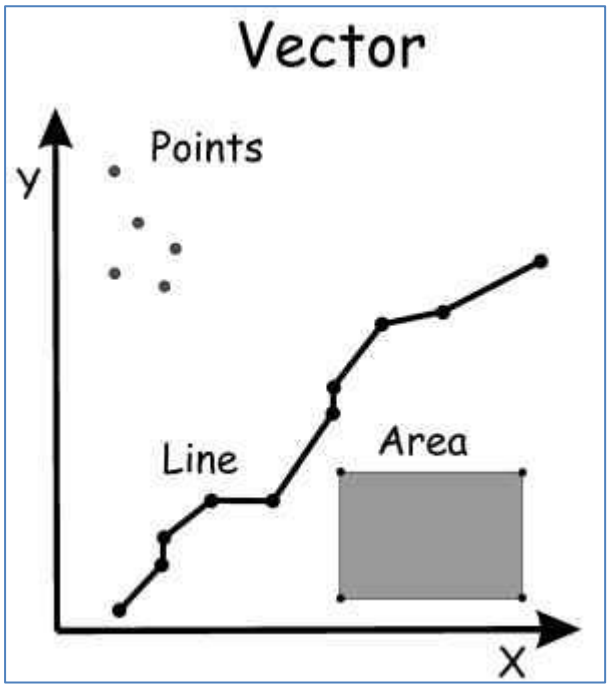


**Figure 3.1: Illustration of vector data (Anon, 2014)**

Raster data, (Figure 3.2) on the other hand, consist of pixels, cells or grids that are coded according to data values. Examples of raster data would be land cover classification, paper maps (2D like maps) and orthophotos. The advantage of using raster data is that the computer can manipulate it quickly, but the output maps from raster data are of a lower quality and less precise than maps created using vector data (Korte, 2001). The reason for this is that the resolution of the data is represented by cells which makes it difficult to illustrate lines and areas. This can be seen by comparing the line feature of Figure 3.1 and Figure 3.2: the bigger the cells, the lower the resolution. Other advantages and disadvantages of raster data according to Gobi (2007) include:

Advantages:

- Each cell's geographic location is implied by its position within the cell matrix.
- Due to the data storage technique, data analysis is usually easy to program and quick to perform.
- Raster data are ideal for mathematical modelling and quantitative analysis.
- The grid-cell system associated with raster data is very compatible with raster-based output devices, for example graphic terminals.

Disadvantages:

- The resolution of the represented data is determined by the cell sizes. The bigger the cell sizes the weaker the resolution.
- The cell resolution makes it difficult to represent linear features. This will lead to a misrepresentation of the line and would then be not only less precise, but also inaccurate.
- Many of the output maps from a grid-cell system do not conform to the high quality cartographic standards.
- Most of the data will have to be converted since it is in the vector data format.

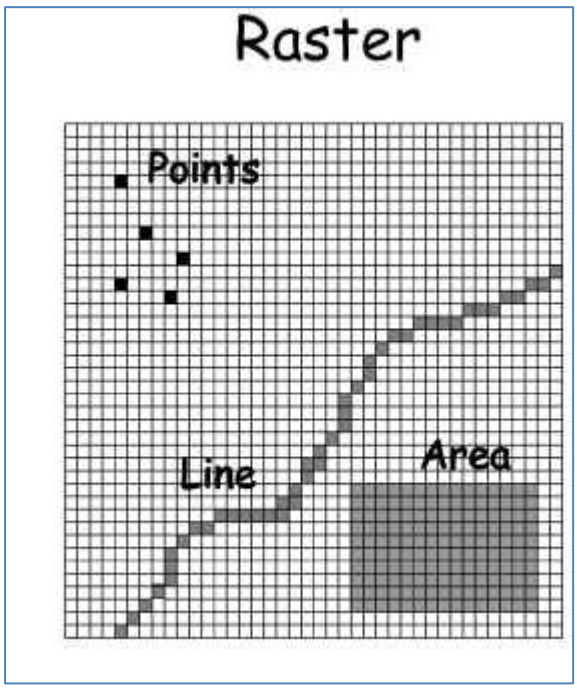


**Figure 3.2: Illustration of raster data (Anon, 2014)**

Both the vector and raster data can then be captured in a geodatabase. According to ESRI (2013) a geodatabase is known as a data storage and management framework used in ArcGIS. By combining the spatial data (geo) with data repository (database) a central data repository for spatial data storage and management is created. This is done by making use of ArcCatalog. A geodatabase stores geographic features with the same geometry type, the same attributes and the same spatial reference. Homogeneous features such as highways and secondary roads can be grouped into one unit for data storage purposes by making use of feature classes. The feature class will then be named “roads”. Feature classes include points, lines or polygons (ESRI, 2013).

According to Tavakoli (2008) a geodatabase should be considered when it comes to the study of geology, because as a tool, the geodatabase of a geological study can contain data of spatial locations and shapes of geological or geographical structures which are saved as lines, points and polygons. The various advantages of a geodatabase can also be seen as another reason why a geodatabase can be considered an important step. These advantages are as follows (Childs, 2009):

- It improves versatility and usability.
- It optimises performance.
- Few size limitations.
- Easy data migration.
- Improved editing model.
- It stores rasters.
- Customisable storage configuration.
- It allows updates to spatial indexes.
- It allows the use of data compression.

After the data have been sorted in the geodatabase, the geological terrain surface data could be displayed in ArcScene. The data are displayed through using surface models, namely TINs and raster surfaces / DEMs. These two surfaces are explained below.

According to ESRI (2013) a triangulated irregular network (TIN) surface is vector-based digital geographical data which are constructed by triangulating a set of points (vertices). These vertices are connected through a series of edges which form a network of triangles. There are two main interpolation methods used to form a network of triangles, such as Delaunay triangulation and distance ordering. The Delaunay method is supported by the ArcGIS software. The result of this method is that long thin triangles are avoided through maximizing the minimum interior angle of all the triangles. A TIN is made up of three main features, namely nodes, edges and faces.

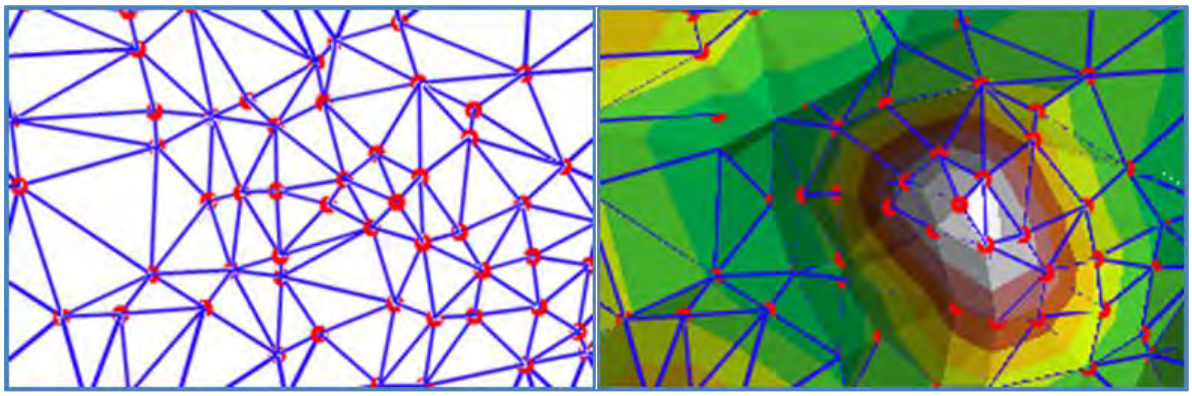

**Figure 3.3: Illustration of the three features a TIN is made of, such as nodes (left), edges (left) and faces (right) (ESRI, 2013)**

When it comes to the Delaunay triangulations method a TIN expects the units to be in feet or metres and not decimal degrees. TINs are known to be more expensive than raster surface models when it comes to the building process, because TINs use good source data, which have a high cost. However; a TIN tends to be less efficient than raster data (DEMs) when it comes to processing, all due to the complex data structure of a TIN model (ESRI, 2013).

Unlike a TIN, a raster surface / digital elevation model (DEM) is a raster (grid) that gives a representation of a continuous surface, generally referencing the earth's surface. The accuracy of these models is primarily determined by its resolution and the data used in creating the DEM. The resolution depends on the distance between the sample points; the greater the distance, the lower the resolution and vice versa (ESRI, 2013).

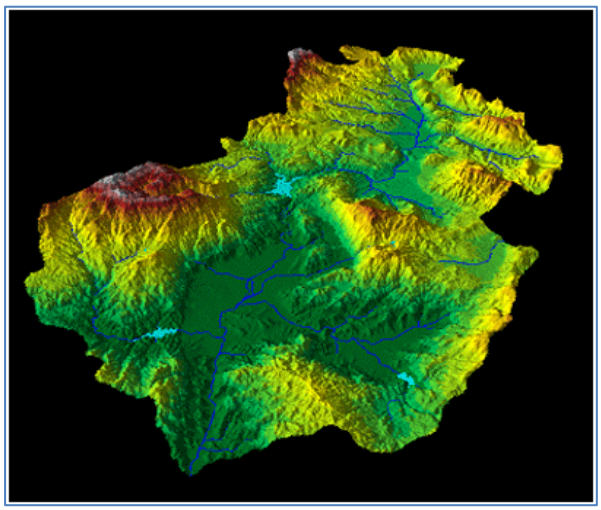

**Figure 3.4: Illustration of a DEM (ESRI, 2013)**

Throughout the literature it is not clear which surface is better to use, because it all depends on what type of analysis needs to be done. For this study the TIN surface type will be used for the first two models (Model A and B) and then the raster surface / DEM type will be used for the third model (Model C). The reason for using the TINs on the first two models is to see what the effect would be when all the breaklines of the TINs, except the boundary lines, are deleted under Model B and compared to those TINs under Model A(a), whose breaklines are not deleted. ESRI (2013) defines breaklines as lines that can and cannot have height measurements. These lines are known to become sequences of one or more triangles' edges. Breaklines represent natural features such as ridgelines and rivers, or constructed features such as roadways. These breaklines can also be divided into two types, namely hard and soft. Hard breaklines capture the sudden changes of a surface and improve the display and analysis of a TIN surface. Soft breaklines allow a TIN surface to capture linear features that will have no effect on the local slope of a surface.

The TINs of Model C that are created from the DEM surfaces will also be compared to those of Model A and Model B. These DEMs will be created from the various borehole data points within the National Groundwater Archive Geodatabase.

To create a raster surface / DEM from a grid of points, various interpolation methods are used, as the Department of Water and Sanitation were not able to drill boreholes throughout the whole area. The interpolation method will estimate the value of points for which there is no information, using the data from the sample points with information (Sárközy, 1998). Some of these methods include:

- **Inverse Distance Weighted Interpolation (IDW) -** According to Li & Heap (2008) IDW is a method that is known to calculate the values of a non-sampled point using a linear combination of sample points weighted by an inverse function of the distance from the non-sampled point to the sampled points. Therefore an assumption can be made that the neighbouring sample points of the non-sampled point are more similar to it than the sample points further away.

- **Spline -** This interpolation method uses a mathematical function to estimate the values of the non-sampled points. This mathematical function is known to minimise the total surface curvature which results in a smooth surface that passes exactly through the sampled points (Azpurua & Ramos, 2010).

- **Kriging -** Kriging, named after South African mining engineer DG Krige (Anderes, 2013), is known to be the best linear unbiased predictor and method of optimal prediction or estimation in geographical space. In this case, "optimal" refers to variance and

unbiasedness. Kriging is also known for its method of “local weighted moving averaging” of the observed values of a random variable (Z) within the neighbourhood (V) (Oliver, 2010).

For this study the Kriging method will be used because according to Oliver (2010) Kriging is being used in a wide variety of disciplines that uses spatial prediction and mapping, such as soil science, geology, hydrology, etc. There are many forms of Kriging; these include, among others, Ordinary Kriging, Universal Kriging, Simple Kriging, and Empirical Bayesian Kriging (EBK). Of these, the most original form of Kriging is called Ordinary Kriging. It is also known to be the most robust and often used method of Kriging (Oliver, 2010). This type of Kriging is known to be linear, since its estimates are weighted linear combinations of the data available. Ordinary Kriging is unbiased since it attempts to get the error or mean residual close or equal to 0 (Edward *et al*., 1989). According to Cilliers (2013) and ESRI (2013) a few conditions need to be met when it comes to creating a surface by making use of Kriging. These conditions are as follows:

- Is the data normally distributed?
- Check for outliers (there should be none).
- Data needs to be stationary.
- No visible clusters in the data.
- No visible trends in the data.

Meeting these conditions will ensure a Root-Mean-Square Standard Error (RMSES) = close to 1 and a Root-Mean-Square Error (RMSE) = close to 0. Getting these results will ensure that the produced raster surface / DEM is accurate (Cilliers, 2013).

For this study the Empirical Bayesian Kriging method, which falls under the Geostatistical Wizard of ArcGIS, will be used. According to ESRI (2013) the Empirical Bayesian Kriging method is a geostatistical interpolation method that automates the difficult aspects when it comes to building an effective Kriging model, in order to get the results mentioned above. Unlike the other Kriging models that require manually adjusted parameters to receive accurate results, the Empirical Bayesian Kriging method automatically calculates the parameters through a process of subsetting and simulations. When it comes to the semivariogram (Figure 3.6) the other Kriging methods calculate the semivariogram from data locations that are known and use this semivariogram to make the predictions for the unknown locations, whereas the Empirical Bayesian Kriging method accounts for the error that is introduced by estimating the underlying semivariogram. A semivariogram illustrates the semivariogram cloud which is created when the

distance between two points are measured and then plotting the difference squared between the values at the locations.

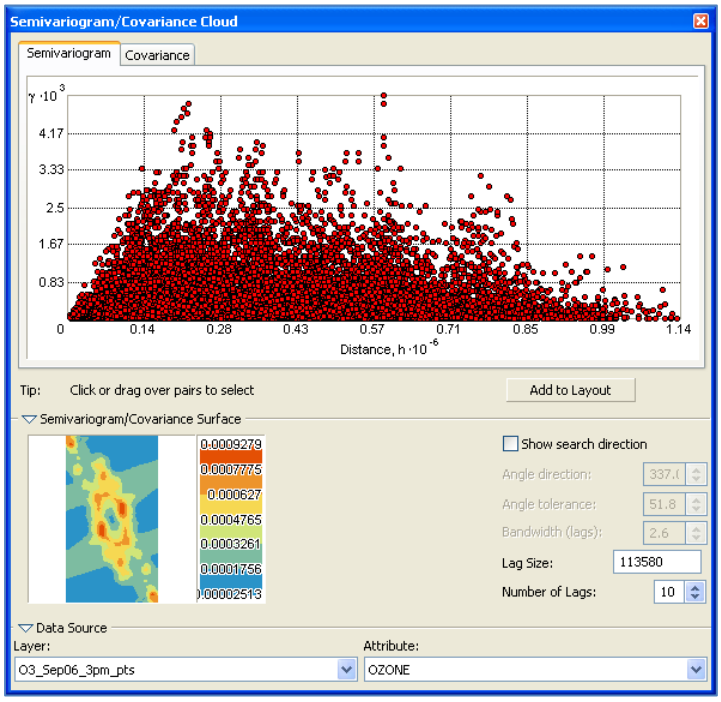


**Figure 3.5: Example of a semivariogram (ESRI, 2013)**

The advantages and disadvantages for this type of Empirical Bayesian Kriging as mentioned by ESRI (2013) are as follows:

Advantages

- Minimal interactive modelling is required.
- Unlike other Kriging methods the standard errors of prediction are more accurate.
- Accurate predictions are given when it comes to moderately non-stationary data.
- Known to be more accurate than the other methods when it comes to small data sets.

Disadvantages

- When it comes to raster output, EBK is known to be slower than the other methods.
- The option for co-Kriging and anisotropy is unavailable.

- When it comes to customisation in the semivariogram model, the EBK is limited to a small number of parameters.

- The log empirical transformation is particularly sensitive to outliers. If this transformation is used with data that contains outliers, the predictions might be of magnitude greater or smaller than the values of your input points.

### 3.3 3D GIS

In the modern three-dimensional world of today, the technology is becoming more and more advanced. One of these improvements is the GIS applications that are moving more towards 3D GIS, as it gives a better representation of the real world. 3D reality graphical descriptions are not new, since perspective view drawings date back to the Renaissance period, but it wasn't until the evolution of 3D terrain visualisation in the 1980s that the need for 3D GIS applications existed. These needs came from tremendous demands by geo-browsers such as Google Earth and World Win (Ruzinoor *et al.*, 2012 & Abdul-Rahman & Pilouk, 2007).

According to Abdul-Rahman & Pilouk (2007) 3D descriptions of reality change when it comes to the above-mentioned perspective view, all due to change in the viewing position. Therefore these perspective views were quite dull. This problem was eliminated by traditional maps, due to the use of orthogonal earth projections. But these maps were also offering a very limited 3D impression as they reduce the spatial description of 3D objects to 2D.

All these problems are eliminated when reality is directly transferred into a 3D model when making use of computer technology, such as ArcGIS. According to ESRI (2013) the 3D term is being misused when it comes to software applications today, because this software stores and displays data in a two and a half dimension (2.5D). ArcGIS has a 3D Analyst extension which will be used in this study that is capable of storing raster DEMs, TINs and terrain data sets as functional surfaces. A functional surface according to ESRI (2013) is known as continuous, and all the locations on a surface have only one z-value per x and y coordinates. The true 3D terrain surfaces are sometimes known as a solid model, just like the geological layers that will be created in this study. These solid models are created through multipatch features, which can be seen as an extruded polygon that stores more than one z-value per x and y coordinate. Therefore a multipatch will be created (see section 3.4.4.) for each geological layer to ensure that each geological layer is a complete 3D terrain surface model and not a 2.5D terrain surface model.

According to Ruzinoor *et al*., (2012) the visualisation of a 3D terrain can be divided into four main groups, namely:

1. **Manual 3D Terrain Visualisation** - A big challenge existed over the years for map-makers who manually represented the terrain on 2D maps. Rounded “molehills” were used to represent mountains on a map. These “molehills” were just a simple, uniform, side view of a rounded dome (Table 3.1). Over the years the arrangement of the “molehill” symbols changed to incorporate the various sizes and shapes. They were also shaded to give an impression of illumination. A table was created to categorise the manual representation of the terrain into six different classes. Table 3.1 lists these techniques and an example will be given for each.

**Table 3.1: The six different representation classes according to Ruzinoor *et al*., (2012)**

| | | |
|---|---|---|
| Surface Specific Features | Spot Heights<br>Skeletal Lines |  |
| Slices | Profiles<br>Inclined Profiles<br>ContourLayer Shading | 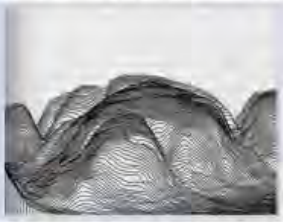 |
| Shading | Stippled Relief<br>Hachures<br>3D Shaded Contour<br>Hill Shading |  |
| Pictorial | Molehill<br>Physiographic<br>Oblique Regional View<br>Block Diagram<br>Sketches |  |
| Photographics | Photomaps | |
| True 3D | 3D Model Globes | |

2. **Automated 3D terrain visualisation** – Automated / Computer 3D terrain visualisation methods consist of mosaics, profiles, contouring, vertices, wire mesh, polygon models, and photo-realism. This type of method holds a big advantage when it comes to terrain visualisation because it is quick and effortless. This method gives a final visualisation / picture that can be seen as bitmap of pixels. Therefore visualisation can be seen as a process that takes 3D information and makes a 2D picture of it.
3. **Online 3D terrain visualisation -** Most of the applications used for 3D terrain visualisation are known to be open-source web-based systems. Together with the emergence and popularity of mobile devices, most of the new 3D visualisation innovations are focusing on mobile applications.
4. **Software 3D terrain visualising -** These include software and toolkits that are commercially available to explore and to display the various types of data. An example, and the software that will be used for this study, is ArcGIS.

Disciplines such as geology, hydrology, civil engineering and environmental engineering all rely on 3D modelling to create a 3D model, which can help to complete their tasks efficiently (Abdul-Rahman & Pilouk, 2007). A 3D model, according to Wainwright & Mulligan (2004), is known to be an abstraction of reality that represents a complex reality in the simplest way that is adequate for the purpose of the modelling. A 3D model also forms the basis of a system which provides the functionality to accomplish the task that is in hand. The best 3D model is that model which attains the greatest realism with the least model and parameter complexity.

Wainwright & Mulligan (2004) states that 3D modelling can thus be seen as canvas on which scientists can develop and test ideas, incorporate a number of ideas, to view the outcome of these incorporated ideas, to integrate and illustrate these ideas to other scientists. Three-dimensional models are usually developed with one or two goals in mind, which could lead restricted uses to which the model may be put. Wainwright & Mulligan (2004) also list seven purposes for which models are usually created:

(1) As an aid to research.

(2) As a tool for understanding.

(3) As a tool for simulation and prediction.

(4) As a virtual laboratory.

(5) As an integrator within and between various disciplines.

(6) As a research product.

(7) As a means of communicating science and the results of science.

When it comes to earth sciences and 3D modelling a suitable tool is the GIS software, which is capable of creating 3D models and is able to represent the real world objects with discrete properties and objects with various properties. One of this software products is ArcGIS, which will be dealt with under 3.4.1. The differences between these two objects are explained in the table below (Abdul-Rahman & Pilouk, 2007):

**Table 3.2: Difference between objects with discrete and varying properties**

| Objects with discrete properties | Objects with various properties |
|---|---|
| • Sampling limited<br>• Readily boundaries, such as buildings, roads, bridges, fault blocks, perched aquifers. | • Definition limited<br>• Defined by means of classification, using properties: soil strata classified by grain-size distribution and moisture content; carbon monoxide in the air by concentration ranges; pollutant by percentage in the water. |

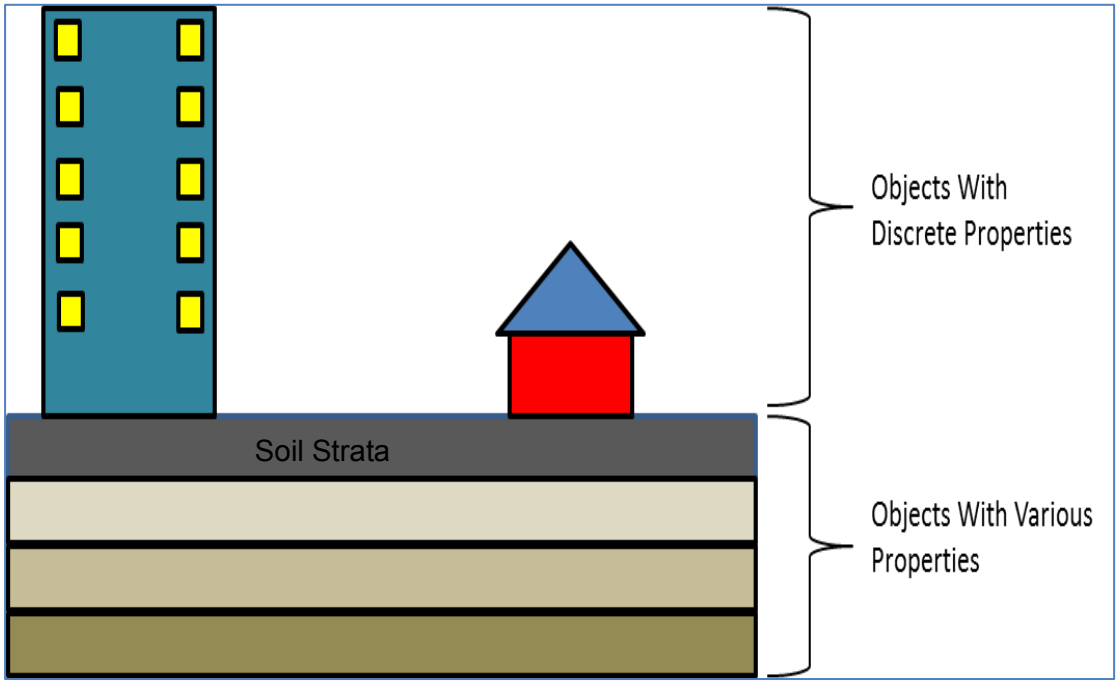


**Figure 3.6: Objects with discrete and various properties adopted from Abdul-Rahman & Pilouk (2007)**

It appears that 3D modelling, especially ArcGIS, proves to be a very effective tool when it comes to city planning, all due to the fact that they use it to bring the abstract project variables like visual impact analysis into the cost-benefit equation. Therefore ArcGIS 10.2 is used in this study to see if the latest GIS with its 3D Analyst Tools will be able to visualise the geology, of the East Rand Basin, three-dimensionally.

There are also other software available which can be GIS related or non-GIS related, that are used to create 3D geological models. A few software examples include:

- Leapfrog
- Rockworks
- Maptek
- Petrel Geology & Modelling
- GeoModeller
- GSI3D Research Consortium

3D modelling with the help of GIS software should not be seen as an alternative to observation methods, since observation is closer to truth and should remain the most important component of a scientific study. 3D modelling must be seen as a powerful tool to understand observations and to develop and test the theory (Wainwright & Mulligan 2004).

### 3.4 Creating the models

There are four main steps (Tavakoli, 2008), as indicated by figure 3.7, that will be used to create the three main 3D models (Model A, Model B and Model C) of the East Rand Basin. Each model will be created with a different method (see section 3.4.4.) and compared in order to determine which method deliver the best results without the extra purchasable tools and models. The first step will be to collect and sort the data for the study area. The second will be to create an appropriate geodatabase for the collected geological data. The third step would be to create the TINs or to run add-in tools. The final step will be to create the three types of 3D models, with the help of ArcGIS, which will illustrate the surface and subsurface geology in order to visualise the geology's characteristics of the East Rand Basin.

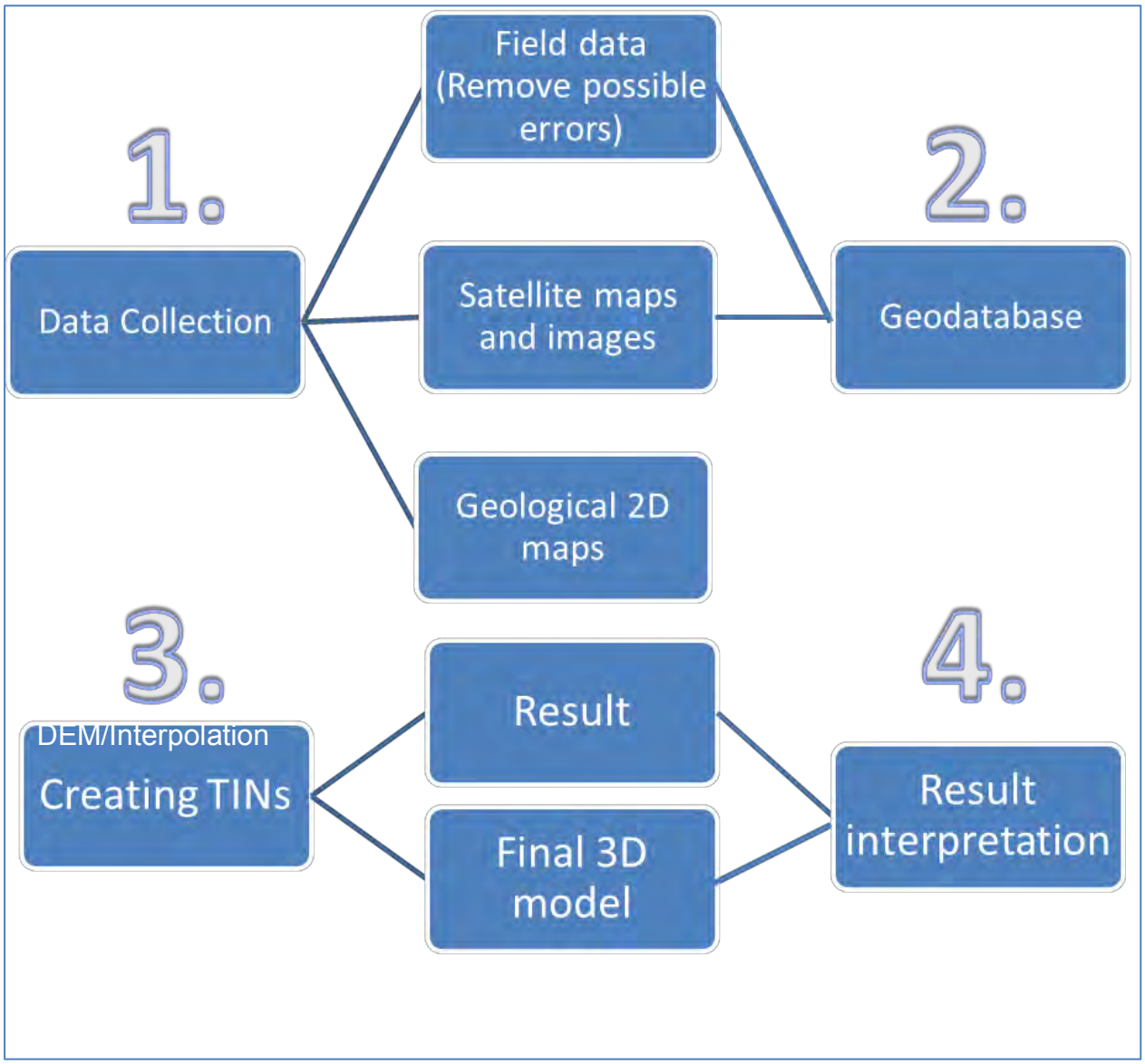


**Figure 3.7: The outline of the main steps that will be used for this study**

### 3.4.1 ArcGIS software

ArcGIS, the software that will be used can be seen as a tool for collecting, managing, analysing, modelling and processing data. ArcGIS allows users to publish geographic information so that it is available to everyone for perusal. ArcGIS as a system is available all around us, on web browsers, mobile devices and desktop computers. According to ESRI (2013) ArcGIS enables you to:

- Create, share and use intelligent maps.
- Compile geographic information.

- Create and manage geographic databases.
- Solve problems with spatial analysis.
- Create map-based applications.
- Communicate and share information using the power of geography and visualisation.

During the study the following ArcGIS software applications were used (ESRI, 2013):

- **ArcCatalog 10.2** - This application is used to manage and store the various geographic data used for this study.
- **ArcGIS 3D Analyst 10.2 -** This toolbox is used to create and edit the various triangulated irregular networks (TINs).
- **ArcGIS Data Management -** The toolbox was used to develop, manage and maintain feature classes, data sets and layers.
- **Geostatistical Wizard -** a dynamic set of pages which is a guide that helps the process of constructing and evaluating the performance of an interpolation model**.**

### 3.4.2 Data collection

The field data that will be used is the x, y and z data from bore logging data, which increase the accuracy of point measurement, since a GPS was used. The borehole data come from the National Groundwater Archive Geodatabase which the Department Water and Sanitation obtained through the boreholes they drilled as the need for groundwater data and information continued to increase to assist in planning, providing water to people, monitoring, drought relief and climate change (DWS, 2014). The National Groundwater Archive Geodatabase consists of four tables (see Table 3.3 for the National Groundwater Archive's lithology codes):

1. **The Basic Information Table** - This table stores the x and y data of a specific borehole.
2. **The Chemistry Table** - This is the table that contains all data related to the chemical compounds of a specific borehole.
3. **The Geology Table** - This table illustrates at which depths a specific geology layer is found. The geology table of the study area consists mainly of the Karoo and Transvaal Supergroups.
4. **Water Level Table** - This is the table that indicates the water level at the time of the drilling of a specific borehole.

**Table 3.3 The National Groundwater Archive (NGA) lithology codes (DWS, 2014)**

| Lithology Code | Lithology | Lithology Code | Lithology |
|---|---|---|---|
| ALVM | ALLUVIUM | LTRT | LATERITE |
| BLCL | BOULDER CLAY | MDSN | MUDSTONE |
| BLDR | BOULDER | MUD | MUD |
| BRCC | BRECCIA | NORT | NOTREITE |
| CHLK | CHALK | NS | NO SAMPLE |
| CHRT | CHERT | QRTZ | QUARTZ |
| CLAY | CLAYSTONE | RBBL | RUBBLE |
| CLCT | CALCITE | SCST | SCIST |
| CLGM | CONGLOMERATE | SDGL | SAND and GRAVEL |
| COAL | COAL | SDSL | SANDSTONE and SHALE |
| DIBS | DIABASE | SHLE | SHALE |
| DLMT | DOLOMITE | SHSL | SHALE and SILTSTONE |
| DLRT | DOLORITE | SILT | SILT |
| DMCT | DIAMICITE | SLSN | SILTSTONE |
| FRCT | FERRICRETE | SLTE | SLATE |
| GNST | GNEISS | SNDS | SANDSTONE |
| GRDS | GRAVEL, SAND and SILT | SOIL | SOIL |
| GRNT | GRANITE | SYNT | SEYENITE |
| LAVA | LAVA | TLLT | TILL |
| LMDM | LIMESTONE and DOLOMITE | TUFF | TUFF |
| LMSM | LIMESTONE | | |
| LOAM | LOAM | | |

Since the geodatabase consists of the Karoo- and Transvaal Supergroups, the deeper geological layers that are not found within this geodatabase will be created through making use of the average depths given by SACS (South African Committee for Stratigraphy) Task Group (2006), since the newly created lithostratigraphic column indicates the average thickness only. Furthermore, the average thicknesses derived from the new lithostratigraphic column and the DEMs provided by the North-West University will also be used to create these deeper geological

layers. Since the database contains all the boreholes of South Africa, the first step would be to select the boreholes that fall within the study area. The best way would be to create a New Area polygon feature class that is slightly larger than the study area, which will increase the accuracy of the models. When it comes to selecting the boreholes that fall within the New Area polygon, the “Clip Tool” found in ArcGIS can be used. This tool allows you to extract the borehole features that overlay the study area features (ESRI, 2013).

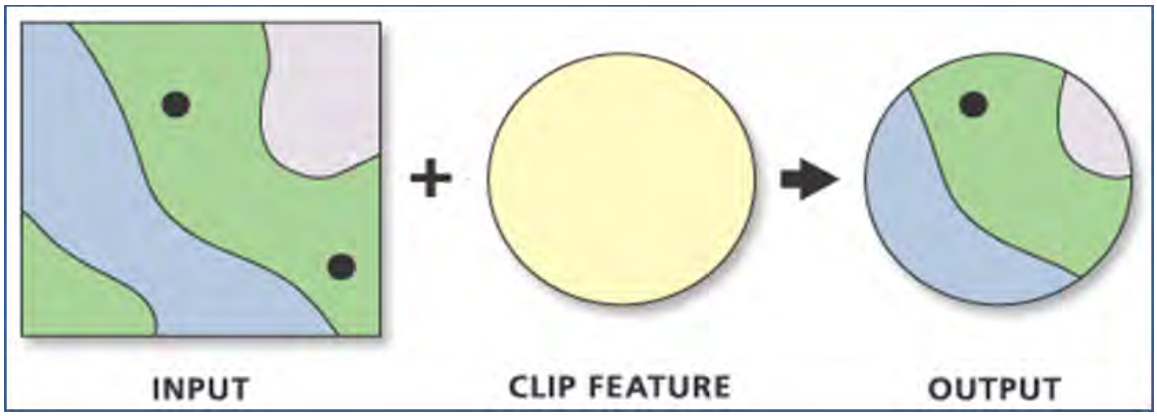


**Figure 3.8: Figure indicating how the clip feature tool works (ESRI, 2013)**

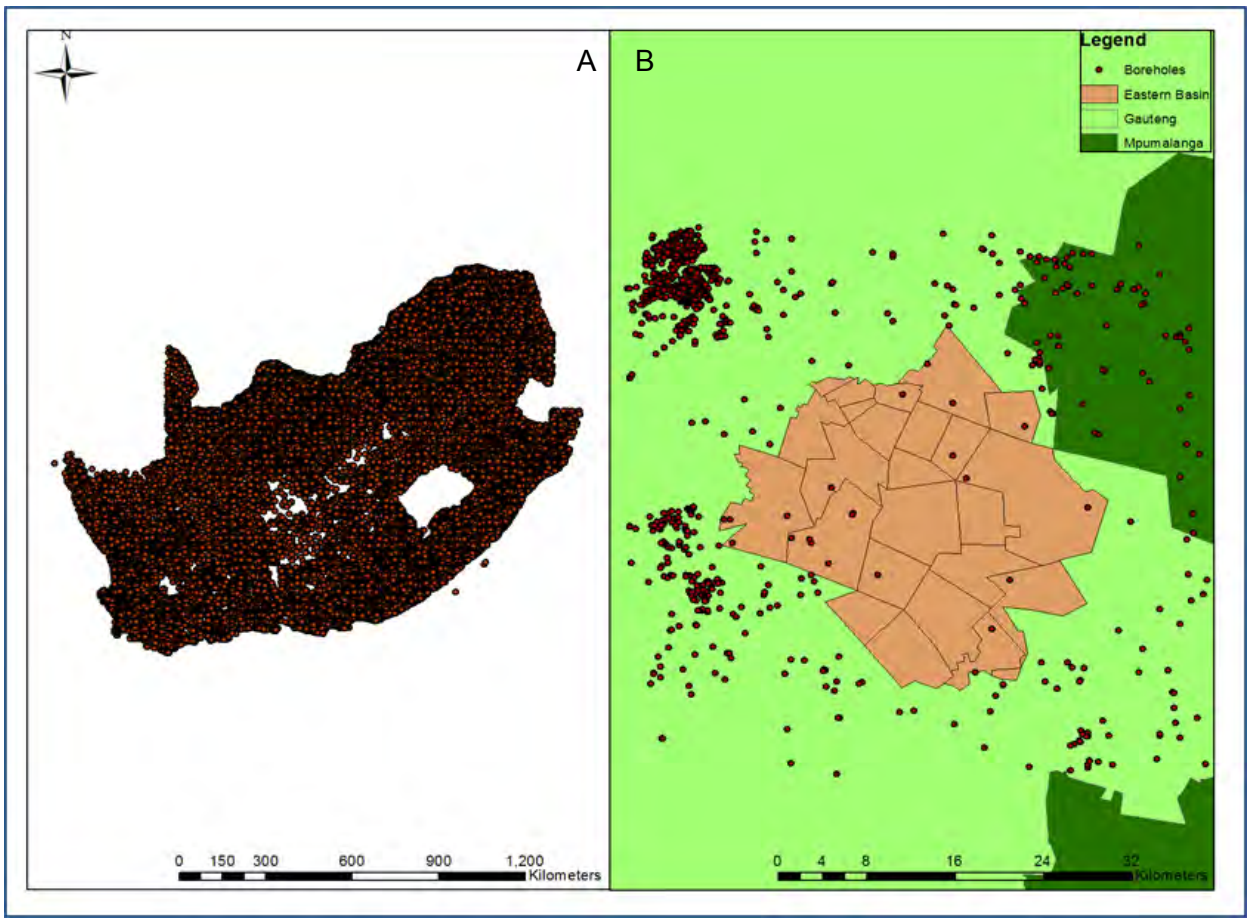


**Figure 3.9:** **(A) Indicates all the borehole points contained within the National Groundwater Archive Geodatabase. (B) Shows the difference after the clipping tool was used to select the boreholes within the study area.**

A new table, Book1, which contains the attributes of the newly selected boreholes, is then added to the National Groundwater Archive Geodatabase in Microsoft Access. A Microsoft Access Query (SELECT*FROM GEOLOGY, BOOK1 WHERE GEOLOGY.SiteName=BOOK1.SiteName) is then used to extract the geology data contained in the Geology Table that correspond with the boreholes used for the study. Before running the query, the output of the results are set to CSV which will be easier to import to Excel.

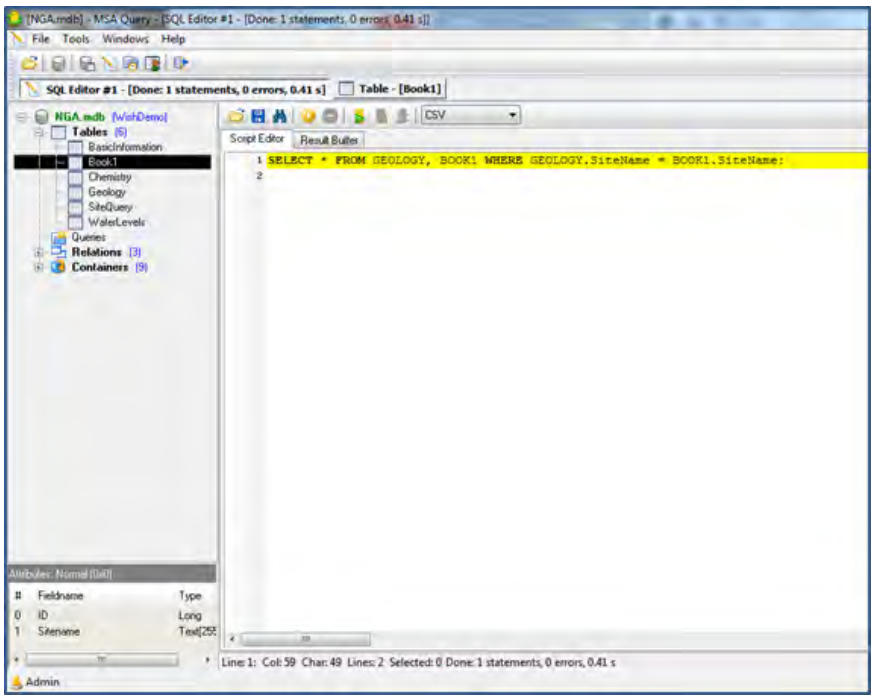


**Figure 3.10: Indicating the various tables within the NGA database and how the query should be entered**

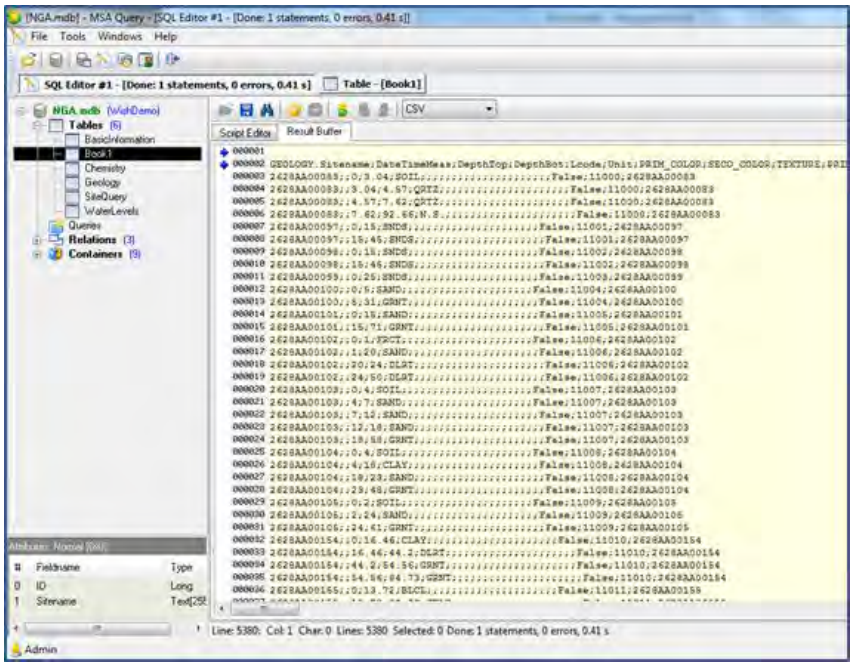


**Figure 3.11: Indication of how the results are presented in the CSV format before it is exported to Excel**

Since the newly created Geology Table contains no x and y coordinate data, it will be merged with the table, Book1, which contains the x and y coordinates. This is done by making use of the

Consolidated Worksheets Wizard trial version from AbleBits. The reason for this was that when joining the tables in ArcGIS, the site names did not contain the right top depth, bottom depth and geology type. This happens because the Geology Table consists of more than one of the same site names whereas the Book1 Table consists of only one site name per x, y and z data. The result produced by the joining function from ArcGIS is shown in Table 3.4. After merging the tables into one table (Figure 3.12), the data could be used to create a geodatabase.

**Table 3.4: The results using the joining function in ArcGIS**

| FID | NAME | x | y | Shape * | Sitename | DepthTop | DepthBot | Lcode |
|---|---|---|---|---|---|---|---|---|
| 109 | 2628AB00123 | 28.44861 | -26.23057 | Point | 2628AB00123 | 0 | -27.43 | CHRT |
| 111 | 2628AB00124 | 28.44862 | -26.23056 | Point | 2628AB00124 | 0 | -19.51 | CHRT |
| 137 | 2628AB00428 | 28.44887 | -26.18555 | Point | 2628AB00428 | 0 | -1.22 | LOAM |
| 151 | 2628AB00432 | 28.42805 | -26.15194 | Point | 2628AB00432 | 0 | -29 | CLAY |
| 117 | 2628AB00436 | 28.40972 | -26.20416 | Point | <Null> | <Null> | <Null> | <Null> |
| 112 | 2628AB00442 | 28.28341 | -26.22702 | Point | <Null> | <Null> | <Null> | <Null> |
| 146 | 2628AB00472 | 28.40555 | -26.17083 | Point | <Null> | <Null> | <Null> | <Null> |
| 143 | 2628AB00480 | 28.36138 | -26.18083 | Point | <Null> | <Null> | <Null> | <Null> |
| 116 | 2628AB00484 | 28.32944 | -26.19444 | Point | <Null> | <Null> | <Null> | <Null> |
| 150 | 2628AB00499 | 28.40805 | -26.16944 | Point | <Null> | <Null> | <Null> | <Null> |
| 147 | 2628AB00500 | 28.40555 | -26.17083 | Point | <Null> | <Null> | <Null> | <Null> |
| 149 | 2628AB00501 | 28.40305 | -26.16972 | Point | <Null> | <Null> | <Null> | <Null> |
| 148 | 2628AB00504 | 28.40361 | -26.17055 | Point | <Null> | <Null> | <Null> | <Null> |
| 108 | 2628AB00507 | 28.43388 | -26.22916 | Point | <Null> | <Null> | <Null> | <Null> |
| 119 | 2628AB00509 | 28.44111 | -26.19444 | Point | <Null> | <Null> | <Null> | <Null> |
| 6 | 2628AD00008 | 28.49472 | -26.33722 | Point | 2628AD00008 | 0 | -6 | CLAY |
| 82 | 2628AD00022 | 28.26278 | -26.28556 | Point | 2628AD00022 | 0 | -39.62 | DLMT |
| 84 | 2628AD00023 | 28.26728 | -26.28555 | Point | 2628AD00023 | 0 | -6.09 | GRVL |
| 81 | 2628AD00024 | 28.26278 | -26.28556 | Point | 2628AD00024 | 0 | -6.09 | SOIL |
| 83 | 2628AD00025 | 28.26279 | -26.28555 | Point | 2628AD00025 | 0 | -6.09 | GRVL |
| 106 | 2628AD00031 | 28.35 | -26.25833 | Point | 2628AD00031 | 0 | -1.22 | SOIL |
| 2 | 2628AD00097 | 28.48056 | -26.37917 | Point | 2628AD00097 | 0 | -6 | SOIL |
| 1 | 2628AD00098 | 28.48056 | -26.37918 | Point | 2628AD00098 | 0 | -6 | SOIL |
| 3 | 2628AD00099 | 28.48057 | -26.37917 | Point | 2628AD00099 | 0 | -6 | SOIL |
| 105 | 2628AD00107 | 28.26889 | -26.26667 | Point | <Null> | <Null> | <Null> | <Null> |
| 102 | 2628AD00108 | 28.27639 | -26.275 | Point | <Null> | <Null> | <Null> | <Null> |

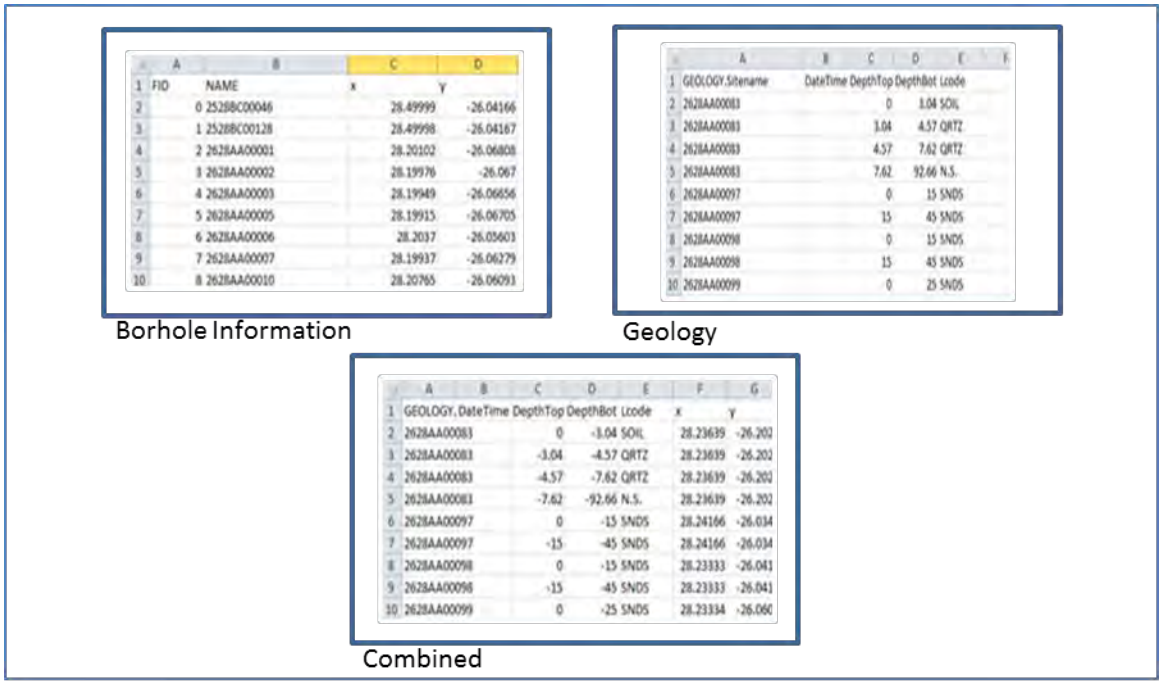


**Figure 3.12: Figure illustrating which tables are combined and the results thereof**

### 3.4.3 Geodatabase development for the East Rand Basin

The geodatabase for each geological model – Model A, B and C of the East Rand Basin – will contain two main feature classes: East Rand Basin Geology and East Rand Basin General. The East Rand Basin Geology feature class will contain all the features that relate to the geology; this includes the TINs and polygons for the various geological layers. The East Rand Basin General feature class will consist of the general features used to create the models. These features include the outline of the East Rand Basin and the New Area polygon. These two data sets will be given a projected coordinate system of UTM35S in which the study area is located.

The Universal Transverse Mercator (UTM) coordinate reference system originates at the equator with a specific longitude. With this reference system the y-coordinates increase negatively to the south (-27°, -28°, etc.) and the x-coordinates increase positively to the east. The number 35S represents the zone (see Figure 3.13) in which Gauteng is located. There are 60 zones that divide the earth's surface, each six degrees wide in longitude and stretching from east to west. Within this zone the x-value is known as the easting value and the y-value is known as the southern value. The southern value is the value given for distance from the equator and the easting value is the value given for the distance from the longitude (central meridian) (Dutch, 2014 & Mitchell, 2011).

The main feature class type that will be used in this study is point and polygon, since the bore logging data is stored as x, y and z coordinates and the geological layers will be illustrated by polygons.

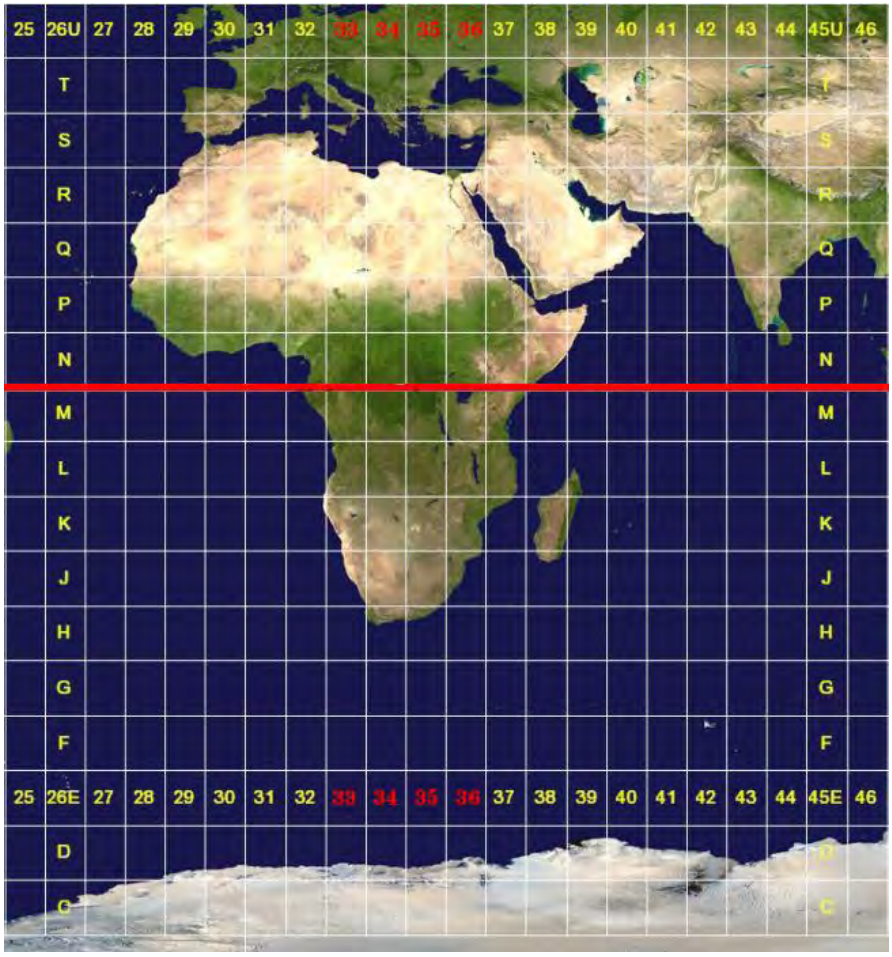


**Figure 3.13: Zones of the Universal Transverse Mercator (UTM) coordinate reference system (Wikipedia, 2014b)**

### 3.4.4 Building the 3D models

Due to the various data sources used in this study, three different 3D models – Model A, Model B and Model C – will be created by using the various tools under 3D Analyst. Model A is subdivided into A(a), A(b) and A(c) so that the completed Models A(b) and A(c) will be used as sub-models in Model B and Model C. Models A(a), B and C will be created from the same borehole data (National Groundwater Archive Geodatabase) whereas Model A(b) will be created from average depths and thicknesses (SACS and the new lithostratigraphic column) and Model A(c) will be created from the DEM surfaces provided by the North-West University. By using the 3D analyst tools the top and bottom depth, in metres, of each geological layer at the various borehole locations (see Figure 3.14), will be converted to 3D surface features. These features include TINs and DEMs. The data, tools and surfaces each model uses are illustrated in Table 3.5.

**Table 3.5: The data, tools and surfaces each model will use**

| Model | Data source | Which surface the data is converted to | 3D Analyst Tools used |
|---|---|---|---|
| Model A (a) | National Groundwater Archive Geodatabase | TIN | • Create TIN Tool<br>• Edit TIN Tool<br>• Extrude Between Tool |
| Model A (b) | Average depths from SACS Task Group and the new lithostratigraphic column | None (only to a polygon) | • None (standard GIS tools used) |
| Model A (c) | DEMs from the North-West University | TIN | • Edit TIN Tool<br>• TIN Edge Tool<br>• Feature to Polygon Tool<br>• Raster to TIN Tool |
| Model B | National Groundwater Archive Geodatabase | TIN | • Extrude Between Tool<br>• Delete TIN Breakline Tool<br>• TIN Editing Taskbar |
| Model C | National Groundwater Archive Geodatabase | TIN and then to a DEM | • Raster to TIN Tool<br>• TIN Editing Taskbar<br>• Extrude Between Tool |

For model A(a), A(b) and B, every geological layer's points needs to be exported to a feature class that represents each specific geological layer. For example, all the borehole points containing data regarding gravel will be exported to the feature class "GRVL" and all the borehole points containing data regarding chert will be exported to the feature class "CHRT". This is done so that an individual TIN can be created for each geological layer's top and bottom depth. Figure 3.15 is an indication of how the placing for each feature class borehole differs after it was exported from the borehole's feature class, mentioned under 3.4.2 and illustrated in Figure 3.9.

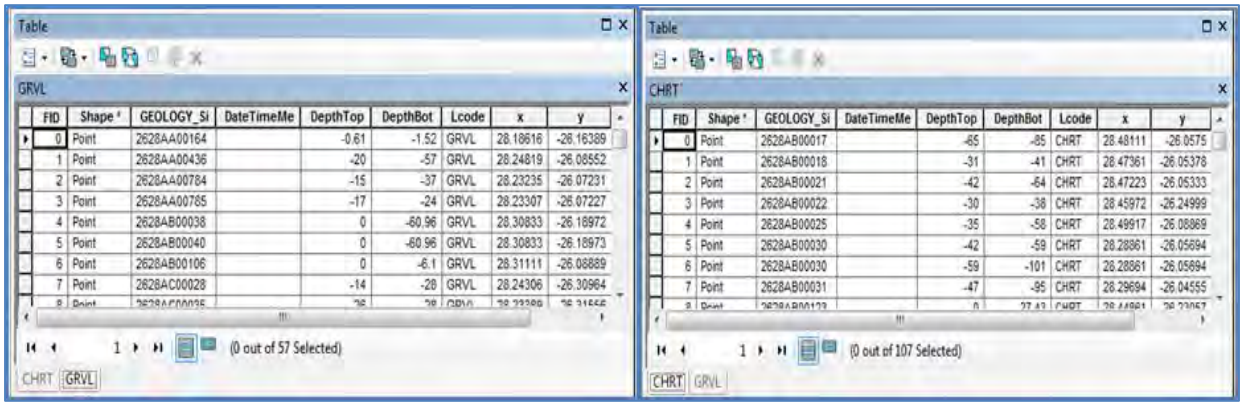


**Figure 3.14: Illustration of the attribute table for each feature class after exporting has taken place.**

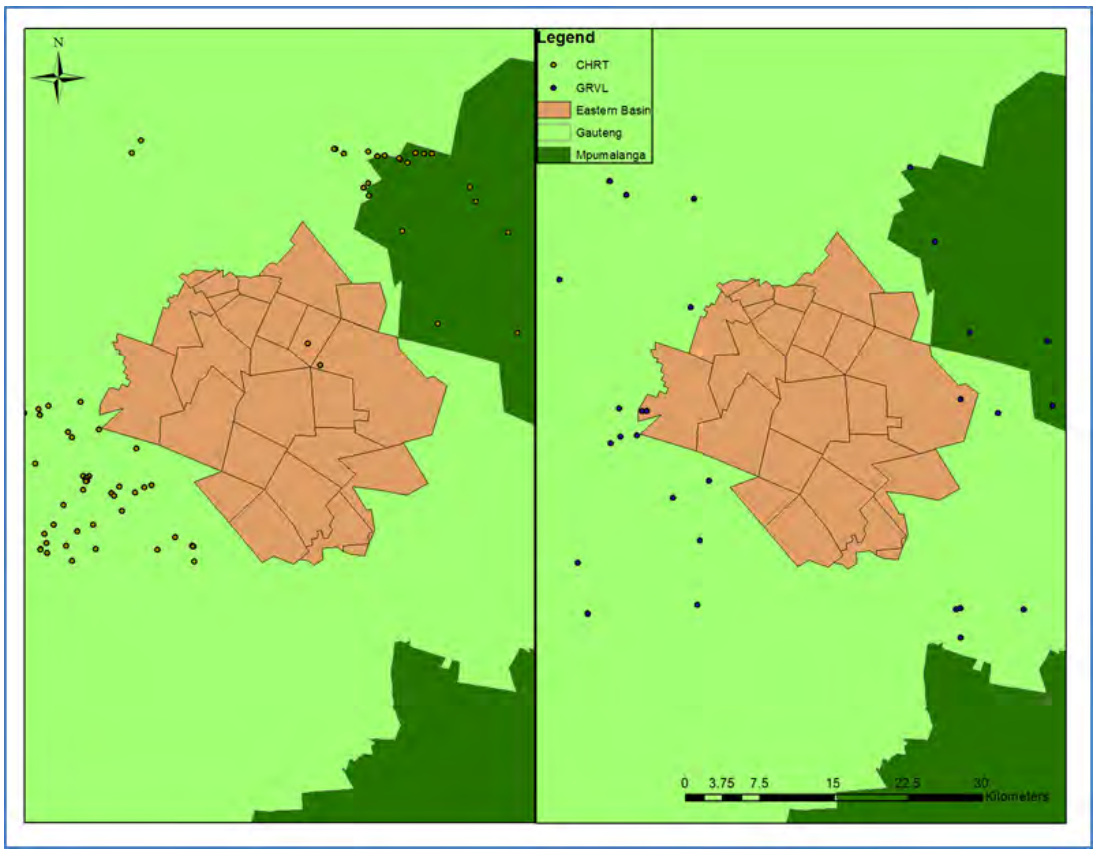


**Figure 3.15: Illustration on how the placing of the Chert borehole points differ compared to those of the Gravel borehole points, after it was exported.**

#### 3.4.4.1 Model A

The first model, Model A(a), will be a very basic model consisting of only a few steps. The first step would be to create a corresponding TIN of the top and bottom depth data for each geological layer. This is done by using the "Create TIN Tool" found under the 3D Analyst Tools. After creating these TINs the "Edit TIN Tool" will be used to clip the top and bottom TINs to the East Rand Basin's polygon feature class. This will ensure that only the data that fall within the study area are used from here onwards. The clipping is done by changing the Height Field to <None>, the Tag Field to <None> and the SF Type to Hard_Clip (see Figure 3.16). The East Rand Basin's polygon feature class can then be extruded between each bottom and top depth TIN. According to ESRI (2014) extrusion is a process that stretches a flat surface, such as the East Rand Basin's polygon feature class, the vertically to create a 3D object. The polygon feature are extruded vertically between the two TINs to create "boxes" (complete 3D geological layers) ESRI (2014). The extruding can be done by using the "Extrude Between Tool". The extruded polygon is known as a multipatch.

*From this point forward only the chert and conglomerate layers will be used as examples under the various models because they cover the whole study area and they have more borehole data contained in their attribute tables.*

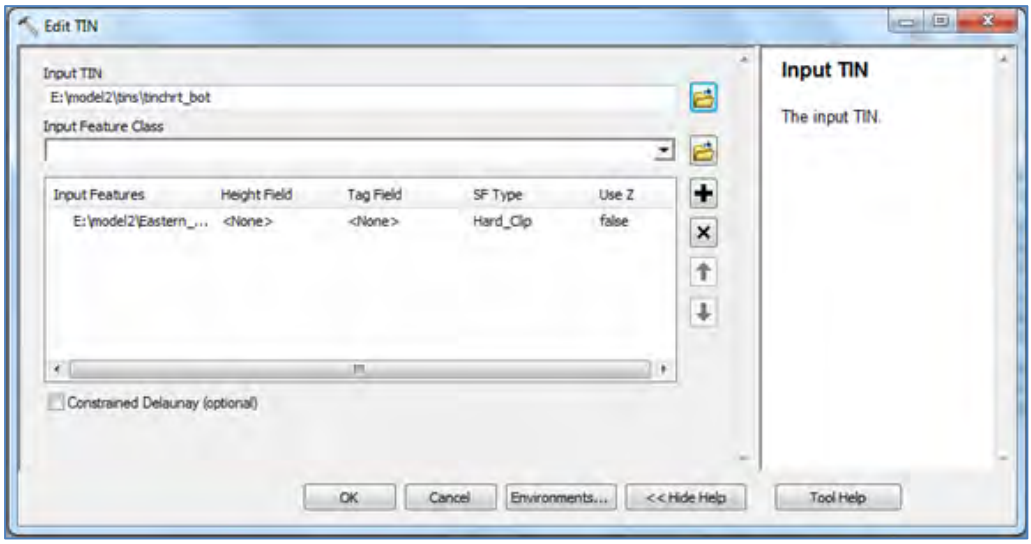


**Figure 3.16: Illustration of how the fields within the Edit TIN Tool should be**

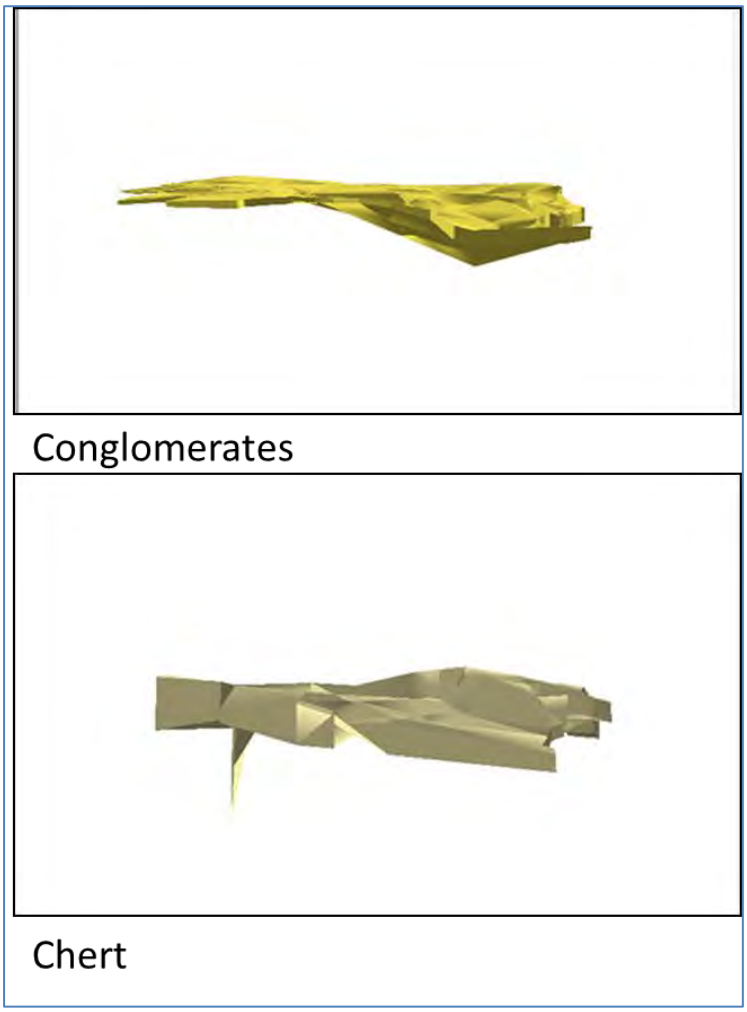


**Figure 3.17: This shows the completed layers for the Conglomerates and Chert for Model A(a)**

Model A(b) will consist of the geological polygon layers created from the average depths provided by SACS and the average thicknesses derived from the newly created lithostratigraphic column in section 2.5. The East Rand Basin's polygon feature class will be used for each of these geological layers, due to the fact that they will only be seen as "basic" layers, because data containing these depths where not available. These layers consist of the Alberton, Mondeor, Elsburg, Doornkop, Booysens, Randfontein and the Main Conglomerate Formations. A z-value field, to which the depth will be added, will be created / added to the attribute table of each geological layer. This will locate the polygon of these layers to their own specific depths. After creating these polygons, they will be extruded to their own specific thickness, which are derived from the new lithostratigraphic column.

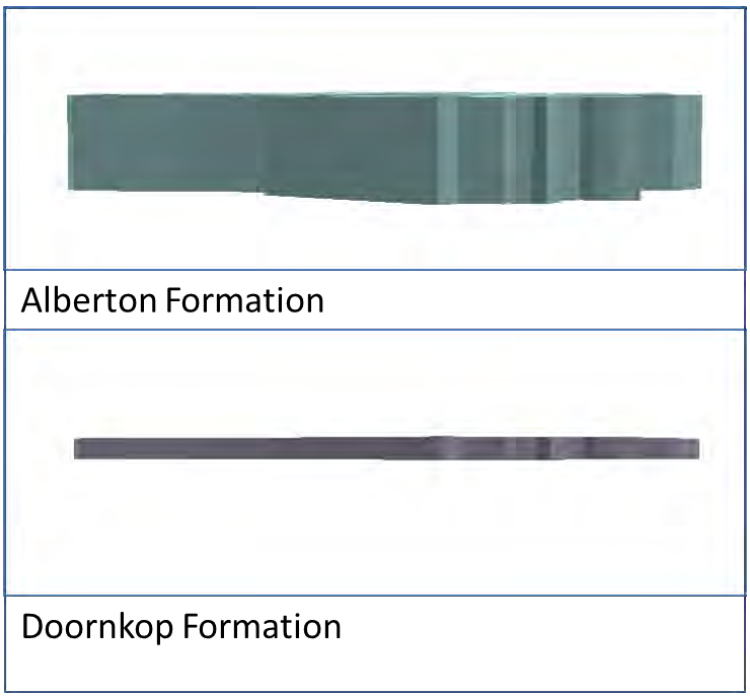


**Figure 3.18: This shows the completed layers for the Alberton Formation and Doornkop Formation for Model A(b)**

When it comes to model A(c) the provided Main Reef, Black Reef and Kimberley Reef DEMs would need to be converted to a TIN (Figure 3.19), after which the TIN would be converted to a polygon. To create the TIN from each DEM the "Raster To TIN Tool" is used. According to ESRI (2013) the "Raster To TIN Tool" creates a TIN from the input raster points to cover the full perimeter of the raster's surface. The raster points are known to be the centre point of each cell / pixel. The TINs are then clipped in the same way as the TINs from Model A(a). After creating the TIN, the "TIN Edge Tool" is used followed by the "Feature To Polygon Tool". The polygons will then be extruded to the maximum average thickness derived from the newly created lithostratigraphic column (Figure 2.18):

- Black Reef = ± 30 meters
- Main Reef = ± 90 meters
- Kimberley Reef = ± 250 meters

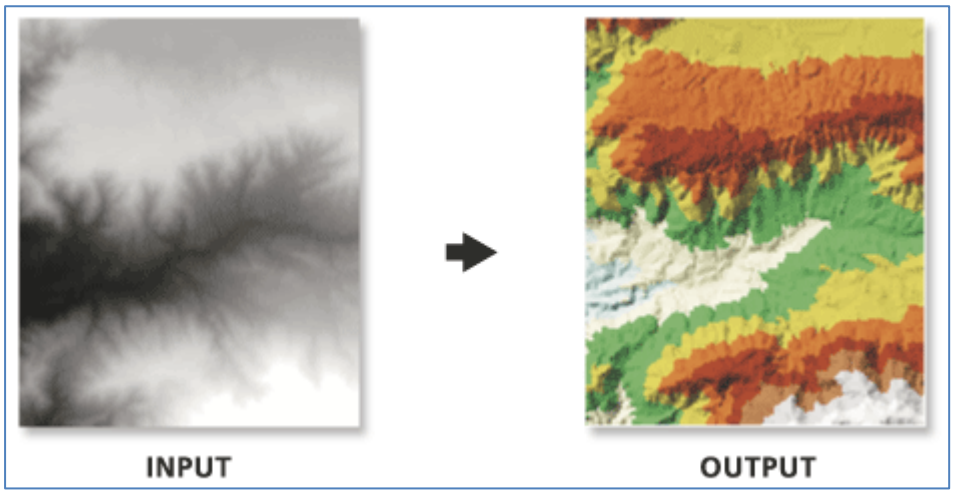


**Figure 3.19: DEM to TIN conversion example (ESRI, 2013)**

Below is the result of the Black Reef after extrusion. The other two Reefs' results will be given in Chapter 4.

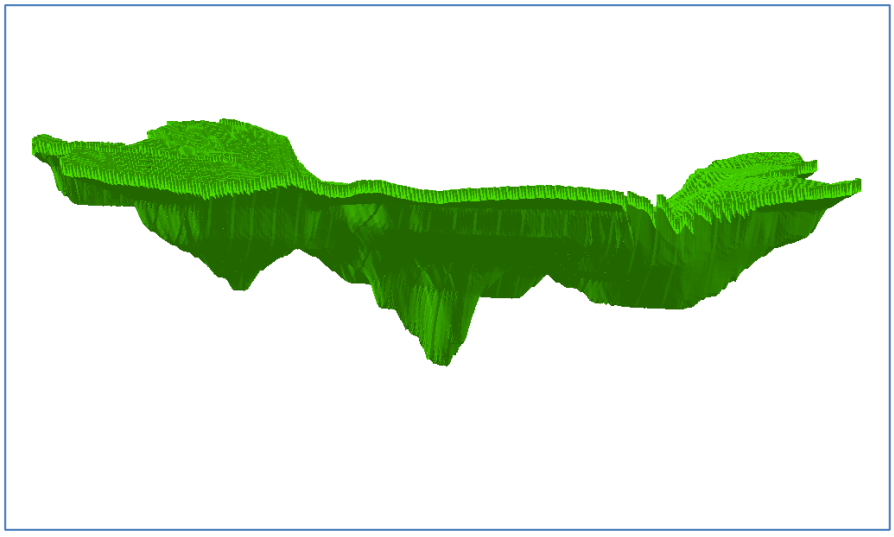

**Figure 3.20: The completed Black Reef layer for Model A (c)**

#### 3.4.4.2 Model B

The second model, model B, is based on the same principles as the first model, but consists of a few more steps and tools. The clipped TINs created from the first model can be used here. The first step to building this model is to delete all the breaklines that are found on top of the TIN surfaces, except for boundary breaklines. This should result in a smoother surface than those of Model A(a), when the "Extrude Between Tool" is used. These breaklines can be deleted by making use of the "Delete TIN Breakline Tool" found under the "TIN Editing Taskbar".

This taskbar only works in ArcMap. After the breaklines are deleted (see Figure 3.21), the same extrusion processes from Model A(a) can be followed to complete the layers for this model.

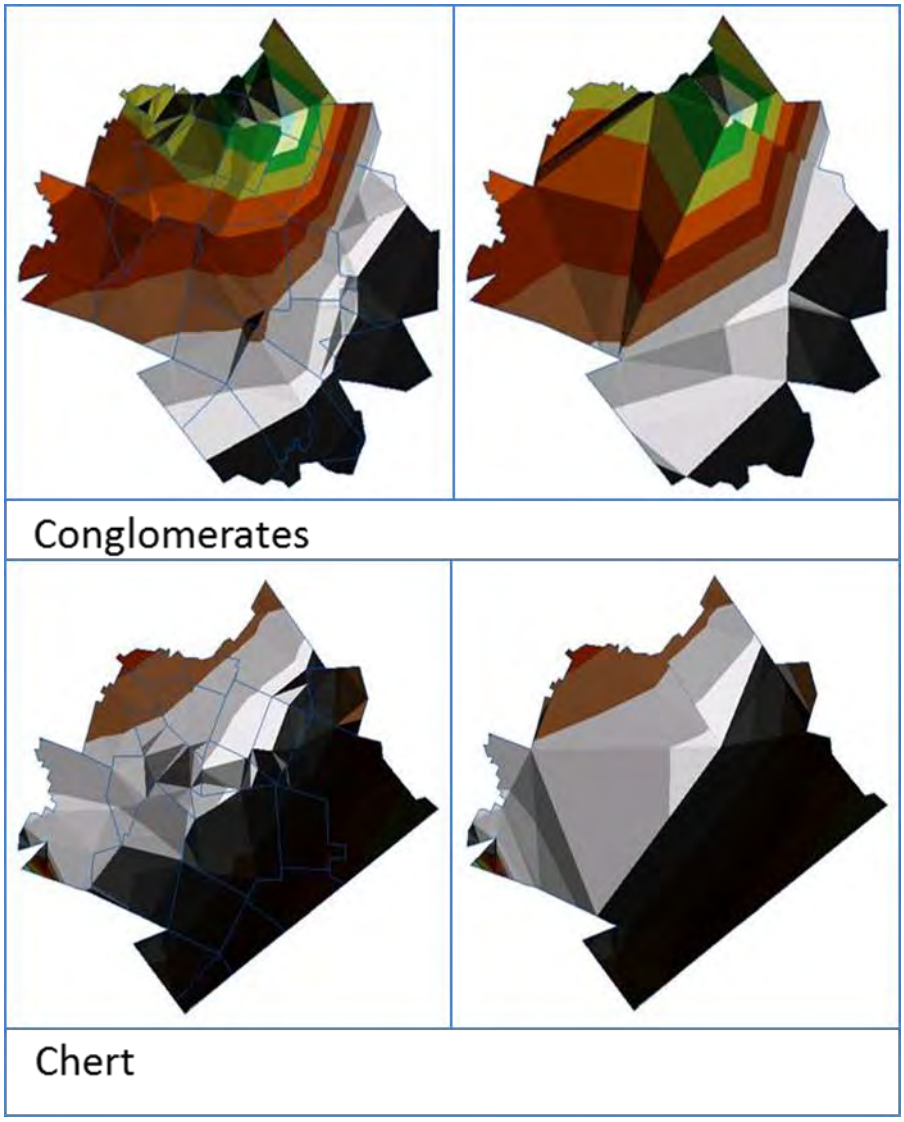


**Figure 3.21: Illustration of how the breaklines should be deleted without deleting the boundary breaklines (Model B)**


**Figure 3.22: This shows the completed layers for Conglomerate and Chert (Model B)**

#### 3.4.4.3 Model C

Model C will be a more advanced type of model, due to the fact that it will be created by making use of Empirical Bayesian Kriging (EBK). This Kriging method is used to create a DEM surface of the top and bottom depths of each geological layer. After creating these DEMs, each DEM will be converted to a TIN by using the "Raster To TIN Tool". After these TINs are created the TINs will undergo the same processes / steps as under Model A (a) but instead of the East Rand Basin's polygon feature the New Area polygon feature will be used to extrude between the TINs. The reason for this is that when the DEM, which was created through Kriging, is converted to a TIN file, the clip method selects the area as a square and not the shape of the study area and therefore the study area will be too small to extrude.

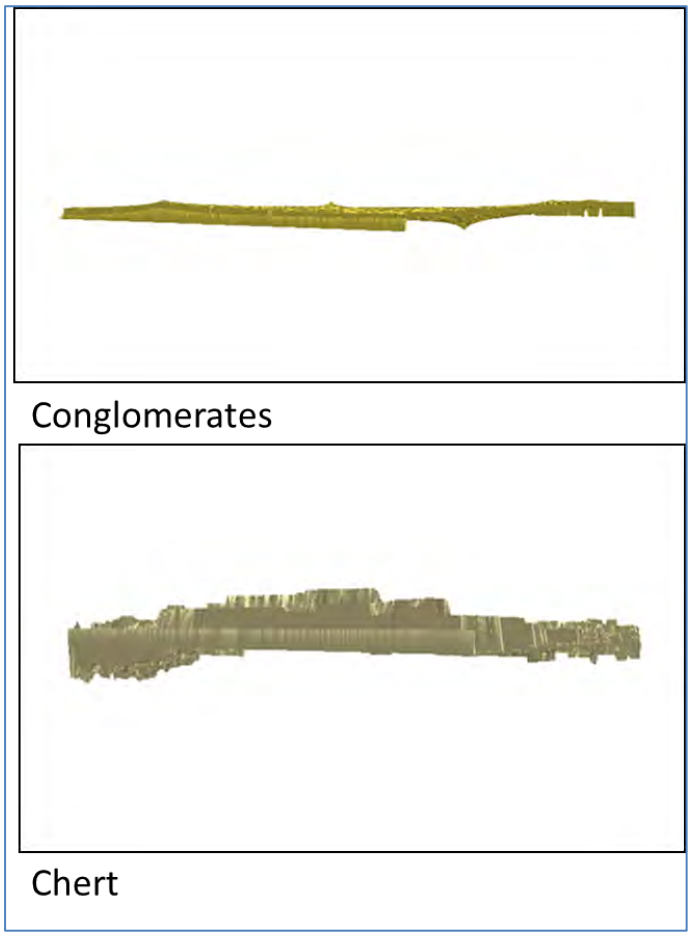


**Figure 3.23: This shows the completed layers for Conglomerate and Chert (Model C)**

If the chert and conglomerate layers form the various models are compared, it can be seen that Model A(a) and B look almost the same, but Model C differs substantially. The reason for this will be described in the chapter that follows.

# Chapter 4: Results

## 4.1 Introduction

The following chapter will deal with the quality of the data and the results of the various ArcGIS spatial analysis methods. Each model's results, the time it took to complete the model, and findings for each model will be given. Only the three main models, Model A(a), B and C, will be compared with one another and other geological cross-section maps to determine their accuracy at the end of this chapter.

## 4.2 Data restrictions

When it comes to the borehole data points and the various methods, the more borehole data points and the deeper the boreholes, the more accurately the geological layers will be mapped. For this study it was found that the total borehole data points that fall within the study area were not enough to ensure a very accurate 3D geological model. Therefore a new polygon (named New Area), which is an area bigger than the study area, was used to select more boreholes for the study (see Figure 4.1). The size of the New Area polygon, 52 km x 52 km, was determined randomly. Selecting this area had a positive influence because more boreholes containing more data about the various geological layers could be selected. This was done because the more data is used, the more accurate the model will be.

Figure 4.1 below clearly indicates that the number of borehole data points within the study area is far less than those that fall within the New Area polygon. Not only does it indicate that the data of the study area is less, but it also indicates that the borehole data points are unevenly distributed. Due to the uneven distribution of the borehole data points, cluttered points are found to the north-western and western parts. The reason for this can be that there are many users contributing (uploading their data) to the National Groundwater Archive Geodatabase in these cluttered areas. A comparison between the study area and another area with more evenly distributed boreholes within the North-west Province is shown in Figure 4.2.

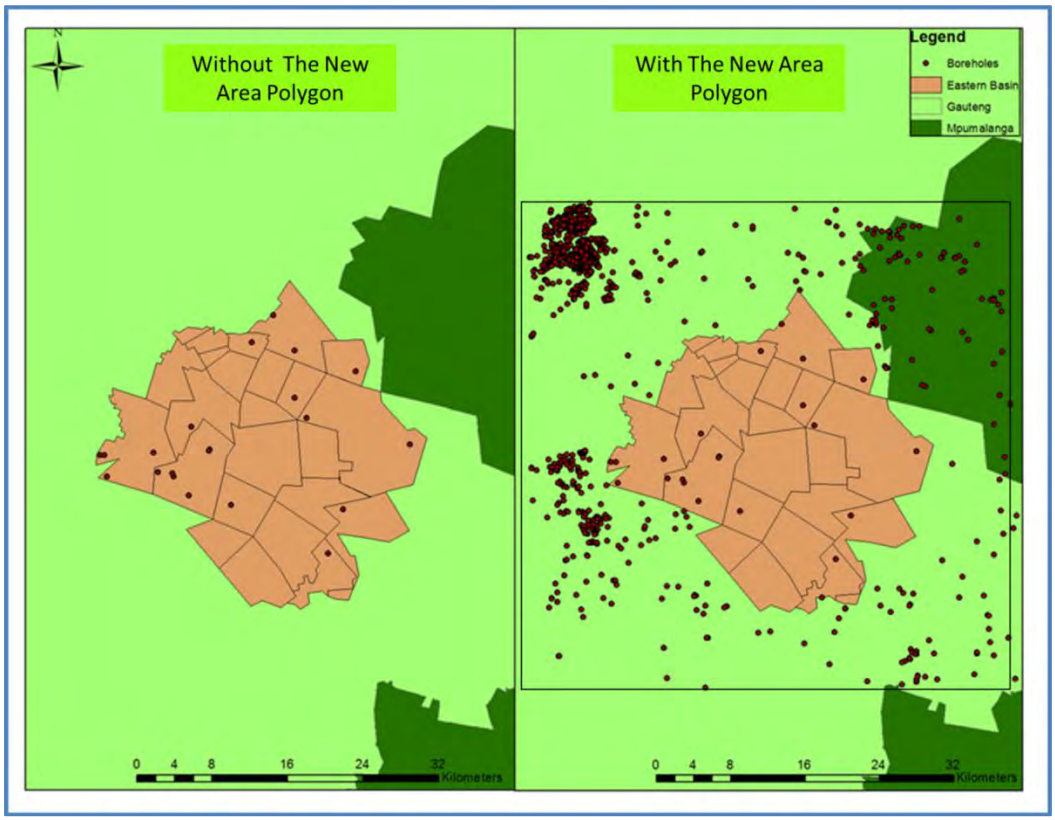


**Figure 4.1: Number of boreholes with and without the New Area polygon.**

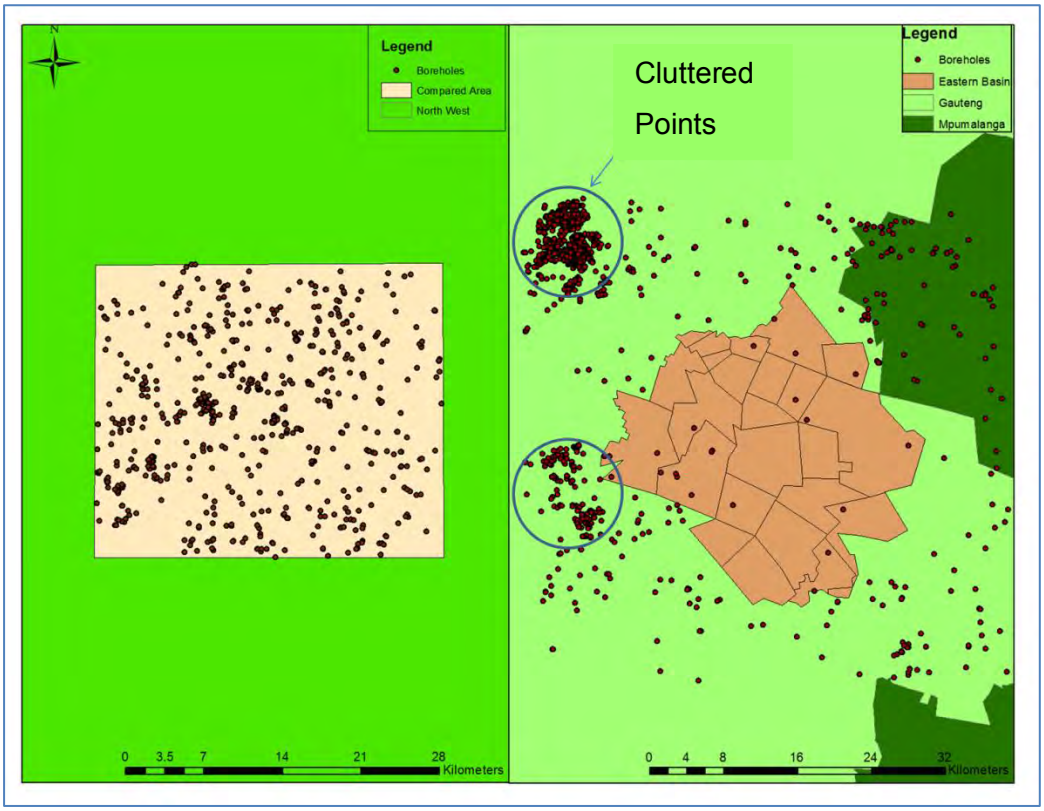


**Figure 4.2:** **Illustration between a more evenly and unevenly distributed data and clusters.**

Challenges with the data were encountered when it came to working with the various depths, because the depths provided by the National Groundwater Archive Geodatabase are an indication of the distance from the surface and not the distance from sea-level. The problem is that it is difficult to link the geological layers to their associated groups and subgroups within a stratigraphic column found in the literature. These columns usually indicate where each group and subgroup is located from the sea-level whereas the borehole data gives the distance from the surface. This then leads to the study of topographic maps in order to determine the surface height of the study area above sea-level. Knowing this height will make it easier to match the geological layers from the borehole data with the stratigraphic columns.

The borehole depths were found to be too shallow since the boreholes were only drilled for hydrological research. The deepest borehole reaches a depth of -351 m and the depth to which the model should be built is that of the Main Reef formation, reaching a depth of -2 330 m. The DEMs of the Main Reef, Black Reef and Kimberley Reef provided by the North-West University were found to be accurate, although it provided only a single depth – the bottom depth – and not both the top and bottom depths. This made it a very limited data source; these limitations will be explained under the results of Model A(c).

The depths derived from the SACS Task Group were found to be accurate, but it also provided the study with some limitations due to the fact that an average depth is provided for each geological layer. The problem with this is that the whole layer will be one solid block with no depth variations across the bottom and top surface; therefore, each of these layers will be inaccurate. To eliminate this, point data for each of these geological layers need to be created. This type of data should be in the same format, containing x, y and z data, as those of the National Groundwater Archive Geodatabase. This will lead to an indication of where the surface for each layer changes and at what depth the specific layer is found.

### 4.3 Results of the ArcGIS spatial analysis methods.

It was found that building a very accurate 3D geological model with the limited data, the various data sources and their own accuracies, and without any help from extension tools, is not possible; however, by using the available data and tools, three basic 3D geological models could be created. The results, the time it took to complete the model, and the findings for each model will be explained below. The results of the conglomerate and chert layers will be used as examples. These two layers were chosen randomly to use as examples. The various types of views that will be used to illustrate the models and their layers and the north to south line used for the profile graphs under 3.3.4, can be seen in Figure 4.3.

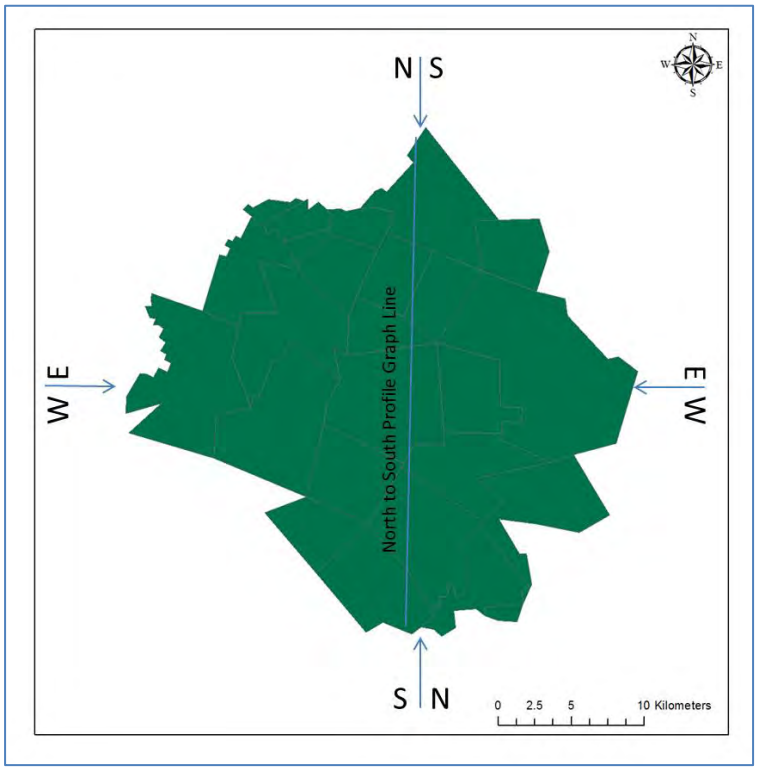


**Figure 4.3: Illustration of the various views**

### 4.3.1 Model A

**Model A (a)** - Creating the corresponding top and bottom depth TINs for each geological layer (Table 4.1) took about two hours to complete, but various geological layers such as alluvium, diamicite and schist could not be completed. The reason for this is that there are less than three boreholes containing these geological layers, and the "Create TIN Tool" needs three or more borehole points to effectively create a TIN surface. There are two main reasons for this shortage of borehole points for the alluvium, diamicite and schist geological layers. Firstly, some of the geological layer boreholes are found close to the boundary while the rest of the data fall outside of the New Area polygon. Secondly, the boreholes fall within an area where there are less boreholes drilled, and therefore there are less data found for these layers (see Figure 4.4 for their spatial location, together with Figure 4.5 for their attribute tables). Using the "Edit TIN Tool" for clipping purposes was effective, but it also took another two hours. The reason for taking two hours was that with each TIN, the fields had to be changed. Using the "Extrude Between Tool" was quick and effective and no problems were experienced here. The time it took using this tool was less than an hour.

**Table 4.1: The created top and bottom depth TINs for the Conglomerate and Chert layers.**

*Take note: ArcScene does not allow one to add a scale or a north arrow like ArcMap, as in ArcScene images are exported through image grab. Therefore the top view is North (top) to South (bottom) and the bottom view is West (left) to East (right).*

| | Top Depth Top View | Top Depth Side View | Bottom Depth Top View | Bottom Depth Side View |
|---|---|---|---|---|
| Conglomerate |  |  |  |  |
| Chert |  |  |  |  |

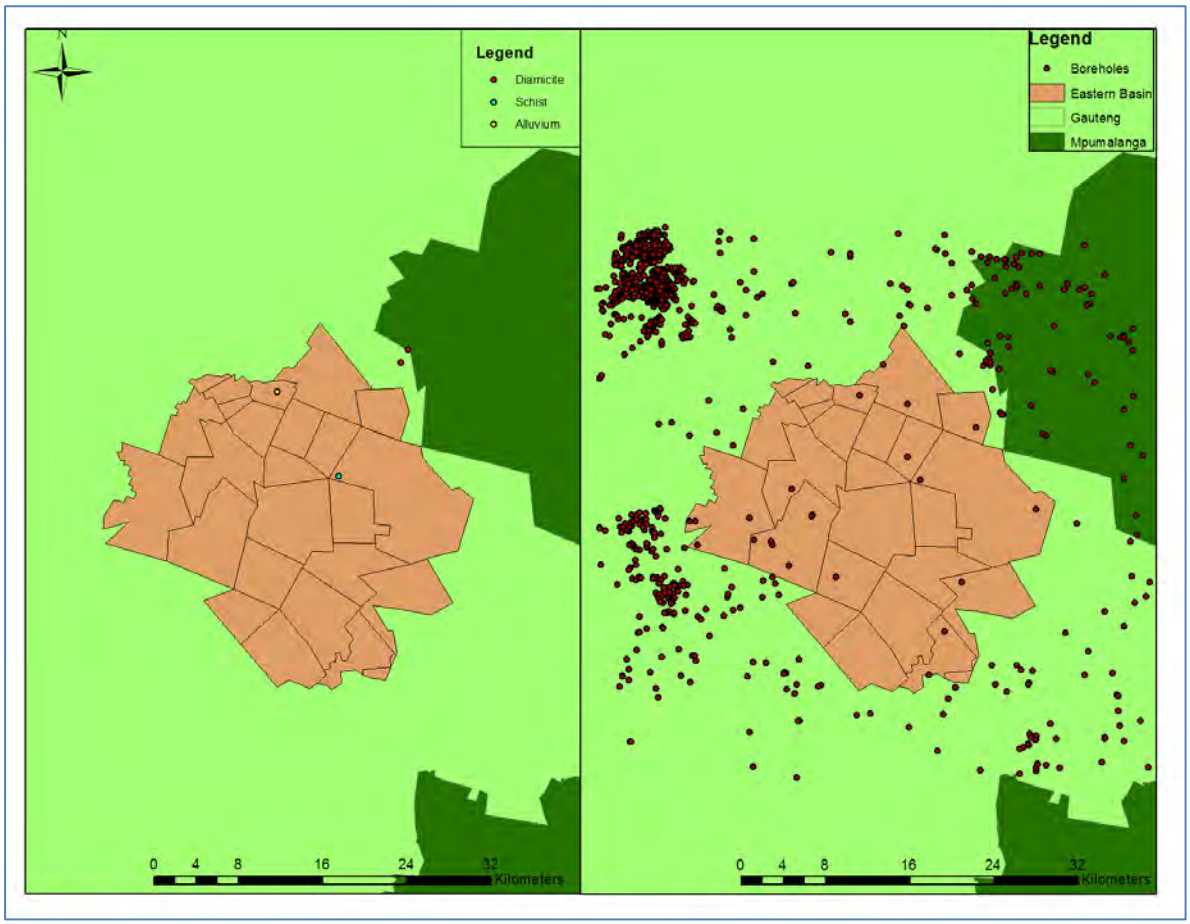


**Figure 4.4: The spatial distribution of the undisplayable layers**

Schist

| FID | Shape * | GEOLOGY_Si | DateTimeMe | DepthTop | DepthBot | Lcode | x | y |
|---|---|---|---|---|---|---|---|---|
| 0 | Point | 2628AB00022 | | -105 | -120 | SCST | 28.45972 | -26.24999 |

Alluvium

| FID | Shape * | GEOLOGY_Si | DateTimeMe | DepthTop | DepthBot | Lcode | x | y |
|---|---|---|---|---|---|---|---|---|
| 0 | Point | 2628AB00036 | | 0 | -21 | ALVM | 28.4075 | -26.17806 |
| 1 | Point | 2628AB00037 | | 0 | -12 | ALVM | 28.40751 | -26.17806 |

DMCT

| FID | Shape * | GEOLOGY_Si | DateTimeMe | DepthTop | DepthBot | Lcode | x | y |
|---|---|---|---|---|---|---|---|---|
| 0 | Point | 2628BA00371 | | -14 | -16 | DMCT | 28.51306 | -26.15333 |
| 1 | Point | 2628BA00372 | | -54 | -57 | DMCT | 28.51917 | -26.1425 |

**Figure 4.5: The attribute tables of the undisplayable layers**

**Model A (b) -** This model was the quickest to build of all the models. It took about one hour to complete this model. The layers from this model are even, smooth, neat and solid. The reason for this is that each layer contains an average depth to which it is extruded. The problem with this is, as mentioned under 4.2., the whole layer is one solid block with no depth variations

across the bottom and top surface; therefore, no geological structures will be visible and because of this the layers can be classified as inaccurate. The exact placement of each geological layer could also be inaccurate, due to the fact that each layer covers the whole basin as the layers were created using the East Rand Basin's polygon feature class. An open space was also found in this model, but this space is where the Black Reef layer is supposed to be situated. This reef was not included in this model because it was created under Model A(c).

**Model A (c) -** This was a quick model to build. It took less than an hour to convert the three provided DEMs to TINs and to clip the TINs to the East Rand Basin's polygon feature class (see Table 4.2). The limitation or problem with this model was the fact that the DEMs contained only bottom depth data and no top depth data, leading to no top depth TIN being created to which a polygon could be extruded. Therefore the polygon had to be extruded to the maximum average thickness that was derived from the newly created lithostratigraphic column. By doing this the layers could also be said to be inaccurate because some features, such as how the layer has been mined, will not be visible.

**Table 4.2: The DEMs and TINs of the three Reefs**

*Take note: ArcScene does not allow a user to add a scale or a north arrow like ArcMap as in ArcScene images are exported through image grab. Therefore the top view is North (top) to South (bottom) and the bottom view is West (left) to East (right).*

| | Black Reef | Kimberley Reef | Main Reef |
|---|---|---|---|
| DEM |  |  |  |
| Top View | 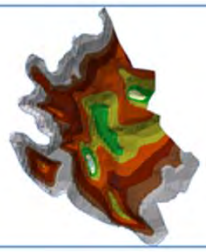 |  | 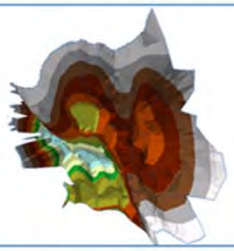 |
| Side View |  |  | 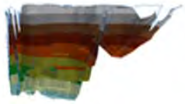 |

**Table 4.3: The completed layers for all three Reefs**

| | Black Reef | Kimberley Reef | Main Reef |
|---|---|---|---|
| S-N View |  |  |  |
| N-S View |  |  |  |
| Top View |  |  |  |

A disadvantage of creating the polygon layers from the TIN surfaces that had been created from the DEMs is that various lines are visible on the top surface. These lines are the edge lines from a TIN surface which was created through connecting the raster points (see 3.4.4.1.). The result is that these lines make the top surfaces look less smooth and more “distorted’ than the bottom surfaces. This can be seen from Table 4.3 above where the top surfaces of the Main Reef looks darker (S-N View) than the smoother bottom surfaces of the Main Reef (N-S View).

### 4.3.2 Model B

Using the “Delete TIN Breakline Tool” is easy and effective, but it took about four to five hours to delete al the breaklines’ lines. The reason for this is that each breakline had to be selected and deleted separately. Another time-consuming problem was that the TIN be edited had to be selected under the “3D Analyst Taskbar” before the tools of the “TIN Editing Taskbar” is activated. This leads to another problem of the editing process not being kept activated for all the TIN surfaces together; it requires the stop of the editing process after each TIN and the start of each editing process before each new TIN surface. The result after the polygons were extruded between the top and bottom depth for each specific geological layer indicated a smoother surface compared to those of Model A(a).

### 4.3.3 Model C

The problem with this model was that it was similar to creating a TIN surface. The Empirical Bayesian Kriging method also requires a number of borehole points to be available for the interpolation, but the Kriging method requires more than a TIN surface. The need for more borehole points resulted in an additional four uncompleted geological layers to those layers mentioned in 4.3.1. These four layers include breccia, calcite, ferricrete and seyenite. The Empirical Bayesian Kriging proved to be sufficient and effective when it came to interpolating the rest of the data, but this method was also quite time-consuming. It took about two hours to interpolate the top and bottom depth data for each remaining geological layer. Converting these DEM surfaces to TINs using the “Raster To TIN Tool” was quick and easy and took less than an hour.

When it came to the clipping of the TINs, it was found that the TINs are not clipped to the shape of the East Rand Basin’s polygon feature, but instead the TINs are clipped in a form of a square (see Table 4.4). The reason for this could be that the interpolation results in a form of a square and after the clipping method a square is produced in order to keep this interpolation results accurately. After the clipping was done, it was found that the top depth TINs were smaller than those of the bottom depth TINs (see Table 4.4), but this had no effect on the results of each layer. Extruding with the East Rand Basin’s polygon feature was impossible because it was found to be smaller than the clipped features and therefore the New Area polygon was used. This extrusion was quick and effective and took less than an hour.

**Table 4.4: Results of the TINs that were created from DEMs**

*Take note: ArcScene does not allow a user to add a scale or a north arrow like ArcMap as in ArcScene images are exported through image grab. Therefore the top view is North(top) to South (bottom) and the bottom view is West (left) to East (right).*

| | Clipped | TIN Top and Bottom Compare | TIN Top and Bottom Side View |
|---|---|---|---|
| Conglomerate |  |  |  |
| Chert | 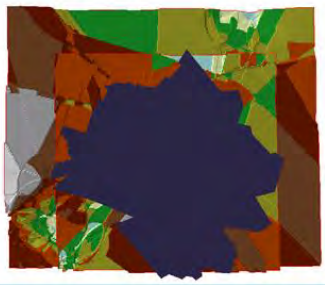 | 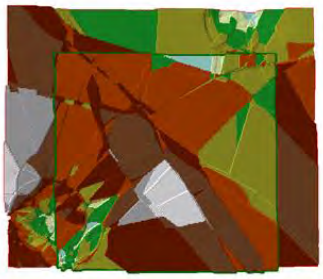 |  |

### 4.3.4 Comparing the models with each other and with geological cross-sections

By comparing the north to south profile graphs (Figures 4.6 and 4.7) of the bottom and top depth TINs that were produced by the various models, it was found that there are no similarities between them. The reason for this is the way each TIN was created. For Models A(a) and B the normal TIN method created triangles with nodes and edge lines from the borehole point data, as explained under Chapter 3.2, and the TINs that where created from a raster surface (DEM) had to create triangles from raster points (explained under 3.4.4.1). Using these raster points which have far more points than those used by the Models A(a) and B, resulted in a uneven profile graph. Some similarities are visible between the profile graphs of Model A(a) and Model B, as the TINs that were used to delete the breaklines from Model B are the same TINs used in Model A(a).

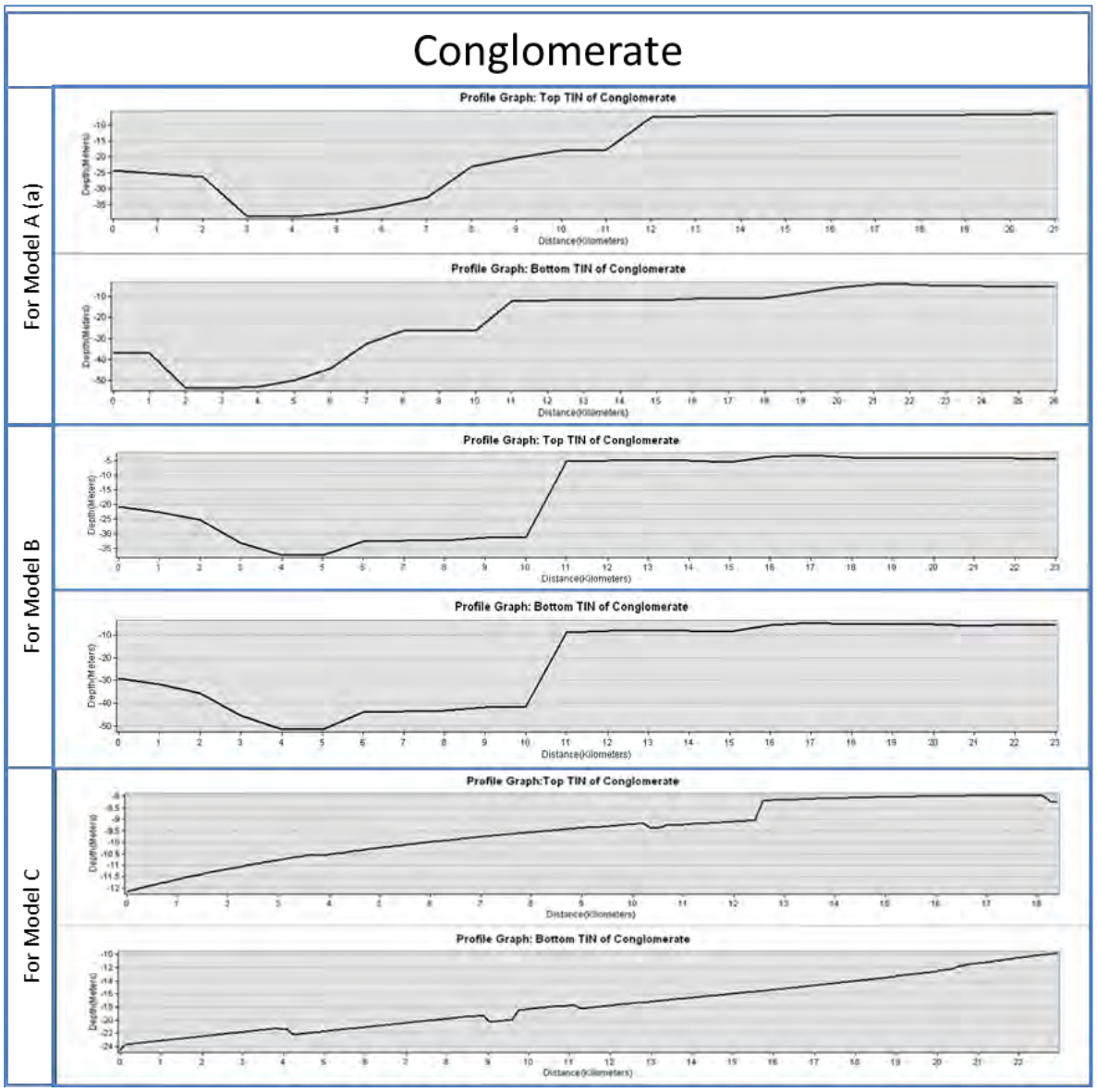


**Figure 4.6: Profile graph of the Conglomerate TIN surfaces of the various models**

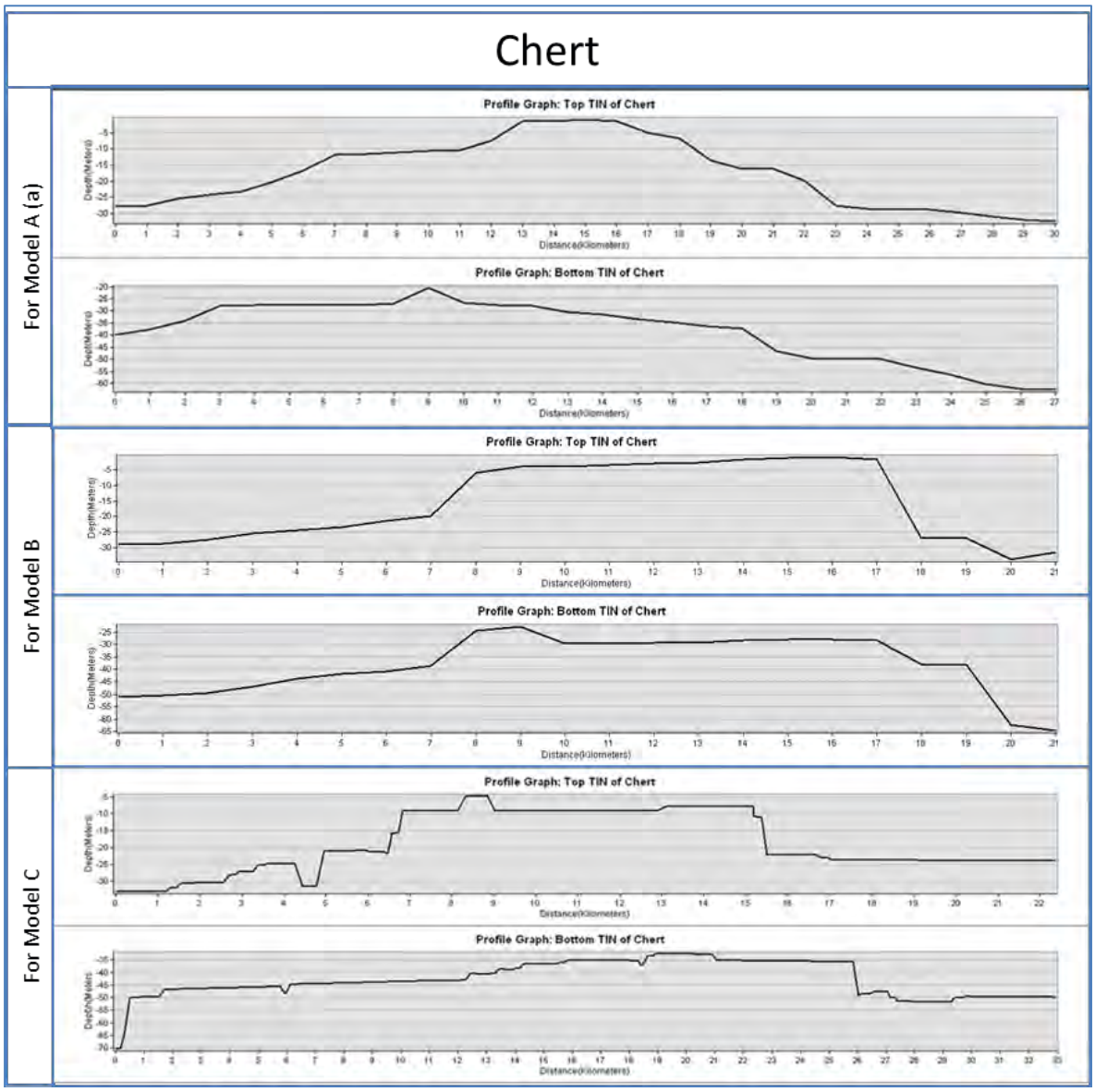


**Figure 4.7: Profile graph of the Chert TIN surfaces of the various models**

*Take note: ArcScene does not allow a user to add a scale or a north arrow like ArcMap as in ArcScene images are exported through image grab. Therefore the views are as follow South to North (S-N), North to South (N-S), East to West (E-W) and West to East (W-E).*

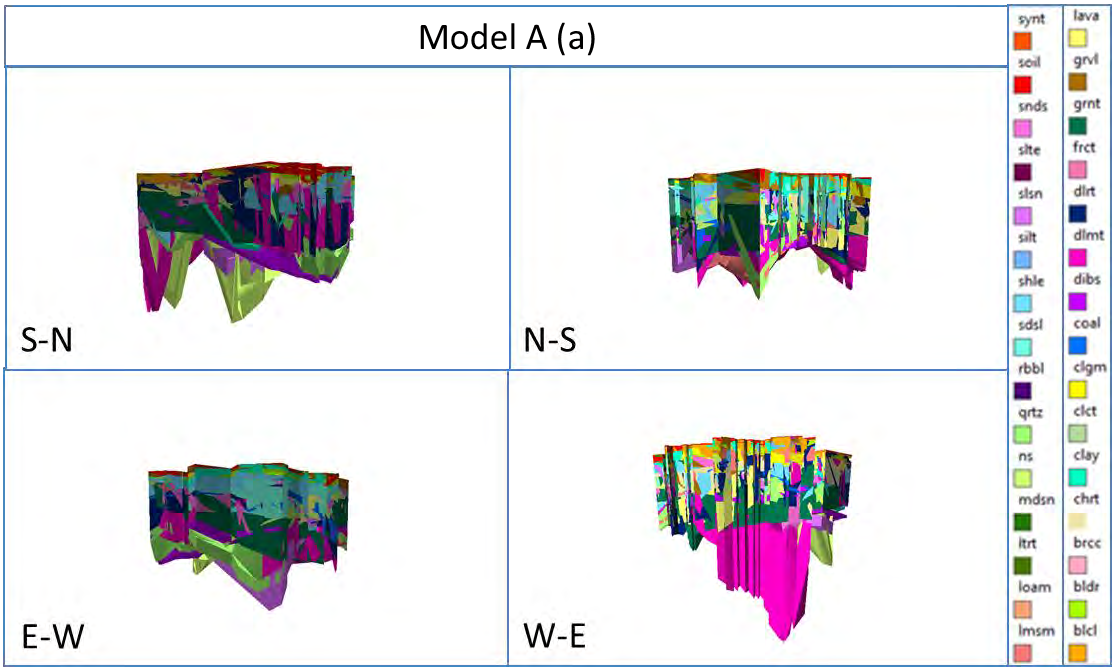


**Figure 4.8: Model A (a) (Annexure I)**

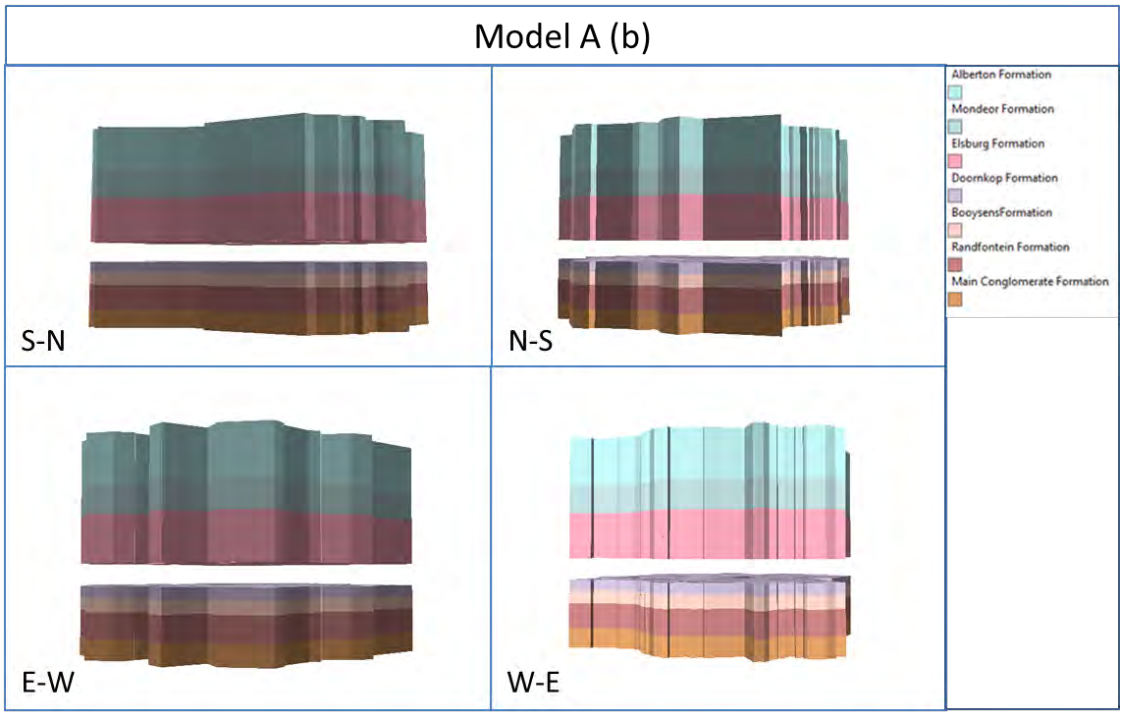


**Figure 4.9: Model A (b) (Annexure J)**

*Take note: ArcScene does not allow a user to add a scale or a north arrow like ArcMap as in ArcScene images are exported through image grab. Therefore the views are as follow South to North (S-N), North to South (N-S), East to West (E-W) and West to East (W-E).*

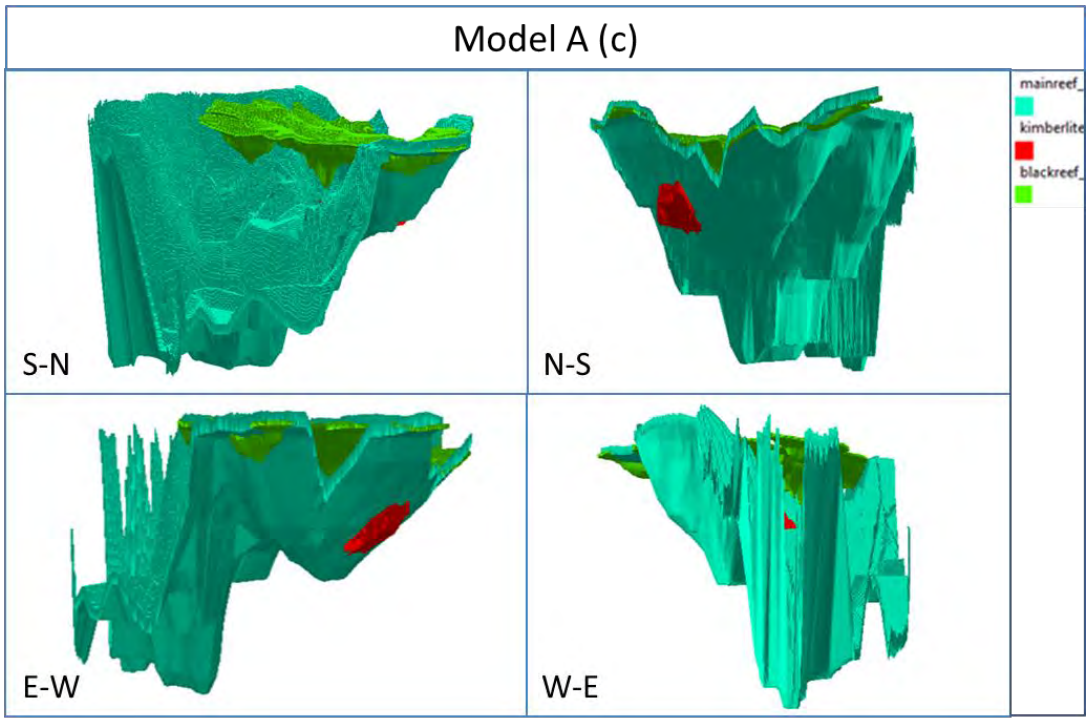


**Figure 4.10: Model A (c) (Annexure K)**

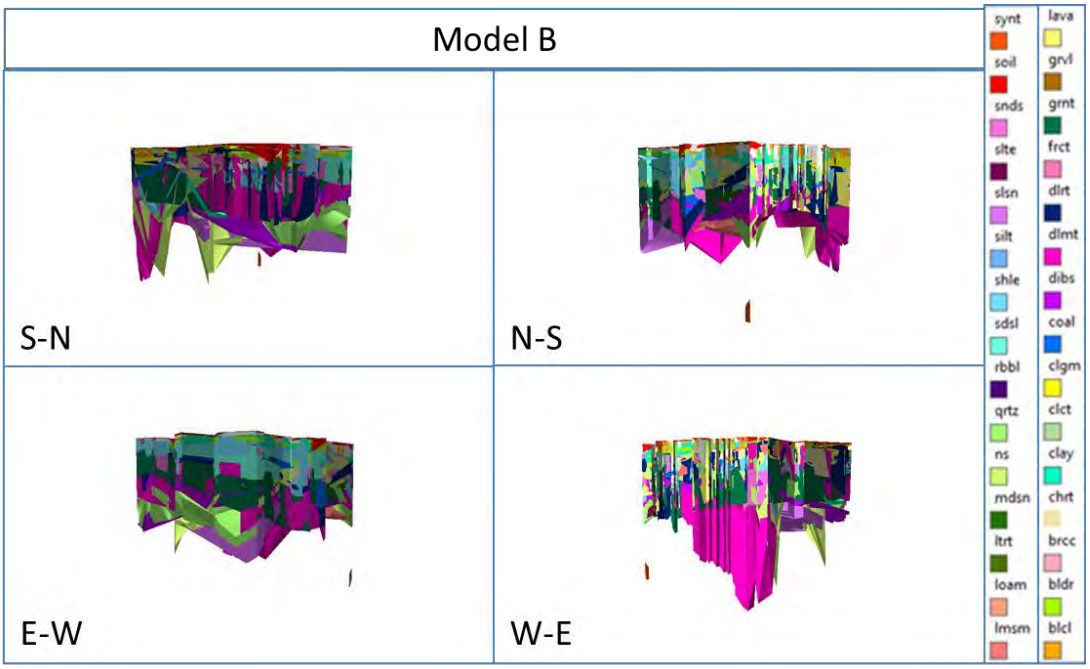


**Figure 4.11: Model B (Annexure L)**

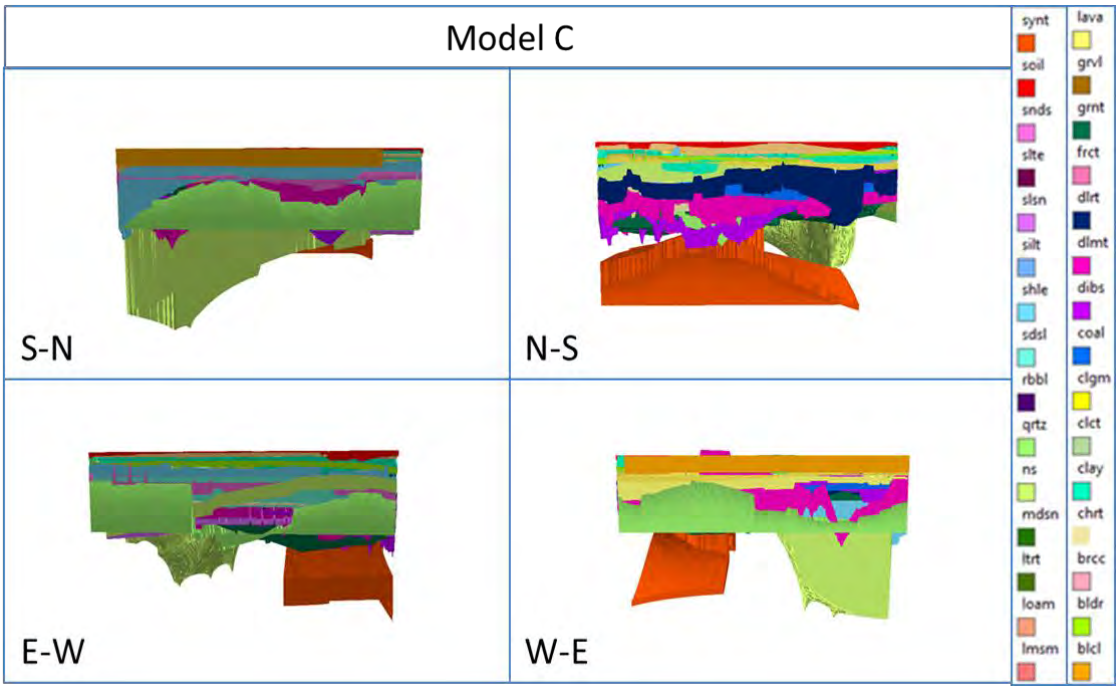


**Figure 4.12: Model C (Annexure M)**

By comparing the various completed models – Model A(a), Model B and Model C – created from the National Groundwater Archive Geodatabase's borehole points, it can be seen that their various angles look quite "chaotic". The reason for this is the boundary lines that cut through one another. It cannot be determined which model, Model A(a), Model B or Model C, is more accurate than the other, since there are no cross-sections available in the literature that indicate the various geological layers of the Karoo and Transvaal Supergroups within the East Rand Basin. However, through an own opinion it can be said that Model C is the most accurate of the three; unlike a TIN that only connects the points, Model C was created using the Kriging method. This method predicted the values of points for which there was no information using the data from the sample points with information. Through this process the Kriging method also attempted to get the error or mean residual close or equal to 0.

Although no cross-sections are found containing the geological layers of the Karoo and Transvaal Supergroups, cross-sections indicating the Black, Kimberley and Main Reef are found in the literature. These available cross-sections will be compared below to the profile graphs of the various reefs. The reason for using profile graphs is that ArcGIS does not come with a cross-section tool although such tools can be purchased. ArcGIS does include a profile graph which draws a surface profile of a TIN. The bottom depth TINs of each reef will be used to create these graphs. Figure 4.13 is an indication on how the cross-sections were taken for the

two cross-sections used below. The same “ABC” and “ab” lines will be used to create the graphs.

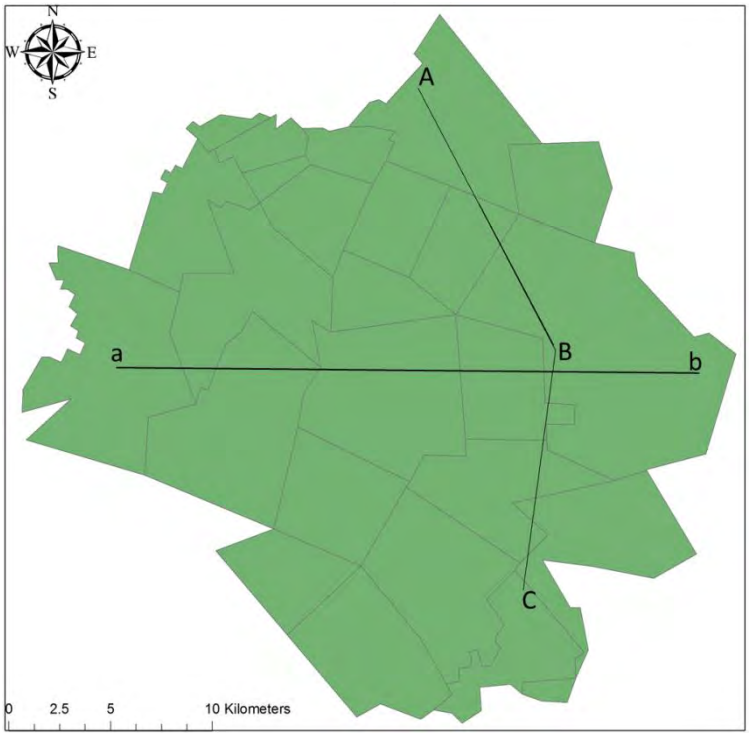


**Figure 4.13: Illustration of the cross-section lines used by DWA (ABC line) and Pitts (ab line).**

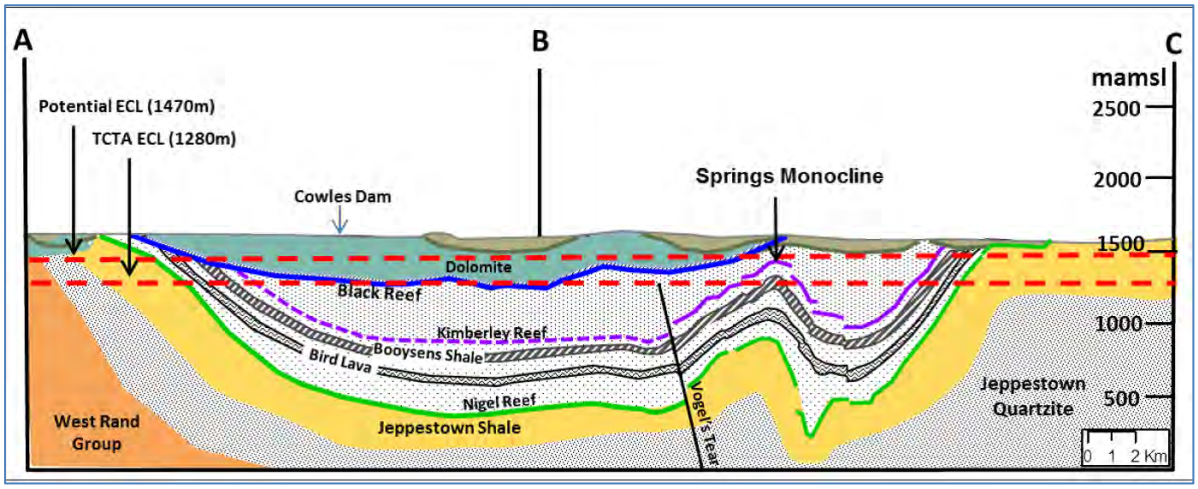


**Figure 4.14: A cross-section in the Eastern Basin in the vicinity of the Blesbokspruit (DWA, 2013).**

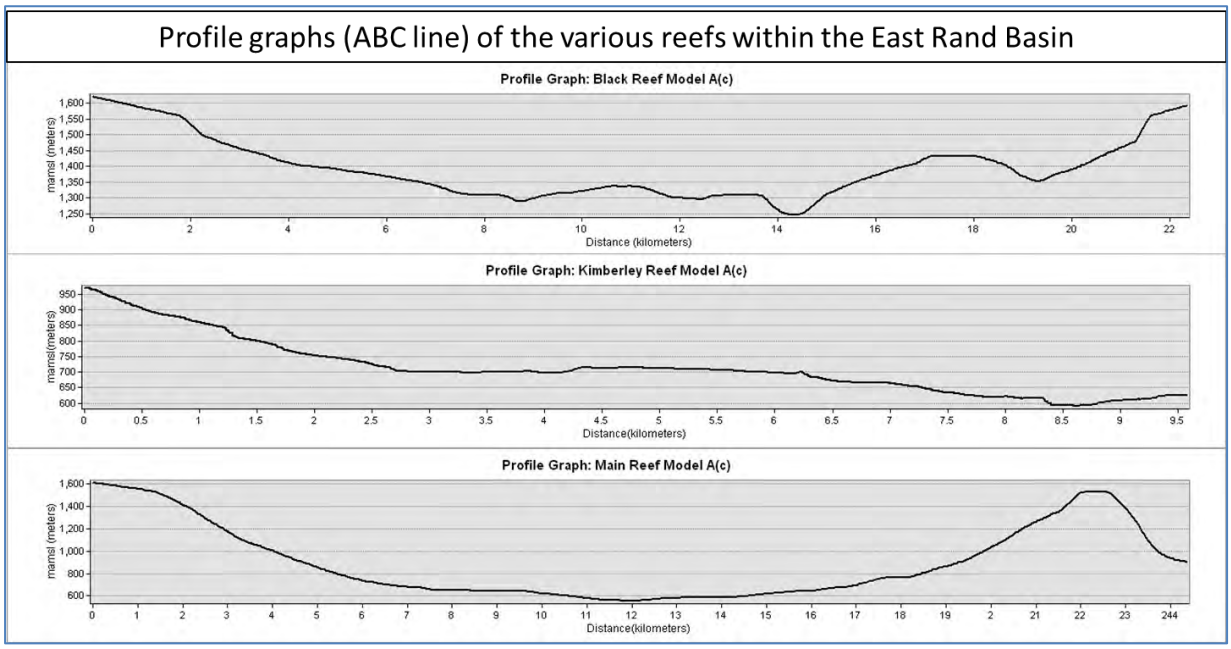


**Figure 4.15: Profile graphs (ABC line) of the various reefs within the East Rand Basin**

By comparing the cross-section ABC from DWA (Figure 4.14) with the profile graphs of the various reefs (Figure 4.15), it can be said that these layers are quite accurate, since all the layers show the same concave upward nature. The Black and Main Reefs' profile graphs also indicate the same climax of the Springs Monocline, which is illustrated by the Black and Main (Nigel) Reef in Figure 4.14.

Below, the cross-section AB (Figure 4.16) that was designed by Pitts (1990) is compared to the profile graphs of the various reefs within the East Rand Basin (Figure 4.17). Due to the absence of the Black Reef in the AB cross-section, the Black Reef's profile graph can't be compared, but it can be given the accurate status due to the fact that its profile also shows the same upward concave nature as the Kimberley and Main Reef in Figure 4.16. The Main Reef's profile graph can also be said to be accurate since it indicates the same concave upward nature and has almost the same profile line as in the AB cross-section.

The Kimberley Reef's profile graph does not indicate any conformity to the two cross-sections and therefore it cannot be said to be accurate in terms of the whole East Rand Basin. The reason for this is that the Kimberley Reef's DEM, which was provided by the North-West University, only covers a certain area in the East Rand Basin on which they did research. Therefore the DEM itself cannot be seen as inaccurate.

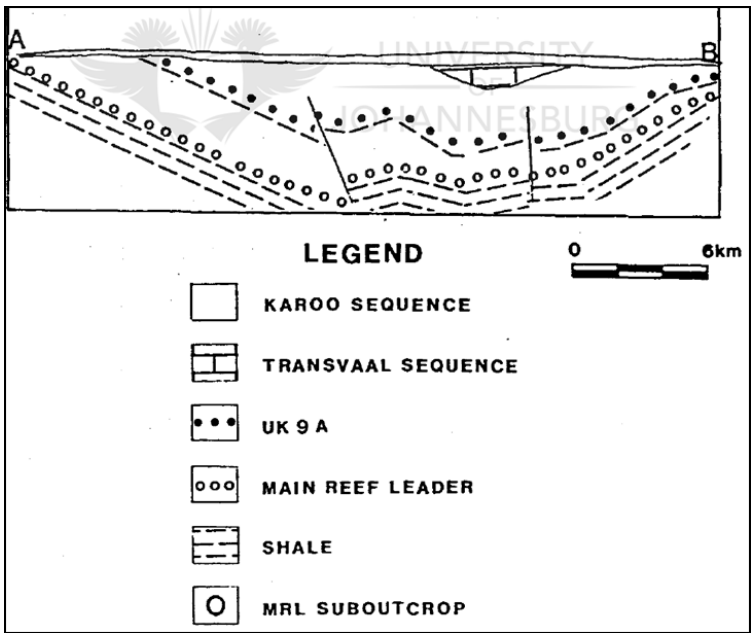


**Figure 4.16: Cross-section in the Eastern Basin (Pitts, 1990)**

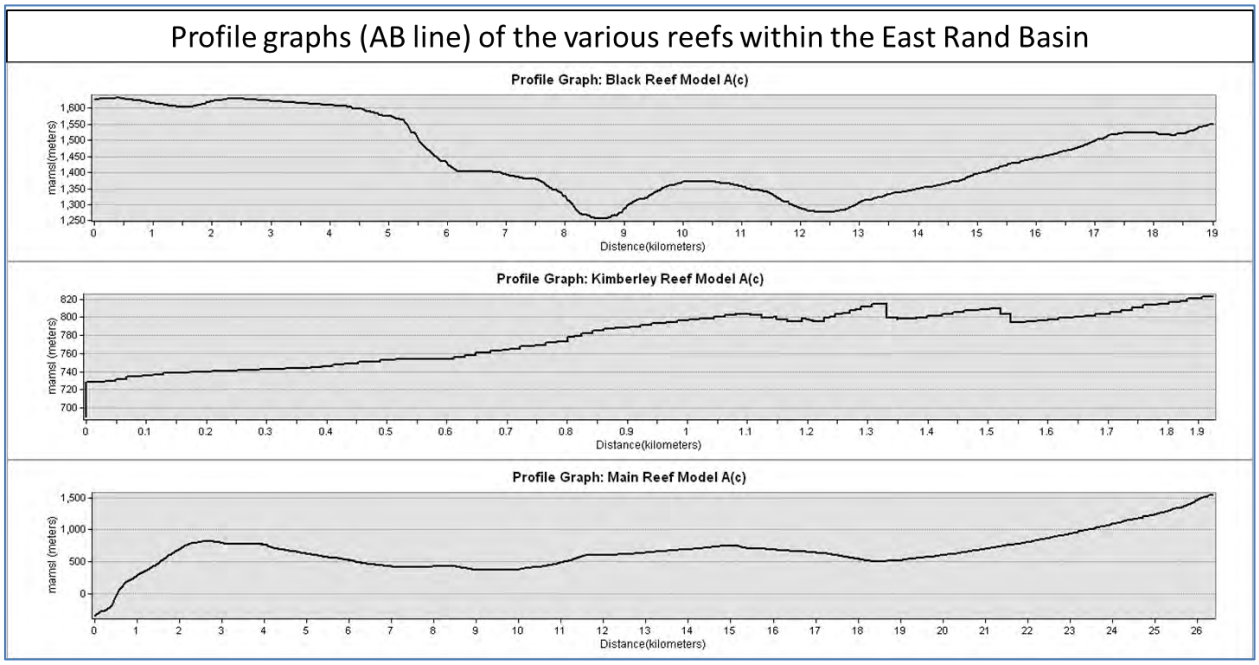


**Figure 4.17: Profile graphs (ABC line) of the various reefs within the East Rand Basin**

# Chapter 5: Conclusion and recommendations

## 5.1 Conclusion

The primary aim of this dissertation was to map the spatial distribution of the geology of the East Rand Basin accurately by creating a 3D geological model with the help of GIS. Three main models, Models A(a), B and C, were created using three main methods in order to achieve this goal. These main methods used TIN and DEM surfaces which were created from borehole data from the National Groundwater Archive Geodatabase. Furthermore, the deeper geological layers that are not found within this geodatabase were created under Models A(b) and A(c). These models were created from average depths and thicknesses provided by SACS (South African Committee for Stratigraphy) Task Group (2006) and Scott (1995) and the DEMs that were provided by the North-West University.

The quality and quantity of the data used for this dissertation were identified as the main problem, as the boreholes were too shallow for the purpose of the study, they were far more in some areas than other areas, and the borehole data points were poorly / unevenly distributed. This was seen through the cluttered points found to the north-western and western parts of the study area. It was concluded that the main cause for these reasons are that there were more users in these cluttered areas uploading their data to the Department Water and Sanitation's (DWS's) database than the other areas. Since the DWS drills for hydrological purposes, the reason for this high need in some areas could be that the state of the hydrology is of high importance.

ArcGIS as a GIS software was found to be capable of constructing the various TIN and DEM surfaces from the various borehole points. Every tool used for this study worked as intended, but it should be added that using these tools are very time-consuming, especially when it comes to creating a bottom and top depth TIN for each geological layer. A small problem was found with displaying the extrusion between polygons, especially the polygon layers from the TINs surfaces that were created from the DEMs. The problem, as mentioned under 4.3.3., is that the top surfaces look less smooth, which gives it a "distorted' look, compared to those of the bottom surfaces. Overall it can be said that ArcGIS and its tools are effective software in respect of basic 3D geological models and that the problem lies with the quality and quantity of the data.

Due to the various data sources and each source's accuracy, the shallow boreholes, the low quantity of data, the distribution of the data and the need to create the complete model using average depths and the "basic" layers (Model A(b) it can be said that a complete model containing all three main models could not be created, as such a model would be inaccurate.

Together with the above information, it should be kept in mind that the three reefs were found accurate as they showed the same concave upward nature when compared to the cross-sections ABC from DWA (Figure 4.14).

However, it is possible to create an accurate model using these methods and data of a higher quality and quantity. In addition, through an own opinion, the method for Model C is rated as the most accurate of the three methods; unlike a TIN that only connects the points, Model C was created using the Kriging method. This method predicted the values of points for which there was no information, using the data from the sample points with information. Through this process the Kriging method also attempted to get the error or mean residual close or equal to 0.

## 5.2 Recommendations

It is recommended that the quantity and the quality of the data available to the public should be increased. The high quality and quantity data will provide accurate 3D geological models with accurate results. It is also recommended that the depth should not be given as a distance from the surface, but as a distance from sea-level. This will ensure that time is not wasted in determining the study area's height above sea-level from 1:50 000 topographical maps. Using the depth as distance from sea-level will also help to link the geological layers found during borehole drilling, with the stratigraphic columns found in literature. The stratigraphic columns within literature always indicate the groups and subgroups according to the depth above and under sea-level.

It is also recommended that when working with these various methods and ArcGIS Tools, concepts and limitations of each be understood to ensure that the results and models are accurately and scientifically correct.

Furthermore, research needs to be done on the various ways to design 3D geological models and all the software will have to be compared with one another in order to determine which software delivers the most accurate results. Each flaw and limitation of each software should be considered in order to develop a 3D geological modelling software that is accurate and user-friendly.

Commercial software and tools are also recommended when it comes to 3D geological modelling. The reason for recommending these tools is that they were specifically designed to create geological layers from boreholes within the ArcGIS software. It also allows the user to create cross-sections within ArcGIS. These commercial tools were not used during the study due to limitation of available funds.

# Bibliography


Abdul-Rahman, A. & Pilouk, M. 2007. Spatial data modelling for 3D GIS. Berlin Heidelberg:Springer. http://books.google.co.za/books?id=X6a2f75ky3gC&printsec=frontcover&source=gbs_ge_summary_r&cad=0#v=onepage&q&f=false Date of access: 15 November 2013.

Allaby, A. & Allaby, M. 1999. Conjugate fault set. (*In* Encyclopedia.com: a dictionary of earth sciences.) http://www.encyclopedia.com/doc/1O13-conjugatefaultset. html Date of access: 11 September 2014.

Anderes, E.B. 2013. Spatial and temporal modelling and analysis. *Encyclopedia of Environmetrics(online)*. 2nd edition. http://www.stat.ucdavis.edu/~anderes/papers/Kriging.pdf . P 3-6.

Anon. 2014. G338-Introduction to GIS. http://www.indiana.edu/~gisci/courses/g338/lectures/introduction_vector.html Date of access: 6 July 2014.

Azpurua, M. & Ramos, K. 2010. A comparison of spatial interpolation methods for estimation of average electromagnetic field magnitude. *Progress in electromagnetics research,* 14:135-145.

Beater, C.D. 1982. The Significance of unconformities in the development of Witwatersrand gold and uranium placers. Grahamstown: Rhodes University. (Dissertation - MSc).

Berlin, J. 2013. Why sinkholes open up: Get the science behind sinkholes and which areas are more prone to them. National Geographic. http://news.nationalgeographic.com/news/2013/08/130812-florida-sinkhole-disney-world-explainer-urban-science/. Date of access: 6 July 2014.

BKS. 2011. Due diligence: Witwatersrand Gold Fields: acid mine drainage (phase 1). http://www.amdshort.co.za/documents/J01599-05%20Due%20Diligence%20-%20Final.pdf Date of access: 20 March 2014.

BLG (Byrn Law Group). 2014. Sinkhole news. http://www.byrnelawgroup.com/practiceareas/sinkholelaw/sinkholenews/. Date of access: 22 October 2014.

Childs, C. 2009. The top nine reasons to use a file geodatabase: a scalable and speedy choice for single users or small groups. http://www.esri.com/news/arcuser/0309/files/9reasons.pdf Date of access: 08 October 2014.

Chrisman, N. 2002. Exploring Geographic Information Systems. 2nd Edition. NY, New York: Wiley.

Cilliers, D. 2013. Kriging. Potchefstroom: North-West University. [PowerPoint presentation].

Council for Geoscience. 2010. Mine water management in the Witwatersrand Gold Fields with special emphasis on acid mine drainage: Report to the inter-ministerial committee on acid mine drainage. Council for Geoscience. Pretoria: South Africa.

Council for Geoscience. 2012. Sinkholes and subsidences. Pretoria. http://www.geoscience.org.za/index.php?option=com_content&view=article&id=994:sinkholes-and-subsidences&catid=165&Itemid=167&showall=1&limitstart= Date of access: 6 August 2014.

Creamer Media. 2011. Sub Nigel shaft closed as water levels rise in East Rand basin. Engineering News. 9 June. http://www.engineeringnews.co.za/print-version/sub-nigel-shaft-closed-as-east-rand-basin-water-levels-rise-2011-06-08 Date of access: 18 April 2015.

De Bever, N.J. 1997. An overview of the early – proterozoic, auriferous black reef placer in the Transvaal Basin. Grahamstown: Rhodes University. (Dissertation - MSc).

De La Vergne, J.N. 2008. Hard Rock Miner's Handbook. 5th Edition. Canada, Alberta: Stantec Consulting.

DeMeritt, 2012. Modelling the terrain below- Creating dynamic subsurface perspectives in ArcScene. Redlands, CA: ESRI.

Durand, J.F. 2012. The impact of gold mining on the Witwatersrand on the rivers and karst system of Gauteng and North West Province, South Africa. *Journal of African earth sciences 68*: volume 68: 24-43.

Dutch, S. 2014. The Universal Transverse Mercator System. University of Wisconsin - Green Bay. https://www.uwgb.edu/dutchs/FieldMethods/UTMSystem.htm Date of access: 27 August 2014.

DWA (Department of Water Affairs). 2013a. Assessment of the water quantity and quality of the Witwatersrand mine voids. volume 3. Pretoria. (Study Report No. 5.2).

DWA (Department of Water Affairs). 2013b. Options for use or discharge of water. volume 3. Pretoria. (Study Report No. 5.3).

DWAF (Department of Water Affairs and Forestry). 2006. Vaal River system: Large bulk water supply reconciliation strategy: Groundwater assessment: Dolomite Aquifers. Pretoria. https://www.dwaf.gov.za/projects/vaal/documents/LargeBulkWater/06_Dolomitic%20Groundwater%20Assessment_Final.pdf Date of access: 18 April 2015

DWS (Department Water and Sanitation). 2014. National Groundwater Information System (NGIS). Pretoria. http://www.dwa.gov.za/Groundwater/NGIS.aspx. Date of access: 5 March 2014.

Edward, H., Isaaks, R. & Srivastava, M. 1989. An introduction to applied geostatistics. NY: Oxford University Press.

EMM (Ekurhuleni Metropolitan Municipality). 2007. Environmental management framework for Ekurhuleni. Ekurhuleni.

Encyclopaedia Britannica Online. 2014a. Springs (South Africa). http://www.britannica.com/EBchecked/topic/561412/Springs Date of access: 17 July 2014.

Encyclopaedia Britannica Online. 2014b. Brakpan (South Africa). http://www.britannica.com/EBchecked/topic/77462/Brakpan Date of access: 17 July 2014.

Engels, J. 2014. What are tailings? - Their nature and production. http://www.tailings.info/basics/tailings.htm Date of access: 5 August 2014.

Environment Canada. 2009. Environmental Code of practice for metal mines. Gatineau, QC.

ESRI. 2013. Resources. http://resources.arcgis.com Date of access: 04 July 2013 - 11 November 2014.

Erikson, P. G., Altermann, W. and Hartzer, F.J. 2006. The Transvaal supergroup and its precursors. In: The Geology of South Africa. Geological Society of South Africa. Pretoria

Gobi, S. 2007. Advanced surveying: Total station, GIS and remote sensing. India, New Delhi: Dorling Kindersley Pvt. Ltd. http://books.google.co.za/books?id=GC6K78Kkou4C&pg=PA43&dq=advantages+and+disadvantages+of+DEM+and+TIN&hl=en&sa=X&ei=Ft3xU_aVEOrG7Aas1oCYAQ&ved=0CBoQ6AEwAA#v=onepage&q=advantages%20and%20disadvantages%20of%20DEM%20and%20TIN&f=false Date of access: 15 November 2013.

GreatMining. 2014. Open Pit Mining. http://www.greatmining.com/open-pit-mining.html. Date of access: 4 August 2014.

Groundwater Dictionary by DWAF. 2014. Groundwater rest level. Pretoria. http://www.dwaf.gov.za/Groundwater/Groundwater Dictionary/index.html?introduction_rest_water_level.htm Date of access: 25 September 2014.

Hamrin, H. 2009. Guide to underground mining methods and applications. Stockholm, Sweden: Atlas Copco.

Hobbs, P.J. & Cobbing., J.E. 2007. A hydrological assessment of acid mine drainage impacts in the West Rand Basin, Gauteng Province. CSIR: Natural Resources and the Environment.

ILO (International Labour Organization). 2011. Techniques in underground mining. Geneva. http://www.ilo.org/oshenc/part-xi/mining-and-quarrying/item/597-techniques-in-underground-mining Date of access: 5 August 2014.

Korte, G.B. 2001. The GIS book. 5th Edition. Albany,NY: On Word Press. http://books.google.co.za/books?id=_C6oPvJ5S_EC&printsec=frontcover&dq=korte&hl=en&sa=X&ei=eNgaVPv9OcHy7AbSmoDwDw&ved=0CB0Q6AEwAA#v=onepage&q=korte&f=false Date of access: 15 November 2013.

Langholt, A. 2013. Why Is the study of geology important?. http://www.life123.com/parenting/education/geology/why-is-the-study-of-geology-important.shtml Date of access: 12 August 2013.

Langran, G. & Chrisman, N.R. 2014. A framework for temporal geographic information. Washington: Washington University.

Li, J. and Heap, A.D. 2008. A review of spatial interpolation methods for environmental scientists. Canberra: Geoscience Australia. (Record 2008/23).

Matsui, K. 2014. Sample chapter civil engineering: underground mining transportation systems. volume 2. Fukuoka: Kyushu University.

McCarthy, T. & Rubidge, B. 2005. The story of earth and life. Cape Town,CT: Struik.

McCarthy, T.S. 2006. The Witwatersrand supergroup. (*In* Johnson, M.R., Anhaeusser, C.R. & Thomas, R.J., *eds*. The geology of South Africa. Pretoria: Council for Geoscience, p.155-186).

McCarthy, T.S. 2011. The impact of acid mine drainage in South Africa. *South African Journal of science*, 107(5/6).

Mine-Engineer. 2012. Basics of an open pit mine. http://www.mine-engineer.com/mining/open_pit.htm. Date of access: 4 August 2014.

MIT (Massachusetts Institute of Technology). 2014. Environmental risks of mining. Massachusetts. http://web.mit.edu/12.000/www/m2016/finalwebsite/problems/mining.html Date of access: 5 August 2014.

Mitchell, A. 2011. An Introduction to coordinate systems in South Africa. Ethekwini: Ethekwini Municipality.

Mosoane, C. 2003. Ore reserve valuation of mined-out areas and remnants at East Rand Proprietary Mines (ERPM). *Journal of The South African Institute of Mining and Metallurgy*, 103(2):87-92.

Ngcobo, T.A. 2006. The risks associated with mines in dolomitic compartments. *The Journal of The South African Institute of Mining and Metallurgy*, 106(4):251-264.

Nigel Business Directory. 2014. History of Nigel. http://www.nigel.co.za/history.htm Date of access: 22 October 2014.

Oliver, M.A. 2010. Geostatistical applications for precision agriculture. London, UK: Springer. http://books.google.co.za/books?id=Is5tnHQRwoC&pg=PA1&lpg=PA1&dq=history+kriging&source=bl&ots=f9oqU9NNJ9&sig=xWQ9sUDfG0-EQInBEtYKNBvbt6g&hl=en&sa=X&ei=-akOVOyFHuOI7Abt0YDABA&ved=0CFwQ6AEwCQ#v=onepage&q=history%20kriging&f=false Date of access: 15 November 2013.

Pitts, A.P. 1990. Aspects of shear strain in the East Rand Basin. Johannesburg: Rand Afrikaans University. (Dissertation - MSc).

Ruzinoor, C.M., Shariff, A.R.M., Pradhan, B., Rodzi Ahmad, M. & Rahim, M.S.M. 2012. A review on 3D terrain visualization of GIS data: techniques and software. Malaysia: University Putra Malaysia, Geospatial Information Science Research Centre (GISRC).

SACS (South African Committee for Stratigraphy). 2006. A revised stratigraphic framework for the Witwatersrand Supergroup. Council for Geoscience. Pretoria: South Africa. (Lithostratigraphic series, volume 42).

SAPA (South African Press Association). 2012. Sinkholes: East Rand families relocated. NEWS24. 19 February. http://www.news24.com/SouthAfrica/News/Sinkholes-E-Rand-families-relocated-20120219 Date of access: 6 July 2014.

Sárközy, F. 1998. GIS functions – interpolation. Budapest: Technical University Budapest. http://www.agt.bme.hu/public_e/funcint/funcint.html Date of access: 21 October 2014.

Satyanarayana, I. 2012 Basics of openpit mining. India: Singareni Collieries Company Limited. http://www.slideshare.net/isnindian/basics-of-openpit-mining= Date of access: 6 July 2014.

SAWEB. 2014. Ekurhuleni Townships: Kwa-Thema (Springs). http://www.saweb.co.za/townships/township/gauteng/kwathema.html Date of access: 17 July 2014.

Scott, R.1995. Flooding of the Central and East Rand Gold Mines: An investigation into controls over the inflow rate, water quality and predicted impacts of flooded mines. Pretoria. (Water Research Report No. 486/1/95).

Schissler, A. 2006. Strip mining. The Encyclopedia of earth. http://www.eoearth.org/view/article/156280/ Date of access: 4 Augustus 2014.

Siabato, W. & Manso-Callejo, M. 2011. Integration of temporal and semantic components into the Geographic Information through mark-up languages part I: definition. Madrid: Polytechnic University of Madrid.

SPC (Secretariat of the Pacific Community). 2014. SPC-EU EDF10 Deep Sea Minerals (DSM) Project:Types of disposal. Noumea, New Caledonia. http://www.sopac.org/dsm/public/files/resources/Deep%20Sea%20Minerals%20in%20the%20Pacific%20Islands%20Region%20Brochure%205.pdf Date of access: 6 July 2014.

Swanson, J. 1996. The three dimensional visualization & analysis of geographic data. Wasington: BioMedware. http://maps.unomaha.edu/Peterson/gis/Final_Projects/1996/Swanson/GIS_Paper.html Date of access: 27 August 2014.

Tavakoli, S. 2008. Construction of a solid 3D model of geology in Sardinia using GIS methods. Gävle: University of Gävle. (Dissertation - MSc).

Truswell, J.F. 1977. The geological evolution of South Africa. Cape Town: Alice Kelly Purnell.

Van Der Merwe, W. & Lea, I. (2003). Towards sustainable mine water treatment at Grootvlei mine. (*In* Nel, P. J. L. 2003. Mine Water and the Environment (Proceedings, 8th International Mine Water Association Congress). South Africa: Johannesburg. p. 25-36, 4 fig., 9 tab.).

Van Wyk, E., Mokgatle, T. & De Meillon, N. 2013. Witwatersrand mine voids – Their hydrochemistry and hydrodynamic characteristics. Midrand: Golder Associates.

Van Wyk, J. J. & Munnik, R. 1998. Dewatering of the Far East Rand Mining Basin: A critical evaluation of Government's approach towards solving the associated environmental problems. Pretoria: Department of Water Affairs and Forestry.

Water Encyclopedia Science and Issues. 2013. Hydrogeologic mapping. http://www.waterencyclopedia.com/Hy-La/Hydrogeologic-Mapping.html Date of access: 30 July 2013.

Wainwright, J. & Mulligan, M. (eds). 2004. Environmental modelling: Finding simplicity in complexity. Chichester: John Wiley & Sons.

Wikipedia. 2014a. Surface map. http://en.wikipedia.org/wiki/Surface_map Date of access: 20 March 2014.

Wikipedia. 2014b. Universal Transverse Mercator coordinate system. http://en.wikipedia.org/wiki/Universal_Transverse_Mercator_coordinate_system Date of access: 27 August 2014.

Winde, F. & Stoch, E.J. 2010. Threats and opportunities for post-closure development in 71 dolomitic gold-mining areas of the West Rand and Far West Rand (SouthAfrica) – a hydraulic view part 1: Mining legacy and future threats. Potchefstroom: North-West University.

Water Institute of South Africa. 2015. RAMSAR sites in South Africa. http://www.ewisa.co.za/misc/wetlands/defaultramsar.htm Date of access: 12 April 2015

Wisegeek. 2014. What is shaft mining. http://wisegeek.com/what-is-shaft-mining.htm Date of access: 5 August 2014.

Zanchi, A., Francesca, S., Stefano, Z., Simone, S., Graziano, G. 2007. 3D reconstruction of complex geological bodies: Examples from the Alps. Elsevier.

## Annexure A

# A locality map of the East Rand Basin

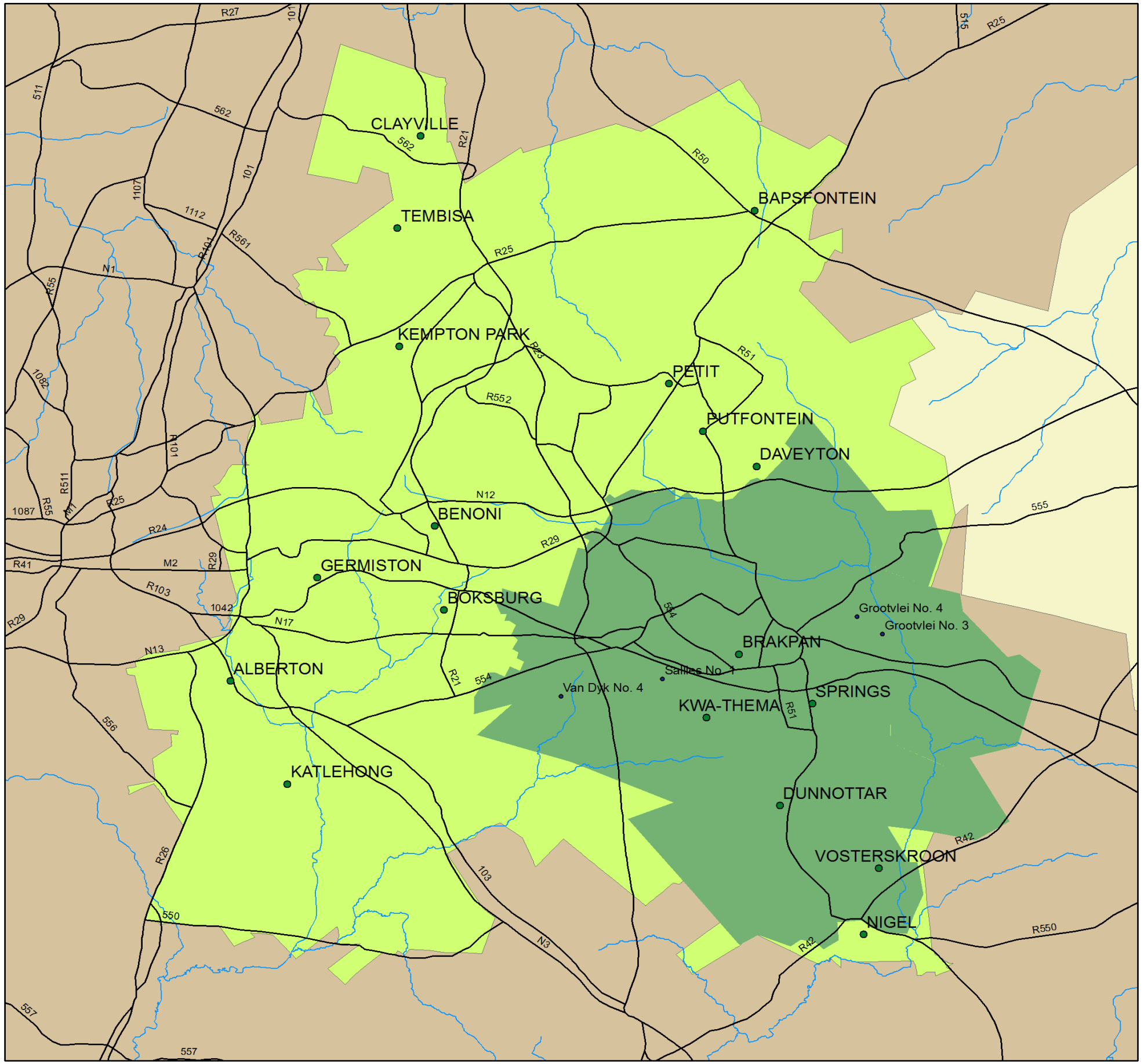


## Legend

- Towns
- Shafts
- Mainroads
- Main Rivers
- Eastern Rand Basin
- Ekurhuleni Municipality
- Gauteng

N

W E

S

0 3.25 6.5 13 Kilometers

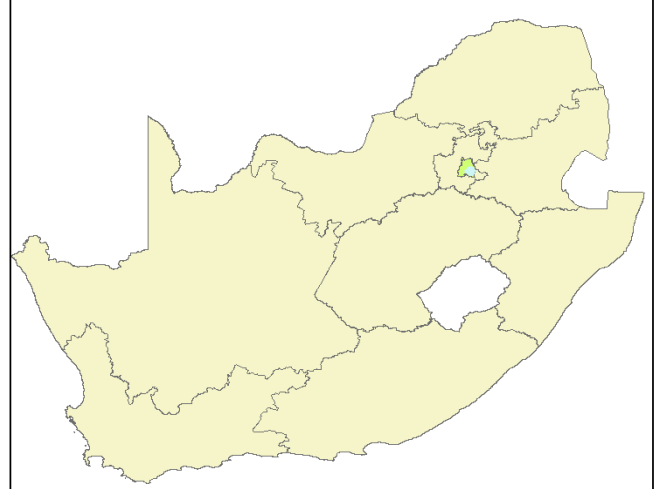

## Annexure B

EKURHULENI METROPOLITAN MUNICIPALITY
ENVIRONMENTAL MANAGEMENT FRAMEWORK 2007

# Current Use of Land

**Map 10**

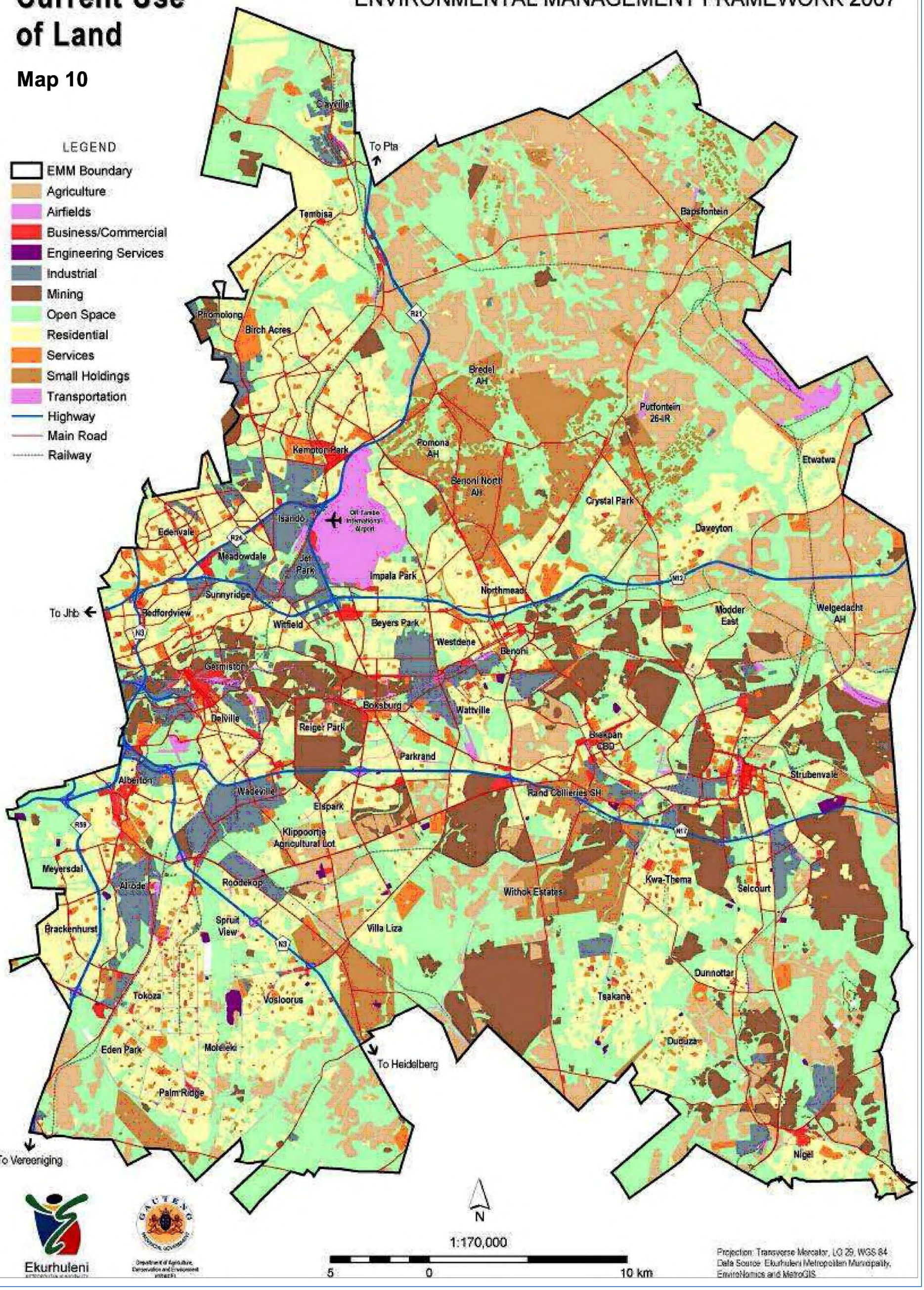

## Annexure C

# The Hydrology Of The East Rand Basin

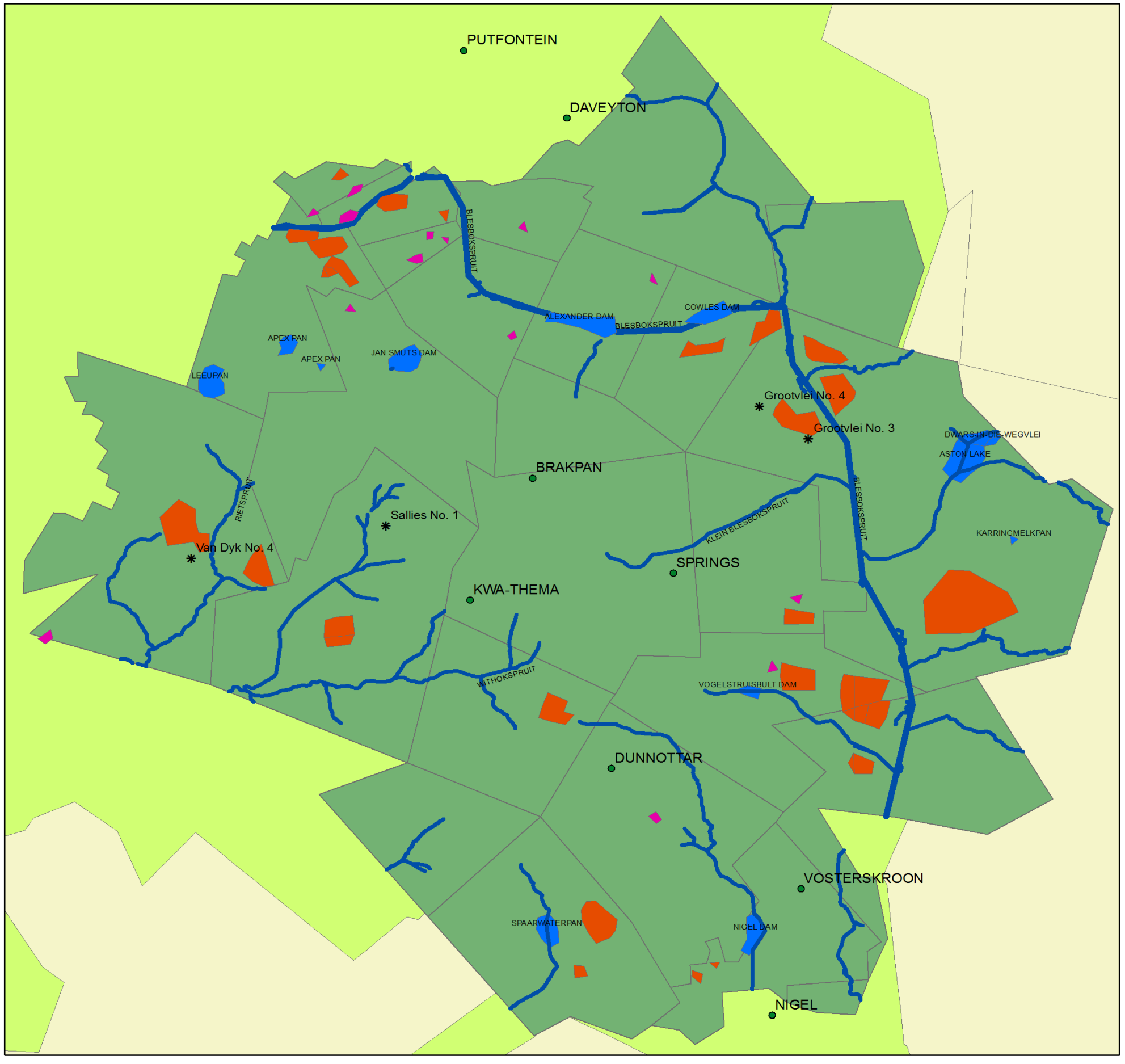


## Legend

- Shafts
- Towns
- Rivers & Spruits
- Mine Dumps
- Slime Dams
- Dams
- **East Rand Basin**
- **Ekurhuleni Municipality**

N
W E
S

0 1.75 3.5 7 Kilometers

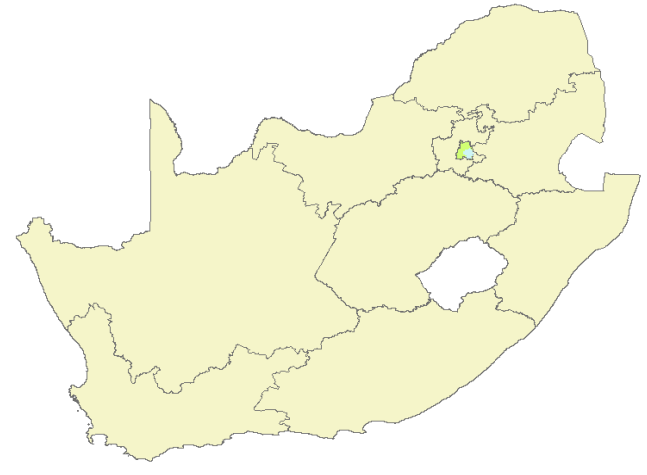

## Annexure D

# Extensively Mined Out Areas On The Main Reef

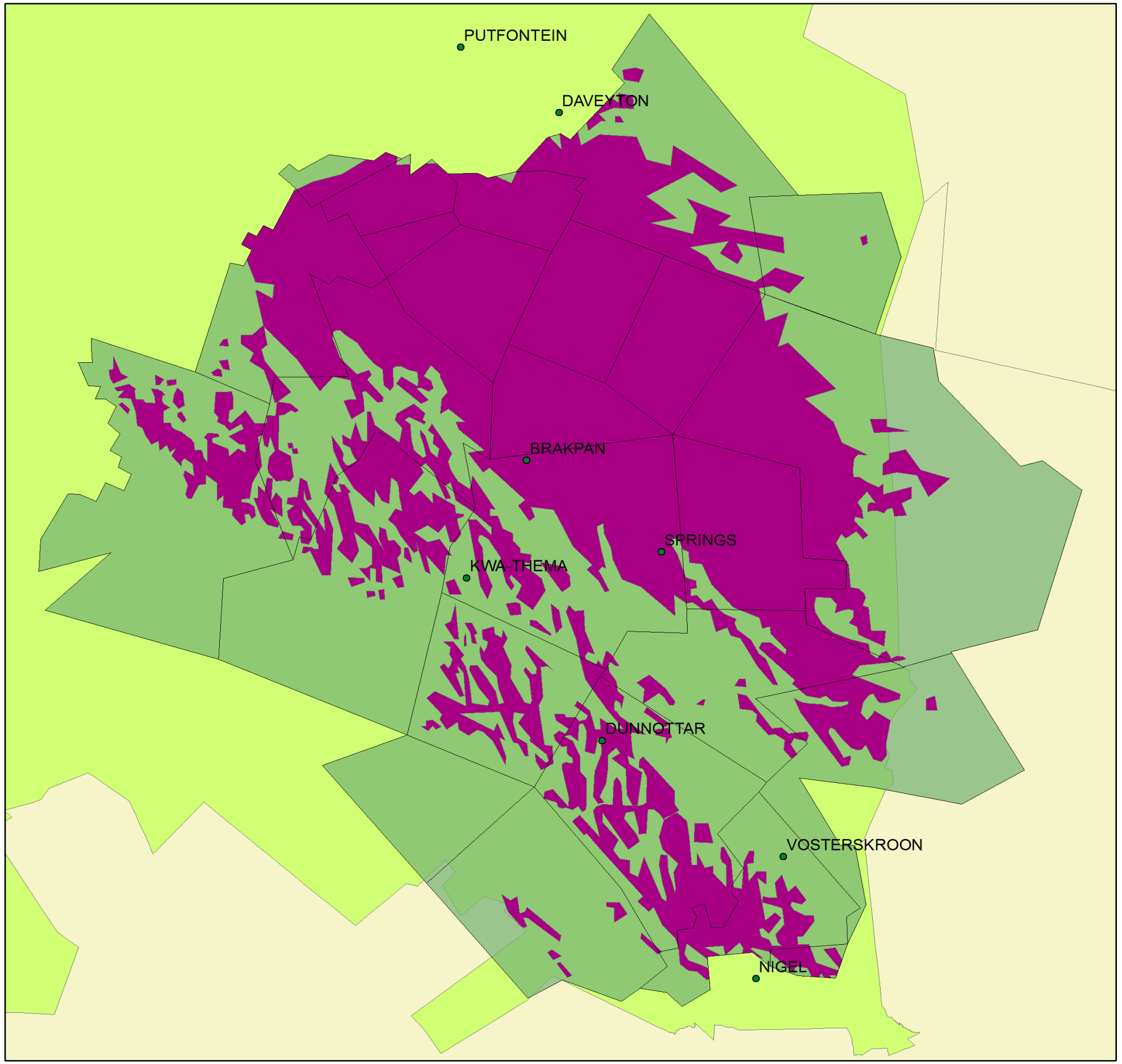


## Legend

- Towns
- Main Reef
- Eastern Rand Basin
- Ekurhuleni Municipality

N
W E
S

0 1.75 3.5 7 Kilometers

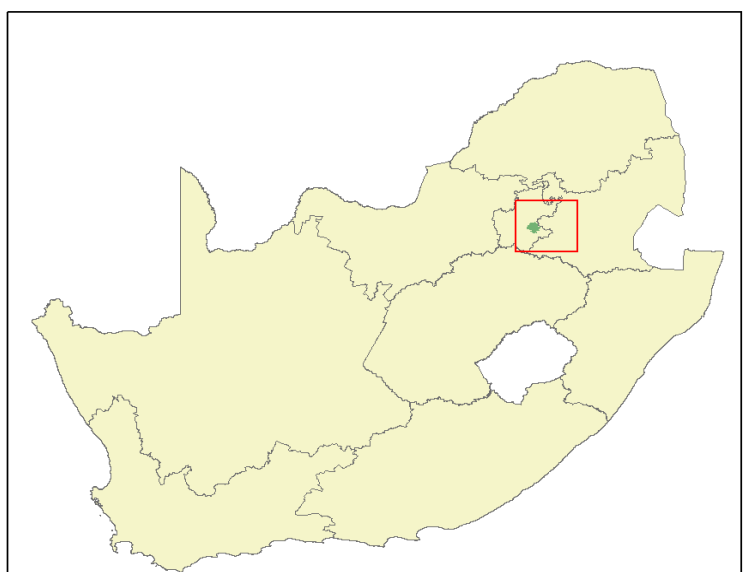

## Annexure E

# Extensively Mined Out Areas On The Kimberley Reef

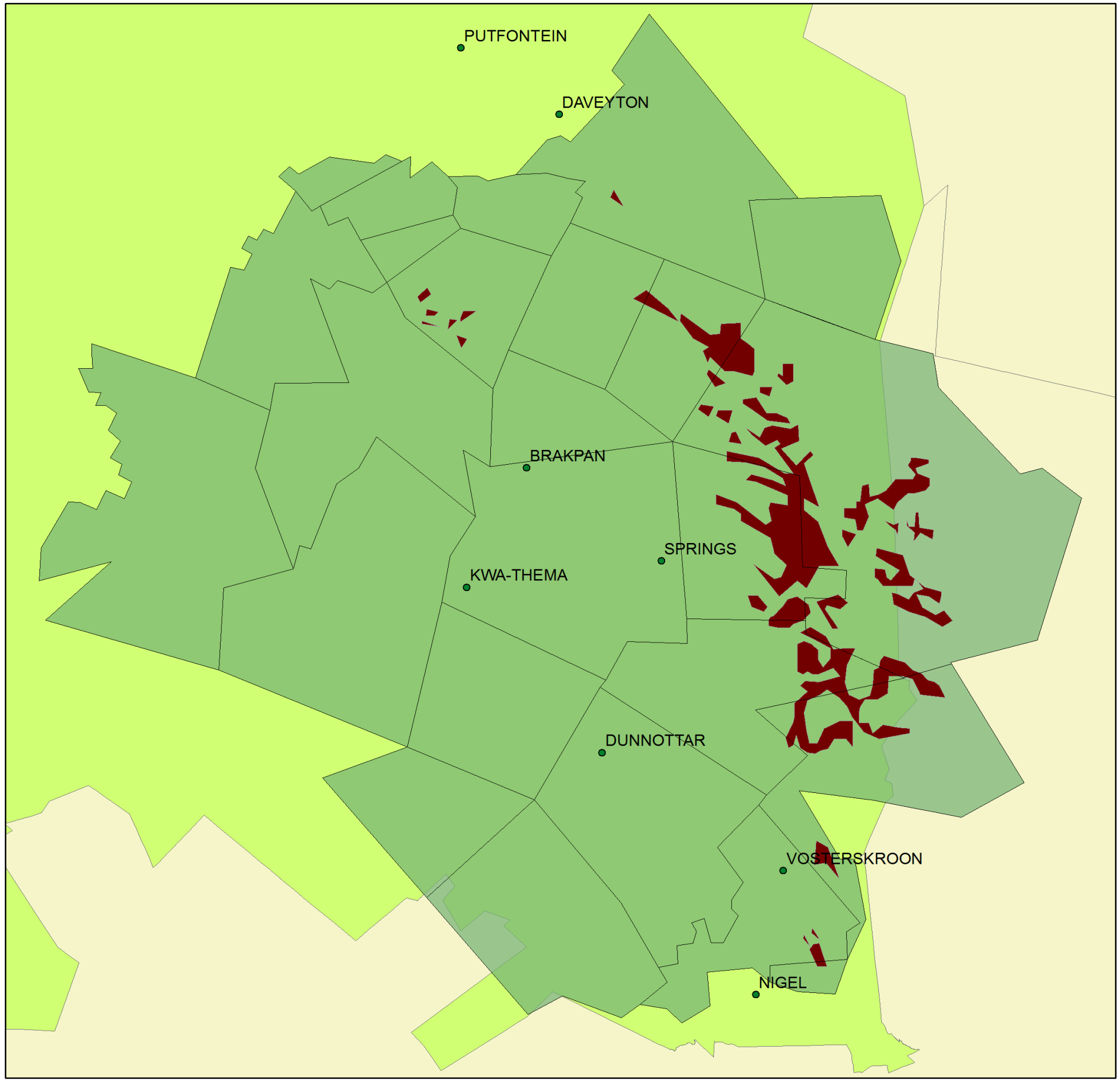


## Legend

- Towns
- Kimberley Reef
- Eastern Rand Basin
- Ekurhuleni Municipality

N
W E
S

0 1.75 3.5 7 Kilometers

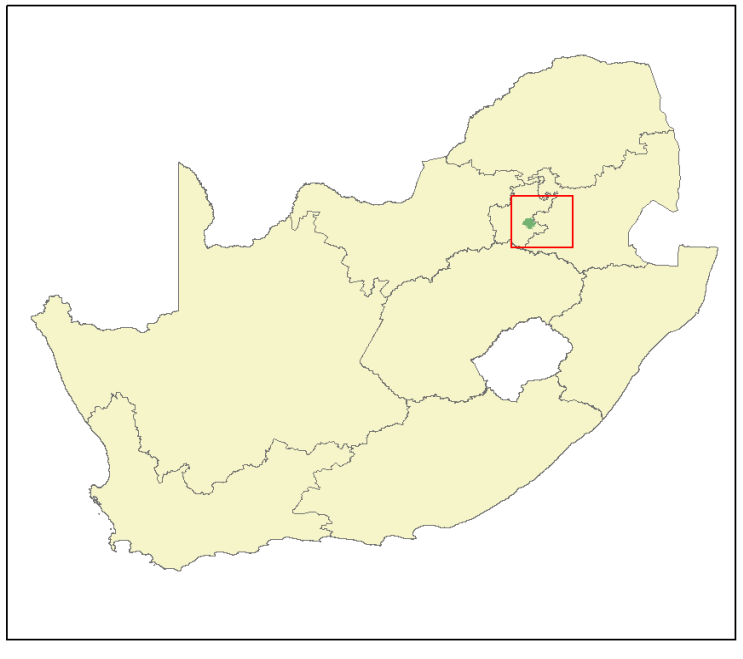

## Annexure F

# The East Rand Basin Mine Lease Areas

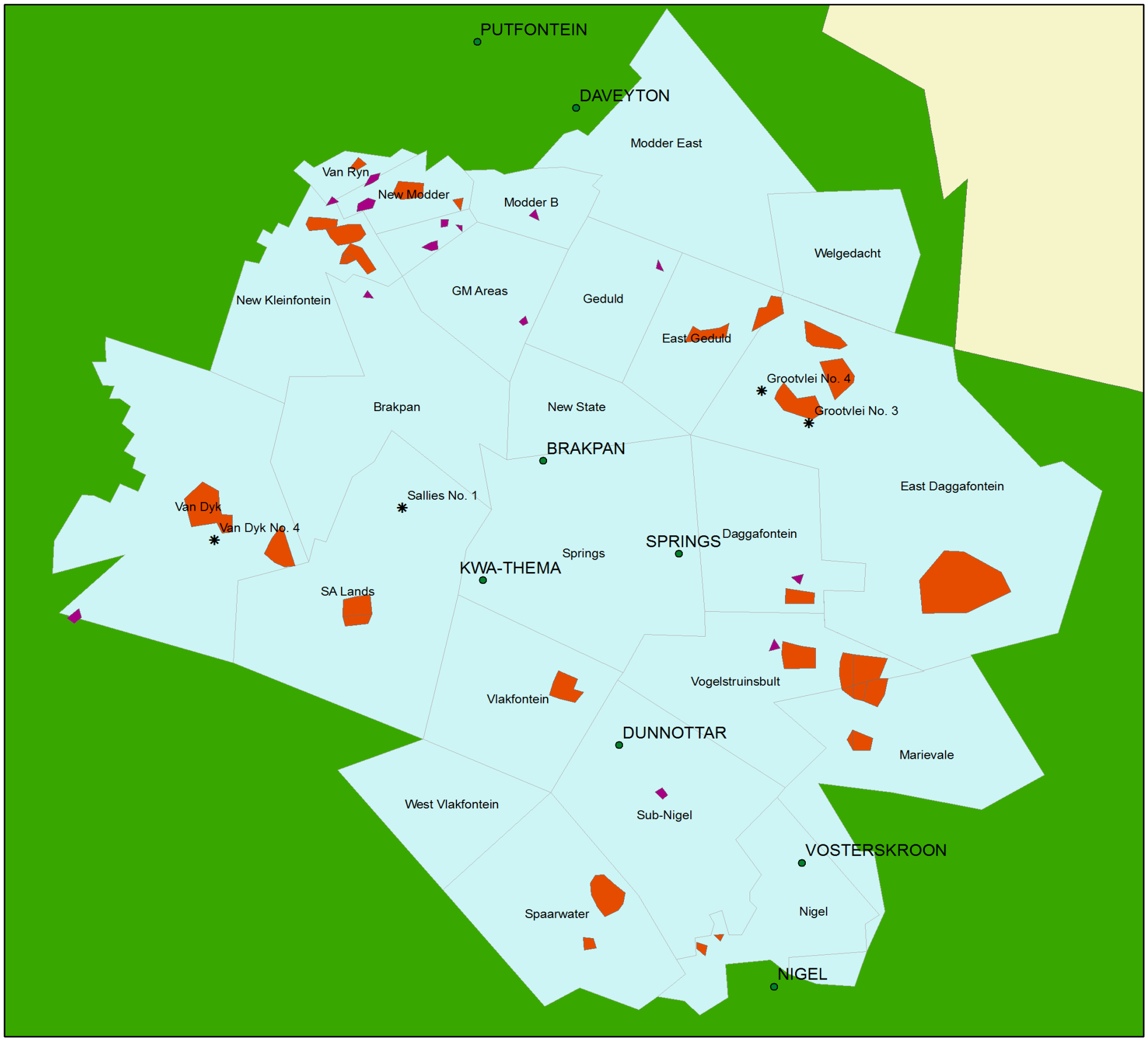


## Legend

- Shafts
- Towns
- Slime Dams
- Mine Dumps
- Mine Lease Areas/Boundaries
- Gauteng

N
W E
S

0 2 4 8 Kilometers

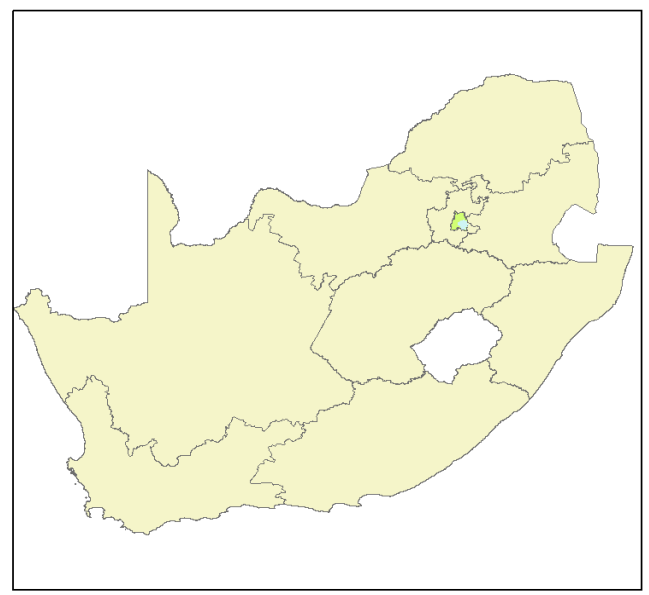

## Annexure G

# The Geology and Mine Leases Of The East Rand Basin

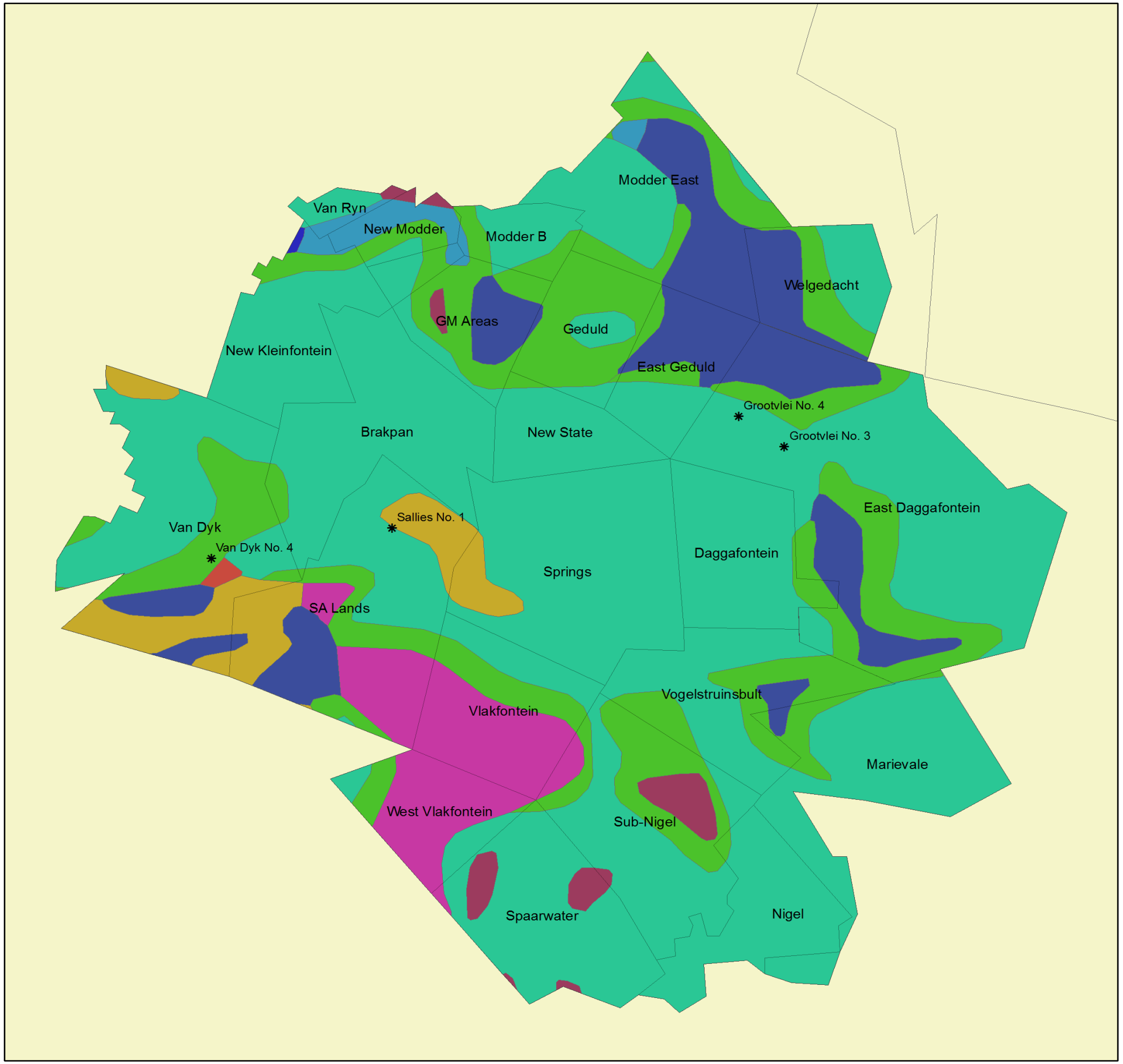


## Legend

- Shafts
- **Mine Leases**

**Geology**

**Stratname**

- Black Reef, Transvaal Spgrp
- Dwyka Grp, Karoo Spgrp
- Jeppestown Sbgrp, West Rand Grp
- Johannesburg Sbgrp, Central Rand Grp
- Karoo Dolerite Sui
- Klipriviersberg Grp, Ventersdorp Spgrp
- Madzaringwe Fm, Karoo Spgrp
- Malmani Sbgrp, Chuniespoort Grp
- Turffontein Sbgrp, Central Rand Gr

N
W E
S

0 1.75 3.5 7 Kilometers

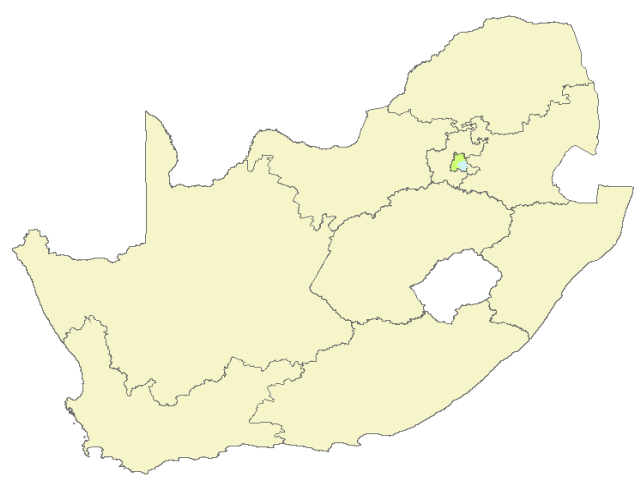

## Annexure H

# The Geology and Structural Features Of The East Rand Basin

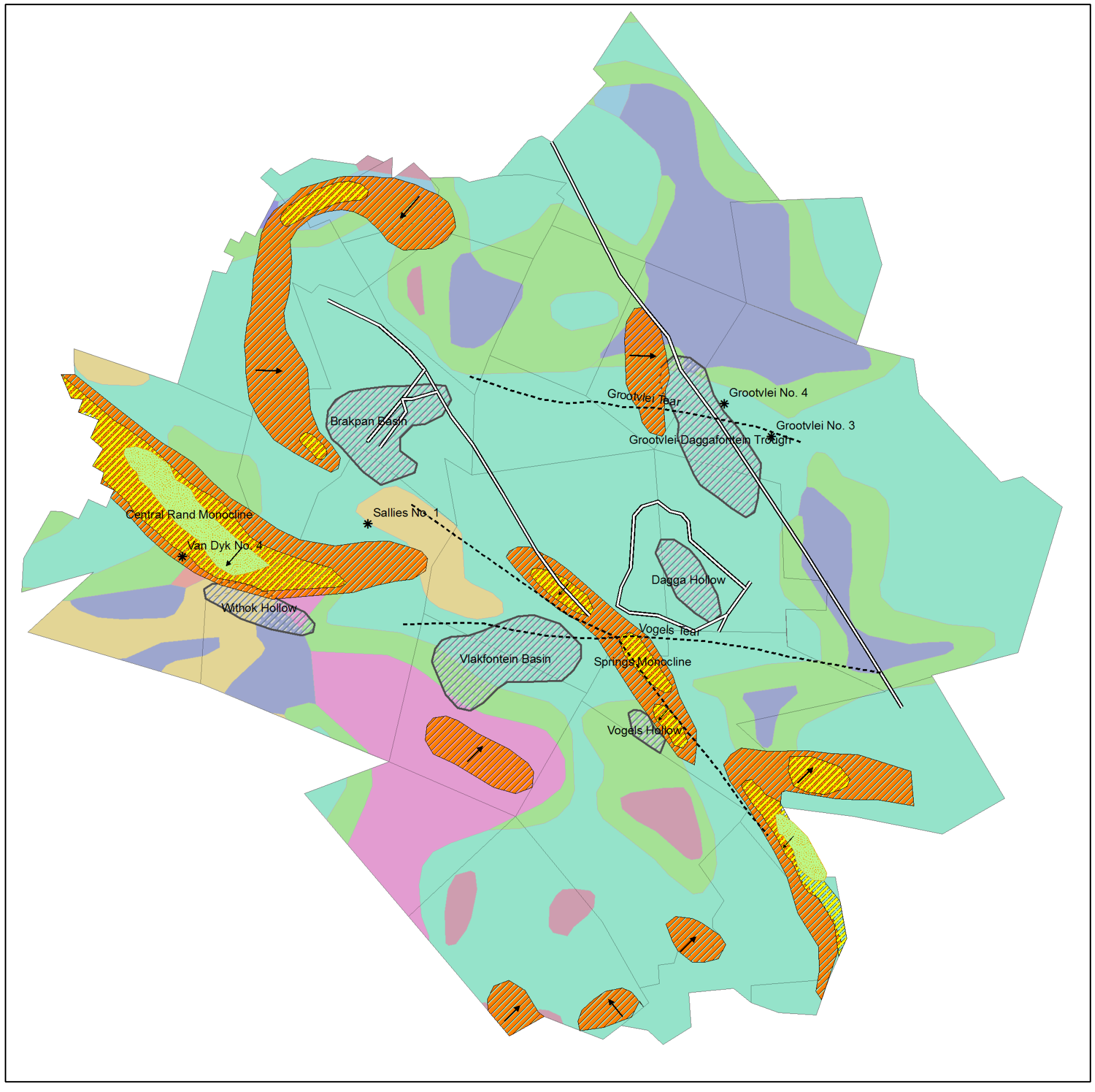


## Legend

- Shafts
- Fault
- Dyke
- Very Steep Dips 45 Degrees
- Steep Dips Over 30 Degrees
- Moderate Dips 20-30 Degrees
- Discrete Basin
- **Mine Leases**

**Geology**

**Stratname**

- Black Reef, Transvaal Spgrp
- Dwyka Grp, Karoo Spgrp
- Jeppestown Sbgrp, West Rand Grp
- Johannesburg Sbgrp, Central Rand Grp
- Karoo Dolerite Sui
- Klipriviersberg Grp, Ventersdorp Spgrp
- Madzaringwe Fm, Karoo Spgrp
- Malmani Sbgrp, Chuniespoort Grp
- Turffontein Sbgrp, Central Rand Gr

N
W E
S

0 1.75 3.5 7 Kilometers

## Annexure I

# Model A (a)

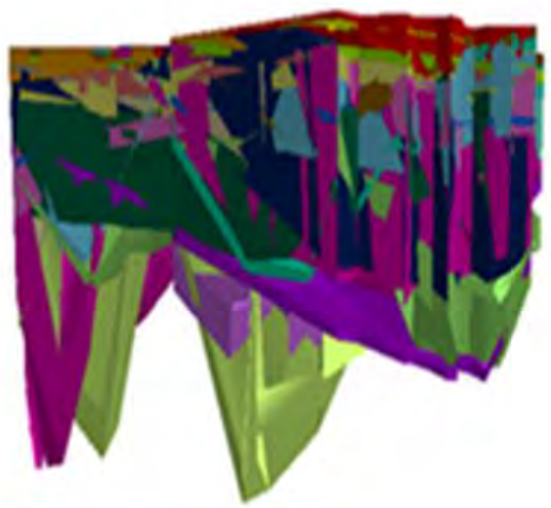

S-N

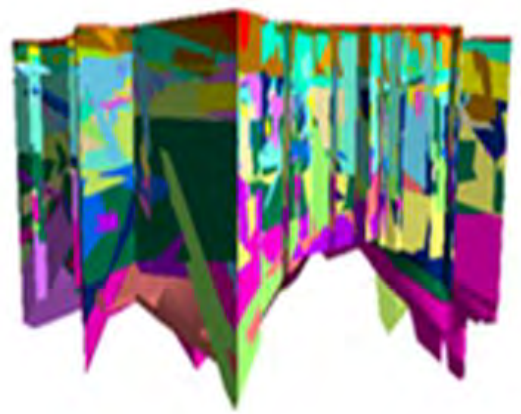

N-S

E-W

W-E

## Annexure J

# Model A (b)

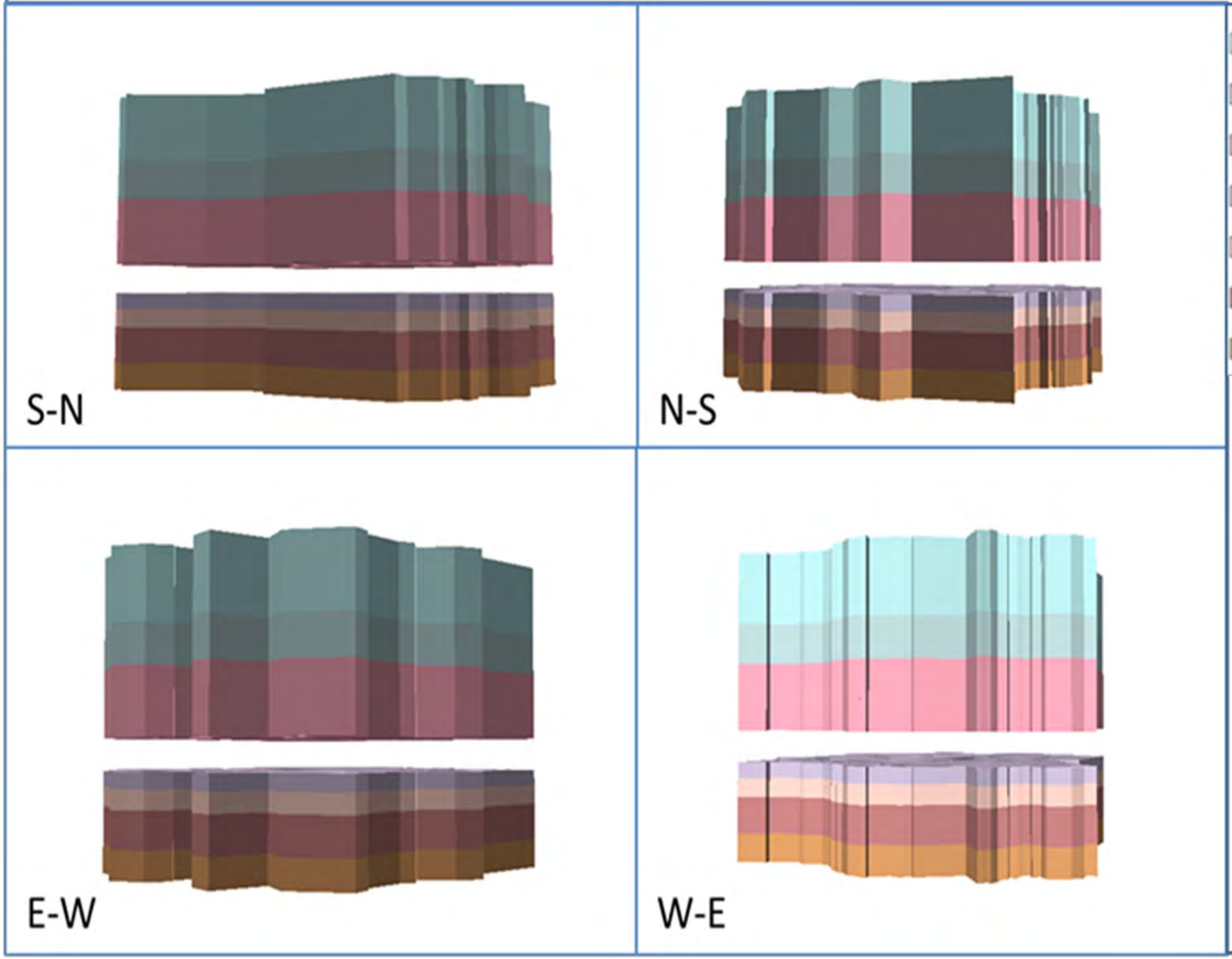
S-N
N-S
E-W
W-E
Alberton Formation
Mondeor Formation
Elsburg Formation
Doornkop Formation
BooysensFormation
Randfontein Formation
Main Conglomerate Formation

## Annexure K

# Model A (c)

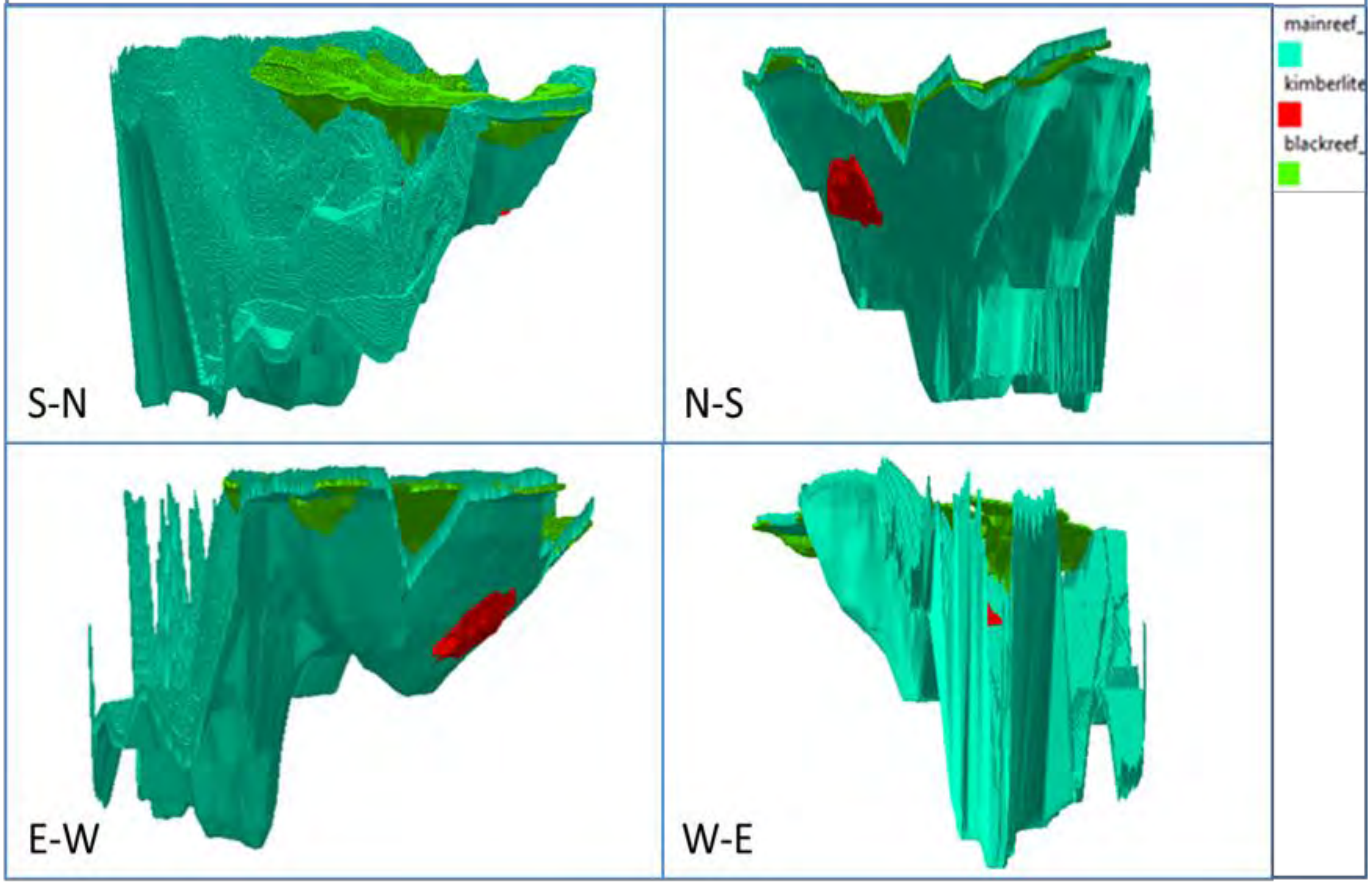

## Annexure L

# Model B

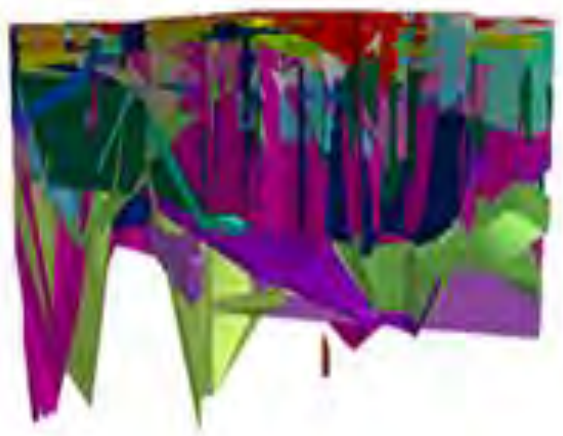

S-N

N-S

E-W

W-E

synt
soil
snds
slte
slsn
silt
shle
sdsl
rbbl
qrtz
ns
mdsn
ltrt
loam
lmsm

lava
grvl
grnt
frct
dirt
dlmt
dibs
coal
clgm
clct
clay
chrt
brcc
bldr
blcl

## Annexure M

# Model C

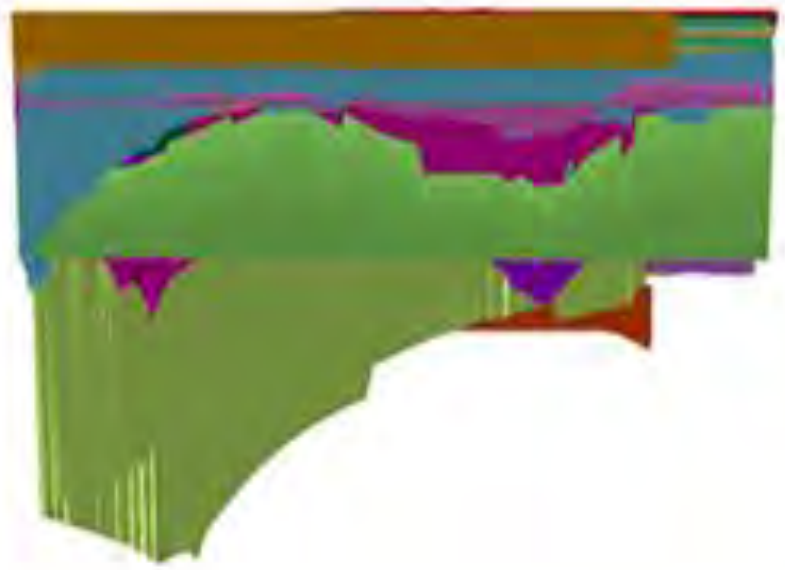

S-N

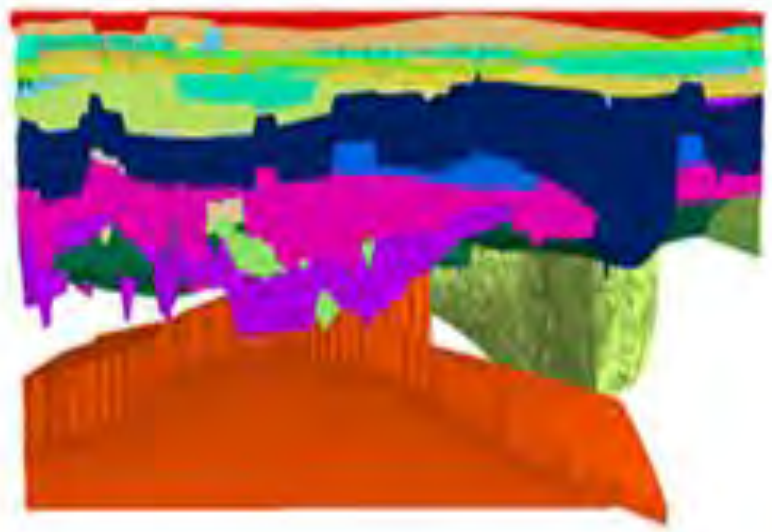

N-S

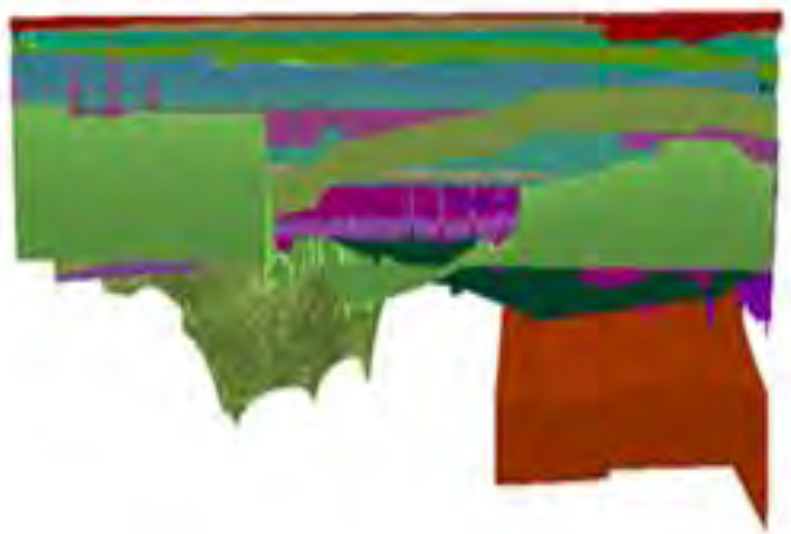

E-W

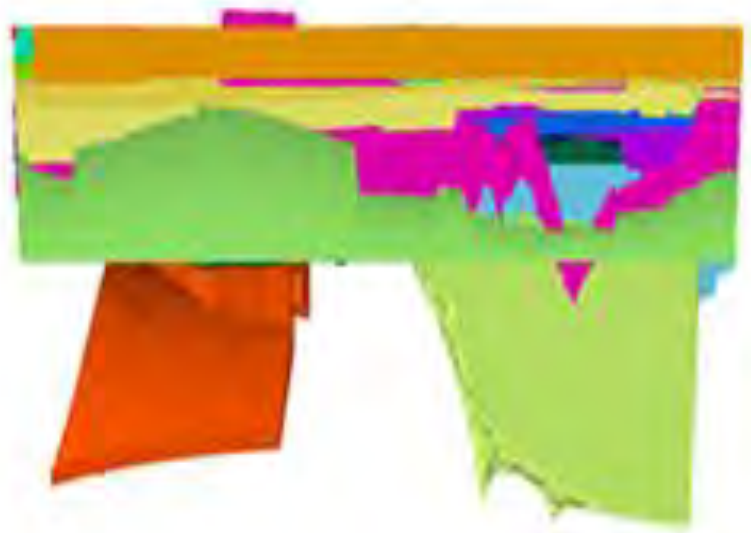

W-E